



The
University
Of
Sheffield.

**Investigating the adsorption and surface active behaviour of
silk fibroin peptides and mixtures of peptide and conventional
surfactants**

By:

Dharana S Jayawardane

A thesis submitted in fulfilment of the requirements for the degree of
Doctor of Philosophy

The University of Sheffield
Faculty of Engineering
Department of Chemical and Biological Engineering

January 2017

“If I have seen further, it is by standing on the shoulders of giants”

Sir Isaac Newton

Abstract

The work herein investigates the surface active properties of short peptides and their interactions with conventional surfactants. Short peptides can be designed to mimic the structures of conventional surfactants such as SDS and C₁₂TAB. Such peptide structures include V₆K peptide, which are attractive in many fields and applications as they can be more biocompatible, biodegradable and environmentally friendlier substitutes to harsh surfactants. Similar peptide structures can also be found naturally occurring in proteins, such as silk fibroin, and can then be liberated by breaking down the protein into its constituent peptides. The interaction of these peptides with conventional surfactants at the air-liquid and solid-liquid interface have not been investigated before. The adsorption behaviour and structures formed at the solid-liquid interface were examined using Ellipsometry and Neutron Reflection. It was found that V₆K could adsorb at the solid interface from solutions containing conventional surfactants and could also be pre-adsorbed at the surface to form bilayers and cylindrical micellar structures which were very stable even upon subsequent surfactant addition. The adsorption of regenerated silk fibroin (RSF) was also investigated at the solid-liquid interface. A stable 80 Å RSF layer was found adsorbed at the interface. However, the layer was found to be susceptible to pH and salt concentration changes and addition of surfactant at high concentration would cause the layer to desorb. At the air-liquid interface, RSF adsorbed and formed a stable layer which was not susceptible to changes in pH or salt concentration. The layer was found to extend up to 40 Å into the water and 15 Å into the air phase. Addition of small amounts of RSF to conventional surfactants resulted in significant lowering of the surface tension making the solutions much more efficient than the pure surfactant solutions. Furthermore, the effects of RSF molecular weight and RSF foaming were also examined.

Acknowledgements

I would like to thank my supervisor, Dr. Xiubo Zhao, for giving me the opportunity to work on this project. It has been a challenging endeavour and I have learnt a lot in the course of these four years.

I'm also immensely grateful to all the people who have helped me along this journey. Claire Hurley and Deborah Hammond at the Sheffield Surface Analysis Centre for scratching their heads with me whenever the ellipsometer misbehaved. Also, I would like to thank all instrument scientist and staff at ISIS neutron facility, for helping set up experiments and making sure everything would run smoothly throughout our stay, and especially Maximilian Skoda and Luke Clifton whom I have bothered a little bit more by asking for help and advice but have always been extremely kind and resourceful.

I would also like to thank Professor Jian R. Lu, at The University of Manchester for supporting our research, as well as Zhiming Lu, Elias Pambou and Zongyi Li with whom I spent days and nights squeezed in the tiny instrument cabins, obsessing over experiments and the neutron beam status, and yet somehow finding time to have a laugh and a good time. A special thanks goes out to Mario Campana, who also squeezed in the cabin with us and shared his enthusiasm towards neutron reflection as well as many much needed coffee breaks (and finding the 'hidden' pool table), but importantly was a wealth of knowledge and has been extremely helpful in explaining things and cheering me on.

Equally, I thank everyone in my department, staff, post-docs and academics for all the guidance and support. Friends (I will not make a list), from Hadfield Building, Pam Liversidge Building and to Kroto you have all contributed to discussions and my general well-being.

On a more personal note, I would like to thank my housemates Kartik Chandrasekhar, Riccardo Innocenti and Thomas Lakey as well as Shalini Weerasooriya for sharing this journey with me through all its ups and downs. Finally, I dedicate this work to my parents who have always believed in me and have given, and keep giving, all the support and love that one could ever ask for.

CONTENTS

ABSTRACT.....	III
ACKNOWLEDGEMENTS.....	IV
LIST OF TABLES	X
LIST OF FIGURES	XII
1 INTRODUCTION.....	1
1.1 SURFACTANTS.....	1
<i>1.1.1 Common structures and subdivisions</i>	<i>2</i>
<i>1.1.2 Surfactant applications</i>	<i>5</i>
<i>1.1.3 Issues with conventional surfactants and search and development of alternatives.....</i>	<i>7</i>
1.2 SURFACTANT AGGREGATION AND ADSORPTION STUDIES	11
<i>1.2.1 Key electrostatic and hydrophobic effects</i>	<i>14</i>
<i>1.2.2 Adsorption at the air-liquid interface</i>	<i>15</i>
<i>1.2.3 Adsorption at solid-liquid interface</i>	<i>18</i>
1.3 PEPTIDES.....	21
<i>1.3.1 Amino acid structure and characteristics</i>	<i>22</i>
<i>1.3.2 Designer peptides.....</i>	<i>24</i>
<i>1.3.3 Surfactant-like peptides.....</i>	<i>26</i>
<i>1.3.4 Alternative peptide sources.....</i>	<i>27</i>
1.4 SILK FIBROIN	29
<i>1.4.1 Molecular structure and composition</i>	<i>29</i>
<i>1.4.2 Regenerated silk fibroin.....</i>	<i>31</i>
1.5 RESEARCH MOTIVATION.....	32
1.6 OUTLINE OF THESIS	33
2 EXPERIMENTAL THEORY.....	34

2.1 NEUTRON REFLECTION	34
2.1.1 Overview	34
2.1.2 Neutron production and facilities	36
2.1.3 Neutron reflection theory	37
2.1.4 Experimental method	46
2.1.5 Contrast variation	48
2.1.6 Neutron data analysis	49
2.2 ELLIPSOMETRY	52
2.2.1 Overview	52
2.2.2 Theory of light reflection for Ellipsometry	52
2.2.3 Experimental method	59
2.2.4 Ellipsometry data	60
2.3 SURFACE TENSION	61
2.3.1 Overview	61
2.3.2 Theory of surface tension	61
2.3.3 Experimental method	64
2.4 FOAMING STUDIES	65
2.4.1 Overview	65
2.4.2 Foaming Theory	65
2.4.3 Experimental method	67
3 V₆K PEPTIDE ADSORPTION	69
3.1 OVERVIEW	69
3.2 INTRODUCTION	70
3.3 EXPERIMENTAL METHOD	73
3.3.1 Materials	73
3.3.2 Spectroscopic Ellipsometry	73

3.3.3 Neutron reflection	74
3.4 RESULTS AND DISCUSSION	75
3.4.1 Adsorption of SDS/V ₆ K mixed solution at solid-liquid interface	75
3.4.2 Interaction of SDS with pre-adsorbed V ₆ K peptide	79
3.4.3 C ₁₂ TAB/V ₆ K mixed solution adsorption at the Solid-liquid interface.....	87
3.4.4 Interaction of C ₁₂ TAB with pre-adsorbed V ₆ K peptide.....	91
3.5 CONCLUSION	93
4 SILK FIBROIN SOLID-LIQUID ADSORPTION.....	94
4.1 OVERVIEW	94
4.2 INTRODUCTION.....	95
4.3 EXPERIMENTAL METHOD.....	97
4.3.1 Silk preparation	97
4.3.2 Spectroscopic Ellipsometry.....	98
4.3.3 Neutron reflection	98
4.4 RESULTS AND DISCUSSION	99
4.4.1 Adsorption of RSF onto SiO ₂ /water interface	99
4.4.2 Effect of pH on the adsorption of RSF	106
4.4.3 Effect of ionic strength on the adsorption of RSF.....	111
4.4.4 RSF/SDS interaction at the SiO ₂ Interface	114
4.4.5 RSF/C ₁₂ TAB interaction at the SiO ₂ interface	118
4.5 CONCLUSION	121
5 SILK FIBROIN AIR-LIQUID ADSORPTION.....	123
5.1 OVERVIEW	123
5.2 INTRODUCTION.....	124
5.3 EXPERIMENTAL METHOD.....	126
5.3.1 Silk preparation	126

5.3.2 Neutron reflection	126
5.3.3 Surface tension.....	127
5.3.4 Foaming experiments.....	127
5.4 RESULTS AND DISCUSSION.....	128
5.4.1 RSF adsorption behaviour and structure as the interface	128
5.4.2 Co-adsorption with SDS and foaming behaviour	141
5.4.3 Co-adsorption with C ₁₂ TAB and foaming behaviour.....	153
5.5 CONCLUSION	163
6 CONCLUSION.....	165
6.1 CONCLUSIONS	165
6.2 FUTURE WORK.....	167
7 REFERENCES.....	169

List of Tables

TABLE 3.1 STRUCTURAL PARAMETERS OBTAINED FROM BEST FITS OF NEUTRON REFLECTION DATA SHOWN IN FIGURE 3.4 FOR THE CO-ADSORPTION OF SDS/V ₆ K IN D ₂ O PH 7. FITTING OF SDS GIVES A THREE LAYER FIT WHILST FITTING OF D-SDS CURVE GAVE A TWO LAYER FIT. (JAYAWARDANE ET AL ¹⁴³ , PUBLISHED BY THE ROYAL SOCIETY OF CHEMISTRY).....	78
TABLE 3.2 STRUCTURAL PARAMETERS OBTAINED FROM THE BEST FITS AS SHOWN IN FIGURE 3.5 FOR 20 MINUTE PRE-ADSORBED V ₆ K AT 20 MG/ML, FOLLOWED BY ADDITION OF 4 MM SDS. (JAYAWARDANE ET AL ¹⁴³ , PUBLISHED BY THE ROYAL SOCIETY OF CHEMISTRY).....	81
TABLE 3.3 STRUCTURAL PARAMETERS OBTAINED FROM MODEL BEST FITS OF NEUTRON REFLECTION DATA SHOWN IN FIGURE 3.7 FOR THE ADSORPTION OF 4 MM SDS ONTO PRE-ADSORBED V ₆ K IN D ₂ O PH 7. (JAYAWARDANE ET AL ¹⁴³ , PUBLISHED BY THE ROYAL SOCIETY OF CHEMISTRY).....	84
TABLE 3.4 STRUCTURAL PARAMETERS OBTAINED FROM MODEL BEST FITS OF NEUTRON REFLECTION DATA SHOWN IN FIGURE 3.10 FOR THE CO-ADSORPTION OF C ₁₂ TAB/V ₆ K IN D ₂ O AT PH 7. (JAYAWARDANE ET AL ¹⁴³ , PUBLISHED BY THE ROYAL SOCIETY OF CHEMISTRY).	90
TABLE 4.1 STRUCTURAL PARAMETERS OF NEUTRON REFLECTION BEST FITS FOR 5-30 KDA SILK FIBROIN PEPTIDES ADSORBED FOR 1HR AT THE SiO ₂ /WATER INTERFACE AT PH 7. REPRINTED WITH PERMISSION FROM JAYAWARDANE ET AL ¹⁷⁵ . COPYRIGHT 2017 AMERICAN CHEMICAL SOCIETY.....	101
TABLE 4.2 STRUCTURAL PARAMETERS OF NEUTRON REFLECTION BEST FITS FOR 30-300 KDA SILK FIBROIN PEPTIDES ADSORBED FOR 1HR AT THE SiO ₂ INTERFACE AT PH7. REPRINTED WITH PERMISSION FROM JAYAWARDANE ET AL. ¹⁷⁵ COPYRIGHT 2017 AMERICAN CHEMICAL SOCIETY.....	104
TABLE 4.3. STRUCTURAL PARAMETERS OF NEUTRON REFLECTION BEST FITS FOR >300 KDA SILK FIBROIN PEPTIDES ADSORBED FOR 1HR AT THE SiO ₂ INTERFACE AT PH7. REPRINTED WITH PERMISSION FROM JAYAWARDANE ET AL. ¹⁷⁵ COPYRIGHT 2017 AMERICAN CHEMICAL SOCIETY.....	105
TABLE 4.4 STRUCTURAL PARAMETERS OF NEUTRON REFLECTION BEST FITS FOR PH EFFECT ON RSF 5-30 KDA ADSORBED FOR 1HR AT THE SiO ₂ /WATER INTERFACE AT A CONCENTRATION OF 3 MG/ML REPRINTED WITH PERMISSION FROM JAYAWARDANE ET AL. ¹⁷⁵ COPYRIGHT 2017 AMERICAN CHEMICAL SOCIETY.	107
TABLE 4.5 STRUCTURAL PARAMETERS OF NEUTRON REFLECTION BEST FITS FOR PH EFFECT ON 30-300 KDA SILK FIBROIN ADSORBED FOR 1HR AT THE SiO ₂ INTERFACE AT A CONCENTRATION OF 3 MG/ML REPRINTED WITH PERMISSION FROM JAYAWARDANE ET AL. ¹⁷⁵ COPYRIGHT 2017 AMERICAN CHEMICAL SOCIETY.	109
TABLE 4.6 STRUCTURAL PARAMETERS OF NEUTRON REFLECTION BEST FITS FOR PH EFFECT ON >300 KDA SILK FIBROIN ADSORBED FOR 1HR AT THE SiO ₂ INTERFACE AT A CONCENTRATION OF 3 MG/ML REPRINTED WITH PERMISSION FROM JAYAWARDANE ET AL. ¹⁷⁵ COPYRIGHT 2017 AMERICAN CHEMICAL SOCIETY.	110
TABLE 4.7 STRUCTURAL PARAMETERS OF NEUTRON REFLECTION BEST FITS FOR NaCl EFFECT ON 5-30 KDA SILK FIBROIN PEPTIDES ADSORBED FOR 1 HR AT THE SiO ₂ /WATER INTERFACE AT A CONCENTRATION OF 3 MG/ML, PH 7. REPRINTED WITH PERMISSION	

FROM JAYAWARDANE ET AL. ¹⁷⁵ COPYRIGHT 2017 AMERICAN CHEMICAL SOCIETY.	111
TABLE 4.8 STRUCTURAL PARAMETERS OF NEUTRON REFLECTION BEST FITS FOR 5-30 kDA SILK FIBROIN 3 MG/ML ADSORBED FOR 1 HR AT THE SiO ₂ /WATER INTERFACE FOLLOWED BY SDS ADSORPTION. REPRINTED WITH PERMISSION FROM JAYAWARDANE ET AL. ¹⁷⁵ COPYRIGHT 2017 AMERICAN CHEMICAL SOCIETY.....	117
TABLE 4.9 STRUCTURAL PARAMETERS OF NEUTRON REFLECTION BEST FITS FOR 5-30 kDA SILK FIBROIN 3 MG/ML ADSORBED FOR 1 HR FOLLOWED BY C ₁₂ TAB ADSORPTION AT THE SiO ₂ /WATER INTERFACE. REPRINTED WITH PERMISSION FROM JAYAWARDANE ET AL. ¹⁷⁵ COPYRIGHT 2017 AMERICAN CHEMICAL SOCIETY	120
TABLE 5.1 STRUCTURAL PARAMETERS FROM THE BEST FIT OF NR CURVES FOR ADSORBED LAYERS FROM SOLUTIONS OF 0.1 MG/ML RSF.....	130
TABLE 5.2 STRUCTURAL PARAMETERS OF RSF 5-30K LAYERS ADSORBED AT THE AIR/WATER INTERFACE.....	134
TABLE 5.3 STRUCTURAL PARAMETERS OF SF1B 5-30K (0.1 G/L) LAYERS ADSORBED AT THE AIR/WATER INTERFACE (PH 7) WITH DIFFERENT NaCl CONCENTRATIONS.....	139
TABLE 5.4 STRUCTURAL PARAMETERS OF SF1B 5-30K (0.01 G/L) LAYERS ADSORBED AT THE AIR/WATER INTERFACE AT DIFFERENT PHs.....	140

List of Figures

FIGURE 1.1 DIAGRAM DEPICTING THE BASIC STRUCTURE OF LINEAR SURFACTANTS AND THEIR FOUR MAIN CATEGORIES.	3
FIGURE 1.2 DETERMINATION OF CMC BY DIFFERENT EXPERIMENTAL TECHNIQUES. ²⁹ ...	13
FIGURE 1.3 MODEL SURFACE TENSION CURVE FOR THE TYPICAL INTERACTIONS BETWEEN A POLYMER AND A SURFACTANT. ³³	17
FIGURE 1.4 ADSORPTION AT THE SOLID-LIQUID INTERFACE ADAPTED FROM PARIA ET AL. ³⁰	20
FIGURE 1.5 AMINO ACID STRUCTURES AND THEIR DIVISION BY PHYSIOCHEMICAL CHARACTERISTICS. (REPRODUCED FROM DAN COJOCARI, PRINCESS MARGARET CANCER CENTRE, UNIVERSITY OF TORONTO UNDER CREATIVE COMMONS ATTRIBUTION-SHARE ALIKE 3.0).....	23
FIGURE 1.6 MOLECULAR STRUCTURE OF SILK FIBROIN CHAINS FROM BOMBYX MORI. REPRINTED WITH PERMISSION FROM HA ET AL. ⁹³ COPYRIGHT 2017 AMERICAN CHEMICAL SOCIETY.....	30
FIGURE 2.1 A MINIATURE MODEL OF THE ISIS NEUTRON FACILITY FOUND AT THE FRONT ENTRANCE TO THE ISIS CONTROL ROOM.	35
FIGURE 2.2 BASIC SPALLATION SOURCE LAYOUT FOR NEUTRON PRODUCTION AND INSTRUMENT FACILITIES AT ISIS.....	36
FIGURE 2.3 A, WAVELENGTHS OF ELECTROMAGNETIC WAVES ACROSS THE ELECTROMAGNETIC SPECTRUM, B, SCHEMATIC OF THE SCATTERING OF ELECTRON, X-RAY AND NEUTRON BEAMS AT THE ATOMIC LEVEL. ¹⁰⁸	38
FIGURE 2.4 WAVEVECTOR AND ANGULAR FREQUENCY OF A NEUTRON SCATTERING EVENT. ¹⁰⁸	41
FIGURE 2.5 VECTOR DIAGRAM FOR A NEUTRON REFLECTION EVENT. ¹⁰⁸	42
FIGURE 2.6 THE INTERFACE BETWEEN TWO BULK MEDIA WITH REFRACTIVE INDICES n_0 AND n_1 , WITH TRANSMITTED AND REFLECTED WAVEVECTORS k_0 AND k_1 , AT ANGLES θ_0 AND θ_1	44
FIGURE 2.7 SETUP OF NEUTRON REFLECTOMETRY INSTRUMENT CHAMBER.....	46
FIGURE 2.8 CONTRAST VARIATION AT THE AIR/LIQUID INTERFACE.	48
FIGURE 2.9 P-POLARISED AND S-POLARISED LIGHT REFLECTING OFF A SURFACE.	53
FIGURE 2.10 INCIDENT LIGHT, I, IS TRANSMITTED INTO MEDIUM n_2 AT AN ANGLE φ	54
FIGURE 2.11 REFLECTION FROM MULTIPLE LAYERS.	57
FIGURE 2.12 ELLIPSOMETER SETUP USED FOR EXPERIMENTS.	59
FIGURE 2.13 COHESIVE FORCES SHOWN ACTING ON MOLECULE IN THE BULK AND AT THE INTERFACE (RED).	61
FIGURE 2.14 LIQUID PULLING ONTO A PLATE, WITH A WETTED PERIMETER L SHOWN IN RED AND A CONTACT ANGLE θ	63
FIGURE 2.15 KRUSS SURFACE TENSIO METER EQUIPMENT.	64
FIGURE 3.1 (A) ADSORPTION ISOTHERMS OF V_6K (\diamond), V_6K_2 (Δ), V_3K (\square) AT THE SILICA/WATER INTERFACE, MEASURED AT PH 7, 100 MG/ML. (B) ADSORBED AMOUNT	

OF V₆K PLOTTED AGAINST SOLUTION PH. REPRINTED WITH PERMISSION FROM PAN ET AL⁷⁹. COPYRIGHT 2017 AMERICAN CHEMICAL SOCIETY..... 71

FIGURE 3.2 IN SITU AFM IMAGES (2 × 2 μM) OF V₆K AT THE SILICA/WATER INTERFACE AT PH 6.0. AFM IMAGES WERE COLLECTED AFTER 30 MIN ADSORPTION. **(A)** HEIGHT IMAGE AND **(A)** THE CORRESPONDING PHASE IMAGE WITH THE PEPTIDE CONCENTRATION FIXED AT 0.05 mM. **(B)** HEIGHT IMAGE AND **(B)** THE CORRESPONDING PHASE IMAGE WITH THE PEPTIDE CONCENTRATION FIXED AT 0.2 mM. THE Z SCALE IS SHOWN ON THE RIGHT (0 - 30 NM). REPRODUCED FROM HAN ET AL¹³⁹ WITH PERMISSION FROM THE ROYAL SOCIETY OF CHEMISTRY. 72

FIGURE 3.3 THE ADSORPTION OF V₆K (×) PEPTIDE AND CO-ADSORPTION OF SDS AND V₆K AT THE SILICA/WATER INTERFACE WITH THE MOLAR RATIO OF SDS: V₆K AT 0.5:1 (□), 0.78:1 (Δ), 1:1 (◇), AND 3.9:1 (*), 7.8:1 (○). V₆K WAS FIXED AT 100 MG/ML, PH 7. (JAYAWARDANE ET AL¹⁴³, PUBLISHED BY THE ROYAL SOCIETY OF CHEMISTRY). ..75

FIGURE 3.4. **(A)** REFLECTIVITY PROFILES FOR SDS/V₆K (0.78/1) MIXTURE (□) AND D-SDS/V₆K (0.78/1) (◇) AT THE SiO₂ INTERFACE IN D₂O PH 7. SOLID LINES THROUGH THE DATA POINTS CORRESPOND TO THE MODEL FITS FOR THE CORRESPONDING MEASURED REFLECTIVITY DATA POINTS. **(B)** SCHEMATIC DIAGRAM SHOWING THE ARRANGEMENT OF V₆K MOLECULES (BLUE), SDS (RED), AT SDS/V₆K=0.78/1. (JAYAWARDANE ET AL¹⁴³, PUBLISHED BY THE ROYAL SOCIETY OF CHEMISTRY). ..77

FIGURE 3.5. A, REFLECTIVITY PROFILES FOR 20 MG/ML V₆K PH 7 (□), 20 MG/ML V₆K PH 7+ 4 mM D-SDS (◇) AND 20 MG/ML V₆K PH 7+4 mM SDS (Δ). SOLID LINES THROUGH THE DATA POINTS CORRESPOND TO THE BEST FITS FOR THE CORRESPONDING REFLECTIVITY DATA POINTS. B, SCHEMATIC DIAGRAM SHOWING THE ARRANGEMENT OF PRE-ADSORBED V₆K PEPTIDES AT 20 MG/ML (BLUE) AND ADSORPTION OF SDS (RED) AT THE SiO₂/ D₂O INTERFACE AT PH 7. (JAYAWARDANE ET AL¹⁴³, PUBLISHED BY THE ROYAL SOCIETY OF CHEMISTRY). 80

FIGURE 3.6 ELLIPSOMETRY DATA SHOWING THE ADSORPTION OF V₆K (100 MG/ML, PH 7) AT THE SILICA/WATER INTERFACE AND WASHED BY WATER AND DIFFERENT CONCENTRATIONS OF SDS (FROM 0.1 mM TO 4 mM). (JAYAWARDANE ET AL¹⁴³, PUBLISHED BY THE ROYAL SOCIETY OF CHEMISTRY). 82

FIGURE 3.7 A, REFLECTIVITY PROFILES FOR: 100 MG/ML V₆K PH 7 (□), 100 MG/ML V₆K PH 7+ 4 mM D-SDS (◇) AND 100 MG/ML V₆K PH 7 + 4 mM SDS (Δ). SOLID LINES THROUGH THE DATA POINTS CORRESPOND TO THE MODEL FITS FOR THE CORRESPONDING REFLECTIVITY DATA POINTS. B, SCHEMATIC DIAGRAM SHOWING THE ARRANGEMENT OF PRE-ADSORBED 100 MG/ML V₆K PEPTIDES (BLUE) AND THE EFFECT OF SDS (RED) ON ITS ARRANGEMENT AT THE SiO₂/ D₂O INTERFACE AT PH 7. (JAYAWARDANE ET AL¹⁴³, PUBLISHED BY THE ROYAL SOCIETY OF CHEMISTRY). ..83

FIGURE 3.8 ELLIPSOMETRY DATA SHOWING THE ADSORPTION OF V₆K (100 MG/ML, PH 7) AT C₈/WATER INTERFACE AND WASHED BY WATER AND DIFFERENT CONCENTRATION OF SDS (FROM 0.1MM TO 4MM). (JAYAWARDANE ET AL¹⁴³, PUBLISHED BY THE ROYAL SOCIETY OF CHEMISTRY). 86

FIGURE 3.9 THE ADSORPTION ISOTHERM OF V₆K AT 100 MG/ML (×) AND C₁₂TAB AT 0.128 mM (○); 2.63 mM (*); 12 mM (□). THE CO-ADSORPTION WAS AT THE MOLAR RATIO OF C₁₂TAB AND V₆K OF 1:1(◇), 20:1(Δ) AND 94:1(+). V₆K WAS FIXED AT 100 MG/ML, ALL AT PH 7. (JAYAWARDANE ET AL¹⁴³, PUBLISHED BY THE ROYAL SOCIETY OF CHEMISTRY). 87

FIGURE 3.10 A, REFLECTIVITY PROFILES FOR: C₁₂TAB/V₆K (20/1) MIXTURE (□) AND D-C₁₂TAB/V₆K (20/1) (◇). SOLID LINES THROUGH THE DATA POINTS CORRESPOND TO

THE MODEL FITS FOR THE CORRESPONDING REFLECTIVITY DATA POINTS. B, SCHEMATIC DIAGRAM SHOWING THE ARRANGEMENT OF V₆K MOLECULES (BLUE), C₁₂TAB (GREEN) AT C₁₂TAB/V₆K=20/1, AT THE SiO₂ INTERFACE IN D₂O PH 7. (JAYAWARDANE ET AL ¹⁴³, PUBLISHED BY THE ROYAL SOCIETY OF CHEMISTRY).. .. 89

FIGURE 3.11 ELLIPSOMETRY DATA SHOWING THE ADSORPTION ISOTHERM OF V₆K (100 MG/ML, PH 7) AT SILICA/WATER INTERFACE AND WASHED BY WATER AND DIFFERENT CONCENTRATION OF C₁₂TAB (FROM 0.1MM TO 4MM). (JAYAWARDANE ET AL ¹⁴³, PUBLISHED BY THE ROYAL SOCIETY OF CHEMISTRY). 91

FIGURE 3.12 ELLIPSOMETRY DATA SHOWING THE ADSORPTION OF V₆K (100 MG/ML, PH 7) AT C₈/WATER INTERFACE AND WASHED BY WATER AND DIFFERENT CONCENTRATION OF C₁₂TAB (FROM 0.1 MM TO 4 MM). (JAYAWARDANE ET AL ¹⁴³, PUBLISHED BY THE ROYAL SOCIETY OF CHEMISTRY)..... 92

FIGURE 4.1 (A) ADSORPTION KINETICS FOR RSF 5-30 kDa AT CONCENTRATIONS OF 0.3 (□), 1 (◇), 3 (Δ) AND 10 (o) MG/ML, PH 7, AT THE SILICA/WATER INTERFACE, STUDIED BY SE. (B) REFLECTIVITY PROFILES FOR RSF 5-30 kDa AT CONCENTRATION OF 0.3 (□), 1 (◇), 3 (Δ) AND 10 (o) MG/ML, PH 7, AT THE SILICA/WATER INTERFACE STUDIED BY NR. SOLID LINES THROUGH THE DATA POINTS CORRESPOND TO THE BEST FITS FOR THE CORRESPONDING REFLECTIVITY CURVES WHICH ARE DETAILED IN TABLE 4.1. REPRINTED WITH PERMISSION FROM JAYAWARDANE ET AL.¹⁷⁵ COPYRIGHT 2017 AMERICAN CHEMICAL SOCIETY..... 100

FIGURE 4.2 (A) ADSORPTION KINETICS (MEASURED BY SE) FOR 0.3 MG/ML (OPEN SYMBOLS) AND 3 MG/ML (SHADED SYMBOLS) RSF AT THE SILICA/WATER INTERFACE, PH 7. (B) ADSORPTION ISOTHERMS FOR SILK FIBROIN PEPTIDES MEASURED BY NR (OPEN SYMBOLS) AND SE (SHADED SYMBOLS). REPRINTED WITH PERMISSION FROM JAYAWARDANE ET AL.¹⁷⁵ COPYRIGHT 2017 AMERICAN CHEMICAL SOCIETY. 102

FIGURE 4.3 REFLECTIVITY PROFILES FOR SF 30-300 kDa PH 7 AT CONCENTRATIONS OF 0.3 (□), 1 (◇), 3 (Δ) AND 10 (o) MG/ML. SOLID LINES THROUGH THE DATA POINTS CORRESPOND TO THE BEST FITS FOR THE CORRESPONDING REFLECTIVITY CURVES WHICH ARE DETAILED IN TABLE 4.2. REPRINTED WITH PERMISSION FROM JAYAWARDANE ET AL.¹⁷⁵. COPYRIGHT 2017 AMERICAN CHEMICAL SOCIETY 104

FIGURE 4.4 REFLECTIVITY PROFILES FOR SF >300 kDa PH7 AT CONCENTRATIONS OF 0.3 (□), 1 (◇), 3 (Δ) AND 10 (o) MG/ML. SOLID LINES THROUGH THE DATA POINTS CORRESPOND TO THE BEST FITS FOR THE CORRESPONDING REFLECTIVITY CURVES WHICH ARE DETAILED IN TABLE 4.3. REPRINTED WITH PERMISSION FROM JAYAWARDANE ET AL.¹⁷⁵. COPYRIGHT 2017 AMERICAN CHEMICAL SOCIETY 105

FIGURE 4.5 (A) ADSORPTION KINETICS FOR RSF 5-30 kDa AT THE CONCENTRATION OF 3 MG/ML AT PH 5 (□), PH 7(◇) AND PH 9(Δ) AT THE SILICA/WATER INTERFACE, STUDIED BY SE.(B) REFLECTIVITY PROFILES FOR 3 MG/ML RSF 5-30 kDa AT PH 5 (□), PH 7(◇) AND PH 9(Δ) STUDIED BY NR. SOLID LINES THROUGH THE DATA POINTS CORRESPOND TO THE BEST FITS FOR THE CORRESPONDING REFLECTIVITY CURVES. REPRINTED WITH PERMISSION FROM JAYAWARDANE ET AL.¹⁷⁵ COPYRIGHT 2017 AMERICAN CHEMICAL SOCIETY..... 106

FIGURE 4.6 REFLECTIVITY PROFILES FOR 3 MG/ML SF 30-300 kDa AT PH 5 (□), PH 7 (◇) AND PH 9(Δ).SOLID LINES THROUGH THE DATA POINTS CORRESPOND TO THE BEST FITS FOR THE CORRESPONDING REFLECTIVITY CURVES WHICH ARE DETAILED IN TABLE 4.5. REPRINTED WITH PERMISSION FROM JAYAWARDANE ET AL.¹⁷⁵. COPYRIGHT 2017 AMERICAN CHEMICAL SOCIETY..... 109

FIGURE 4.7 REFLECTIVITY PROFILES FOR 3 MG/ML SF >300 kDA AT PH 5(\square), PH 7(\diamond) AND PH 9(Δ). SOLID LINES THROUGH THE DATA POINTS CORRESPOND TO THE BEST FITS FOR THE CORRESPONDING REFLECTIVITY CURVES WHICH ARE DETAILED IN TABLE 4.6 . REPRINTED WITH PERMISSION FROM JAYAWARDANE ET AL. ¹⁷⁵ . COPYRIGHT 2017 AMERICAN CHEMICAL SOCIETY.....	110
FIGURE 4.8 (A) ADSORPTION KINETICS FOR RSF 5-30 kDA 3 MG/ML WITH NaCl CONCENTRATIONS OF 5 (\square), 20 (\diamond), 50 (Δ), 150 (o) AND 500 (*) mM, AT THE SILICA/WATER INTERFACE, PH 7 STUDIED BY SE. (B) REFLECTIVITY PROFILES FOR RSF 5-30 kDA PH 7 WITH NaCl CONCENTRATIONS OF 5 (\square), 20 (\diamond), 50 (Δ), 150 (o) AND 500 (*) mM STUDIED BY NR. SOLID LINES THROUGH THE DATA POINTS CORRESPOND TO THE BEST FITS FOR THE CORRESPONDING REFLECTIVITY CURVES. REPRINTED WITH PERMISSION FROM JAYAWARDANE ET AL. ¹⁷⁵ COPYRIGHT 2017 AMERICAN CHEMICAL SOCIETY.....	112
FIGURE 4.9 EFFECT OF NaCl CONCENTRATION ON THE ADSORPTION OF 3 MG/ML SILK FIBROIN MEASURED BY SE AT THE SILICA/WATER INTERFACE, PH 7. REPRINTED WITH PERMISSION FROM JAYAWARDANE ET AL. ¹⁷⁵ COPYRIGHT 2017 AMERICAN CHEMICAL SOCIETY.....	114
FIGURE 4.10 (A) FINAL ADSORPTION VALUES FOLLOWING SEQUENTIAL ADSORPTION OF 3 MG/ML SILK FIBROIN (1 HR) AND DIFFERENT CONCENTRATIONS OF SDS MEASURED BY SE AT THE SILICA/WATER INTERFACE PH 7. (B) REFLECTIVITY PROFILES FOR RSF 5-30 kDA PH 7 WITH 1 mM SDS (\square), 1 mM D-SDS (\diamond), 10 mM SDS (Δ) AND 10 mM D-SDS (o). SOLID LINES THROUGH THE DATA POINTS CORRESPOND TO THE BEST FITS FOR THE CORRESPONDING REFLECTIVITY CURVES. (C) SCHEMATIC MODEL SHOWING THE ARRANGEMENT OF RSF MOLECULES (BLACK), SDS (RED) AT 1 mM AND 10 mM SDS. REPRINTED WITH PERMISSION FROM JAYAWARDANE ET AL. ¹⁷⁵ COPYRIGHT 2017 AMERICAN CHEMICAL SOCIETY.....	115
FIGURE 4.11 (A) FINAL ADSORPTION VALUES FOLLOWING SEQUENTIAL ADSORPTION OF 3 MG/ML RSF (1 HR) AND C ₁₂ TAB MEASURED BY ELLIPSOMETRY AT THE SILICA/WATER INTERFACE, PH 7. (B) REFLECTIVITY PROFILES FOR RSF 5-30 kDA PH 7 WITH 0.2 mM C ₁₂ TAB (\square), 0.2 mM D-C ₁₂ TAB (\diamond), 20 mM C ₁₂ TAB (Δ) AND 20 mM D-C ₁₂ TAB (o). SOLID LINES THROUGH THE DATA POINTS CORRESPOND TO THE BEST FITS FOR THE CORRESPONDING REFLECTIVITY CURVES. (C) SCHEMATIC MODEL SHOWING THE ARRANGEMENT OF RSF MOLECULES (BLACK), C ₁₂ TAB (BLUE) AT 0.2 mM AND 20 mM SDS. REPRINTED WITH PERMISSION FROM JAYAWARDANE ET AL. ¹⁷⁵ COPYRIGHT 2017 AMERICAN CHEMICAL SOCIETY.....	119
FIGURE 5.1 EQUILIBRIUM SURFACE TENSION RESULTS FOR RSF PEPTIDES WITH AN SDS SURFACE TENSION CURVE FOR COMPARISON.	128
FIGURE 5.2 FITTED CURVES OF NR DATA FOR ADSORPTION OF 0.1 MG/ML RSF IN NRW: IN ORDER FROM TOP TO BOTTOM, 5-30 kDA (GREY), RSF 30-300 kDA (BLUE), RSF >300 kDA (PURPLE).	129
FIGURE 5.3 FROM TOP TO BOTTOM: 10 MG/ML, 3 MG/ML, 1 MG/ML, 0.3 MG/ML, RSF 5-30 kDA AT THE AIR/D ₂ O INTERFACE.....	131
FIGURE 5.4 FROM TOP TO BOTTOM: 0.1 MG/ML, 0.01 MG/ML, 0.005 MG/ML, 0.003 MG/ML, RSF 5-30 kDA AT THE AIR/D ₂ O INTERFACE.....	131
FIGURE 5.5 FROM TOP TO BOTTOM: 10 MG/ML, 3 MG/ML, 1 MG/ML, 0.3 MG/ML, RSF 5-30 kDA AT THE AIR/NRW INTERFACE	132

FIGURE 5.6 FROM TOP TO BOTTOM: 0.1 MG/ML, 0.01 MG/ML, 0.005 MG/ML, 0.003 MG/ML, RSF 5-30 kDA AT THE AIR/NRW INTERFACE	132
FIGURE 5.7 THE TOTAL ADSORBED LAYER THICKNESS AND ADSORBED AMOUNT AS A FUNCTION OF BULK RSF CONCENTRATION AS MEASURED FROM NRW (OPEN SYMBOLS) AND D ₂ O (CLOSED SYMBOLS) RUNS. SQUARES FOR THE SURFACE EXCESS AND TRIANGLES FOR THE LAYER THICKNESS.	135
FIGURE 5.8 SCHEMATIC OF THE SUGGESTED RSF ADSORBED LAYER STRUCTURE AS BULK CONCENTRATION IS INCREASED. RSF IS SHOWN ADSORBED IN A SILK III CONFORMATION PARALLEL TO THE INTERFACE AND AS BULK CONCENTRATION INCREASES THE RSF PEPTIDE IS FOUND TO ORIENT PERPENDICULAR TO THE INTERFACE.	137
FIGURE 5.9 NEUTRON DATA FITTING OF 0.1 MG/ML RSF 5-30 kDA ADSORPTION FROM 10 mM, 30 mM, 300 mM AND 1M NaCl SOLUTIONS (FROM TOP TO BOTTOM).	138
FIGURE 5.10 NEUTRON DATA FITTING FOR ADSORPTION OF 0.01 MG/ML RSF 5-30 kDA AT pH'S (FROM TOP TO BOTTOM) 2, 3, 5, 9 AND 11	139
FIGURE 5.11 SURFACE TENSION CURVES FOR SDS WITH THE ADDITION OF 0.01, 0.1 AND 0.3 MG/ML RSF 5-30 kDA.....	141
FIGURE 5.12 SURFACE TENSION CURVES FOR SDS WITH THE ADDITION OF 0.01, 0.1 AND 0.3 MG/ML RSF 30-300 kDA.....	142
FIGURE 5.13 SURFACE TENSION CURVES FOR SDS WITH THE ADDITION OF 0.01, 0.1 AND 0.3 MG/ML RSF OVER 300 kDA	143
FIGURE 5.14 COMPARISON BETWEEN THE ADDITIONS OF 0.01 MG/ML RSF 5-30 kDA, 30-300 kDA AND OVER 300 kDA FRACTION TO SDS.	144
FIGURE 5.15 COMPARISON BETWEEN THE ADDITIONS OF 0.1 MG/ML RSF 5-30 kDA, 30-300 kDA AND OVER 300 kDA FRACTION TO SDS.	145
FIGURE 5.16 COMPARISON BETWEEN THE ADDITION OF 0.3 MG/ML RSF 5-30 kDA, 30-300 kDA AND OVER 300 kDA FRACTION TO SDS.	146
FIGURE 5.17 FOAMING CAPACITY OF PURE SOLUTIONS OF RSF 5-30 kDA, 30-300 kDA AND OVER 300 kDA.	147
FIGURE 5.18 FOAM ABILITY OF SDS WITH THE ADDITION OF RSF. (A) ADDITION OF 0.01 MG/ML RSF, (B) ADDITION OF 0.3 MG/ML RSF.	148
FIGURE 5.19 ADDITION OF 0.01 AND 0.3 MG/ML RSF 30-300 kDA TO SDS SOLUTIONS OF VARYING CONCENTRATION.	149
FIGURE 5.20 FOAM STABILITY OF SDS AND RSF SOLUTIONS OVER A PERIOD OF 24 H. .	150
FIGURE 5.21 STABILITY OF SDS SOLUTIONS FOLLOWING THE ADDITION OF (A) 0.01 MG/ML RSF, (B) 0.3 MG/ML RSF, OVER A PERIOD OF 24 HOURS.	151
FIGURE 5.22 FOAM STABILITY OF SDS AND MIXTURES WITH RSF ACROSS THE CONCENTRATION RANGE TESTED.	152
FIGURE 5.23 SURFACE TENSION CURVES FOR C ₁₂ TAB WITH THE ADDITION OF RSF 5-30 kDA.	153
FIGURE 5.24 SURFACE TENSION CURVE FOR C ₁₂ TAB WITH THE ADDITION OF RSF 30-300 kDA.	154

FIGURE 5.25 SURFACE TENSION CURVE FOR C ₁₂ TAB WITH THE ADDITION OF RSF OVER 300 kDa.	155
FIGURE 5.26 COMPARISON BETWEEN THE SURFACE TENSION CURVES OF THE THREE RSF MW'S FOLLOWING THE ADDITION OF 0.01 MG/ML TO C ₁₂ TAB SOLUTIONS.	156
FIGURE 5.27 COMPARISON BETWEEN THE SURFACE TENSION CURVES OF RSF MW FRACTIONS AT 0.1 MG/ML ADDED TO C ₁₂ TAB SOLUTIONS.	157
FIGURE 5.28 COMPARISON BETWEEN THE SURFACE TENSION CURVES OF RSF MW FRACTIONS AT 0.3 MG/ML ADDED TO C ₁₂ TAB SOLUTIONS.	158
FIGURE 5.29 FOAMING ABILITY OF C ₁₂ TAB SOLUTIONS WITH THE ADDITION OF (A) 0.01 MG/ML RSF, (B) 0.3 MG/ML RSF.	159
FIGURE 5.30 ADDITION OF 0.01 AND 0.3 MG/ML RSF 30-300 kDa TO SOLUTIONS OF C ₁₂ TAB.	160
FIGURE 5.31 (A) STABILITY OF C ₁₂ TAB, (B) STABILITY FOLLOWING ADDITION OF 0.3 MG/ML RSF 30-300 kDa. ERROR BARS OMITTED FOR CLARITY.	161
FIGURE 5.32 FOAM STABILITY AS A PERCENTAGE OF INITIAL FOAM OF C ₁₂ TAB AND MIXTURES WITH RSF AFTER 4 HOURS.	162

1 INTRODUCTION

This thesis investigates the surface active behaviour of peptides and their adsorption at both the solid-liquid and air-liquid interface. In particular, the adsorption of silk fibroin peptides and their interaction with conventional surfactants. The following literature review gives an introductory account on the current understanding and work carried out in the field of interfacial surfactant adsorption and frames the importance and relevance of the work carried out.

1.1 Surfactants

The term surfactant arises from the shortening of surface-active-agent and refers to a molecule (agent) which has the ability to considerably lower the thermodynamic free energy of a surface (surface active). Surfactants achieve this by adsorbing at the surface in large amounts. In this context, surface refers to any interface between two immiscible phases, such as solid-liquid or air-liquid. Surfactants are able to adsorb at the surface because they are amphiphilic molecules, i.e. their molecular structure incorporates both a polar and a non-polar moiety. For example, at an aqueous interface, these moieties would

be hydrophobic (water-hating) and hydrophilic (water-loving). This general amphiphilic structure is what drives surfactants to the interface and will be discussed further in section 1.1.1. In simple terms, the higher the adsorbed amount at an interface, better the surfactant. Furthermore, given the right conditions and interactions, surfactants are known to aggregate and self-assemble into supramolecular structures such as micelles and bilayers (discussed further in section 1.2). This is a very attractive feature of surfactants which can be used in a wide range of applications from personal care products to biotechnology (examples in section 1.1.2).

It should be noted that the self-assembly of molecules is ubiquitous to biological systems found in nature and play an essential role in their function. Perhaps the most common example is the cell membrane, which is a bilayer composed primarily of amphiphilic surfactant-like molecules known as phospholipids. This highlights a significant distinction in the use of the term surfactant. The term surfactant is conventionally used in reference to compounds that to some degree are manmade or processed by man. However, as will be discussed in this thesis, this does not preclude biological molecules found in nature from having surface active properties and structures similar to conventional surfactants.

1.1.1 Common structures and subdivisions

The hydrophobic/hydrophilic partitioning of surfactant molecules is essential for their function as surface active agents, and it's thus a common feature to all surfactants. One of the simplest and most common surfactant structures are the linear surfactants. They consist of a linear chain of hydrophobic segments covalently joined to hydrophilic segments. In the literature, these two segments are more commonly described as the

hydrophobic tail and the polar hydrophilic head (as depicted in Figure 1.1). In addition to the basic linear structure, there is a variety of structures which include branched or cyclic tails and even surfactants which have multiple heads or tails. However, the most common way to categorise surfactants is not by their structure but by identifying them by their head group. This is mainly because the polar head group will strongly influence the way the surfactant interacts with other molecules and surfaces and therefore surfactants with the same head group will broadly follow similar interactions. Hence the main subdivisions of surfactant structures divide surfactants into four categories: anionic (negatively charged), cationic (positively charged), zwitterionic (mixed charge) and non-ionic surfactants, shown in Figure 1.1.

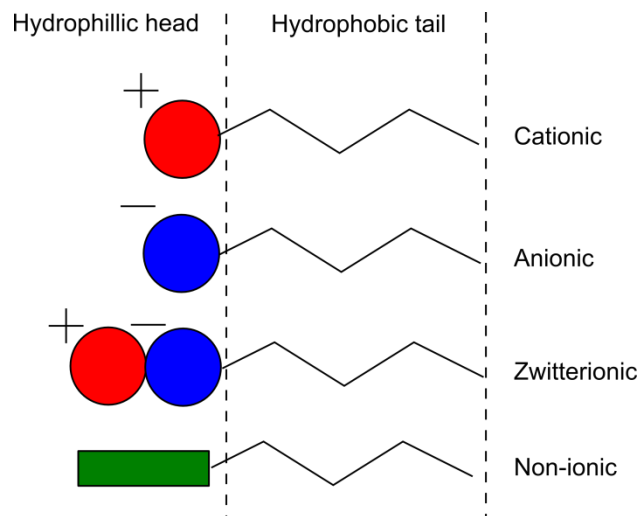


Figure 1.1 Diagram depicting the basic structure of linear surfactants and their four main categories.

Typical anionic surfactants head group species include carboxylates, sulphates, sulphonates, and phosphates. Carboxylates are found in soap and are the most common anionic surfactants.¹ However, one of the major draw backs of carboxylate surfactants is their susceptibility to hard water which causes them to precipitate out (forming scum).

Cationic surfactants are mainly characterised by quaternary ammonium compounds and amines, with the latter having a pH dependant charge rather than a fixed positive charge. As such amines are susceptible to high pH as they need to be protonated. On the other hand surfactant ester quats (quaternary ammonium compounds with two hydrophobic alkali chains bonded via weak ester linkages) are used as fabric softener and are extremely susceptible to hydrolysis at pH's above 5-6.²

Zwitterionic surfactants possess both charged species in their head group, and can hence be net negative or positively charged, and may have a pH dependant charge depending on its composing species. They are the smallest class of surfactants and are generally more expensive to produce. They are very compatible with a variety of conditions and work well in the presence of other surfactants and have low eye/skin irritation and therefore are a preferred choice in personal care products. Common zwitterionic molecules include betaines and lecithins (industry term for extracts mainly comprising of phospholipids).

Non-ionic surfactants, on the other hand, have no charge, they are mainly composed of oxygen, hydrogen and carbon atoms. They are the second largest class of surfactants by volume.¹ Non-ionic surfactants include fatty alcohols, alkyl ethoxylates and other long chain molecules giving non-ionics a wide range of complex structures. Fatty alcohol ethoxylates are the most important non-ionic surfactant type, used in liquid and powder detergents. Non ionics are also commonly used to stabilise oil-in-water emulsions and in the case of polysorbates are excellent for use in food products as they degrade to sugar and fatty acid.³

In addition to the chemistry of the head group, the tail also impacts on a surfactants behaviour. Generally conventional surfactants have alkyl chains made from 8-18 carbon atoms and the choice of carbon tail length will affect the surfactants behaviour.¹ Factors

such as toxicity and irritation are known to sometimes peak at a specific chain length, since as chain length increases the critical micelle concentration falls (Refer to chapter 1.2) resulting in a lower concentration of free monomers. Also mentioned earlier there are surfactants which have more complex structures, branched cyclic or simply having multiple tails and heads. For example Gemini surfactants are a group of dimeric surfactants, essentially two surfactants joined together via a spacer and are very efficient at lowering the surface tension.^{4,5} However discussion of all these surfactants structures is beyond the scope of this thesis which focuses only on linear surfactant structures.

1.1.2 Surfactant applications

World surfactant production is over 20 million metric tons per year.¹ Anionic surfactants are the most used surfactant type by volume, representing around 70% of the total surfactant consumption. Surfactant use ranges from household products, industrial applications to food and biotech applications. The following section will give a brief account of some of the ways the physiochemical properties of surfactants have been exploited for applications in so many fields. For more information, surfactant use has been reviewed for applications in food industry⁶, drug delivery⁷, biopharmaceutics⁸ and biotechnology⁹.

In the food industry, surfactants have been used to help stabilise different phases in food products and make emulsions, these include products from mayonnaise to salad creams and ice creams. These mainly include non-ionics as well as lecithins as they tend to be more biocompatible.⁶ Surfactants ability to modify wettability of solids and both stabilise and destabilise dispersions has been widely exploited by several industries. In the agrochemical industry surfactants are used in the dispersion of herbicides as well as

reduce the surface tension and hence improve the spreading and wetting of leaf surfaces for improved herbicidal uptake by weeds.¹⁰ Improved uptake is also achieved since surfactants amphiphilic nature allows them to penetrate in the otherwise water impermeable waxy layer of leaves helping deliver herbicide or alternatively deliver nutrients past the outer waxy barrier. Surfactant formulations have been used to enhance dispersion of single walled carbon nanotubes by improving colloid stability and enhance their antibacterial activity.¹¹ On the other hand their destabilising ability can be exploited in flocculation and floatation. For example, industrial floatation of minerals or particulates can be accomplished by addition of suitably charged surfactants and adjustment of ions, pH and other solution properties. Surfactants ability to modify the surface properties upon adsorption has, for example, been used to improve filtration of ultrafine particles by changing surface properties such as with micro porous polypropylene membrane filters, which are treated with cationic surfactants which help to filter out negatively charged nanoparticles increasing filter efficiency from 10% to 95%.¹² Similarly, they are being used in the metal working industry to coat and impart anticorrosive properties.¹³ As well as being used as surface coating on surgical or medical implants, increasing surface biocompatibility and reducing nonspecific protein binding and cell or bacteria adhesion. Alternatively, they can also be used to remove molecules from a surface through their detergent action.¹⁴ Surfactants in the biotech industry have been used in a range of applications from drug and gene delivery vectors to helping maintain biopharmaceuticals products.⁷ For example, cationic surfactants can be used to bind with negatively charged DNA molecules for delivery through the cell membrane. Though cationic surfactants generally have high toxicity which limits their efficiency as transfection agents such as with Oligofectamine®, a cationic surfactant lipid used as a standard transfection reagent but suffers from toxicity problems. Biomolecules such as IgG antibodies, insulin and other hormones used as biopharmaceutics suffer from stability issues such as aggregation,

denaturation and precipitation which affect their activity and place constraints on their storage and use.⁸ Non-ionic surfactants such polysorbates (Tween®) and poloxmer (Pluronic® F68) used in formulations adsorb at the air/water and solid/water interfaces and form a barrier which stops biomolecules from adsorbing and denaturing as well as helping stabilise the molecules in the bulk solution.⁸

The above brief account on surfactants abundantly showcases the wide variety of ways in which surfactant molecules have and can be employed. Common to all is the surfactants ability to exploit its interfacial adsorption and or interactions with other molecules through either electrostatic or hydrophobic interactions Each application requires a specific surfactant and therefore understanding surfactant adsorption and interaction is of fundamental importance for the development of new technologies and applications based on these classes of molecules.

1.1.3 Issues with conventional surfactants and search and development of alternatives

As discussed earlier surfactants have found application in numerous fields and are intensively used in many industries resulting in an estimated production of over 20 million metric tons per year. Unfortunately, many conventional surfactants have come under fire due to concerns on their environmental impact from production to disposal. This is especially the case with surfactants which rely on the petrochemical industry to provide the raw material for their production. Pollution occurs both indirectly from the petrochemical industry as well as directly from surfactant synthesis and release into the environment which can cause adverse toxicity to wildlife and other organisms.¹⁵

Green chemistry is a relatively new field within chemistry. It attempts to find ways of reducing the impact chemical processes can have on the environment and on human health. The basis and founding motives of green chemistry date back to the 1960's, following the increased coverage and awareness by the media and the scientific community of the potentially catastrophic effects of pesticides such as Dichlorodiphenyltrichloroethane (DDT) on humans, environment and wild life. This led to growing concerns and fears regarding the exposure to toxic chemicals which resulted in increased regulatory pressures from environmental agencies around the world. The main focus was on the prevention of pollution from industrial processes by reducing or eliminating hazardous substances from reagents, solvents, products and by-products of chemical processes. Anastas and Warner were the first to define green chemistry in their book, *Green Chemistry: Theory and Practice*, setting examples on how to approach the reduction or elimination of hazardous chemicals at each step from design, and manufacture to the application of chemicals.¹⁶ Since then the principles of green chemistry have permeated across fields, and scientists and engineers alike are expected to optimise reaction conditions by improving energy efficiency, designing and using environmentally friendly chemicals and shifting towards renewable and sustainable resources.

As a result, the European Union has developed REACH legislation, registration evaluation authorization and restriction of chemicals, placing Europe at the forefront of environmental and human safety. Their motto is "No data, no market".¹⁷ REACH regulation in the EU has been active since December 2006. It covers the production and use of chemicals and covers surfactant use as well. One of the major policy changes is that companies must prove safety and publish test results making them publicly available for scrutiny.

Generally, surfactant manufacturers are driven by the profit motive and hence focus on finding ways to increase demand and minimise the manufacturing cost. The shift in the market requirements to green surfactants is now forcing the industry to also take environmental impact into account and is thus a major driving force for new surfactant development.¹ Currently the large majority of surfactants are mostly manufactured by organic synthesis involving harsh chemicals and conditions.¹⁸ Surfactant raw materials are generally based on either oleochemicals or petrochemicals. Oleochemical derived surfactants are based on renewable sustainable raw materials, such as palm oils and other vegetable oils.¹⁹ Whilst surfactants based on petrochemicals are produced from the products resulting from the cracking of naphtha, such as ethylene. Surfactants such as alcohol ethoxylates, alkyl sulphates, alky phosphates have the advantage of being able to be manufactured using either oleochemicals or petrochemicals as their primary source of raw material.¹ In such cases the origin, whether petrochemical or oleochemical, has no bearing on the resulting surfactant product (i.e. no change to harshness or toxicity to the environment by the surfactant). However, in terms of the carbon footprint and greenhouse gas emissions, oleochemical based surfactants are significantly greener and more environmentally friendly in their production. A study found that substitution of oleochemical surfactants for petrochemical surfactants would enable a reduction of 34% of the total fossil CO₂ emissions by the surfactant industry in Germany.²⁰ Due to the regulatory pressures and global market shift away from the petrochemical industry, surfactant manufacturers have already started large scale cultivation of oleochemical sources (such as palm trees) in developing countries in south East Asia and South America. However, it should be noted that this practice is also coming under scrutiny due to massive rainforest clearance and dangers of increased soil erosion and loss of biodiversity.

Furthermore, in addition to the source of the surfactant, their structure and design is also important. Regulations require the safe biodegradation of surfactant in sewage treatment plants before entering water ways thereby thwarting any potential bioaccumulation in the environment and aquatic life.¹⁷ This has recently favoured the use and design of cleavable surfactants. These are surfactants which are designed to have weak bonds which can be chemically or biologically broken making them degradable into non-toxic products. For example ester quats are designed with weak acid cleavable ester bonds which can be easily hydrolysed and have now replaced dialkyl quats due to environmental concerns from severe aquatic toxicity and persistence in the environment.² Similarly, SDS is unstable and rapidly degrades in acidic conditions and begins an autocatalytic degradation as its hydrolysis releases sulfuric acid.²¹ Another example is the move from branched alkylbenzene sulfonates to linear benzene sulfonates.¹ Both these changes resulted in surfactants which can be more easily degraded in the environment resulting in lower toxicity, even though their performance may be limited.

So surfactant design has evolved in order to comply with regulations but the search for alternatives is also fuelled by prospects from new technologies which hope to take advantage of surfactant-like behaviour. For example this has resulted in the development of cleavable surfactants for cleaning of water resistant garments which during the washing process degrade and their hydrophobic moiety adsorbs onto the garment imparting a water repellent finish.²² Cationic surfactants are known to be much more toxic, use of cleavable cationic surfactants can improve its ability for use as personal care products as their irritant/toxic nature would rapidly degrade following application.²³

Surfactant production and design is now shifting to valorise the use of natural building blocks, biodegradability and efficiency (used in lower amounts). One route to improve surfactants use is the formulation of surfactant with milder surfactants. Studies have shown that this can synergistically lower the relative skin irritation and toxicity making

their use more efficient in their respective applications.²⁴ Alternatively, the use of natural sources of surfactant-like molecules is gaining significant research attention. These include surfactants from microorganisms, also known as biosurfactants, and include Rhamnolipids, Hydrophobins and Trehaloses to name a few.²⁵⁻²⁷ Their commercial use is currently limited and constrained by higher costs but has found some use in premium cosmetics and personal care applications. Surfactants are also being developed from peptide molecules which can be carefully designed for specific application (discussed in section 1.3.) but currently these too suffer from high costs. There is therefore a need and a search for novel surface active agents which are green and could be used in conjunction with other surfactants to reduce their impact.

1.2 Surfactant aggregation and adsorption studies

Surfactants are known to aggregate into supramolecular structures above a certain concentration known as the surfactant's critical micelle concentration (CMC). Effectively, the CMC is also a measure of the maximum amount of free surfactant molecules in the solution as beyond the CMC any additional surfactant molecules added to the solution will aggregate.

The aggregation is a result of the unfavourable interactions between the hydrophobic segments of surfactants and the polar water molecules. Hydrophobic segments cause water molecules to structure themselves in the form of a cage which reduces the entropy of the system. Thus aggregation into micelles becomes thermodynamically favourable as it reduces these unfavourable interactions by 'hiding' the hydrophobic moieties and thus helping increase the entropy of the system by releasing the caging water molecules.

Micelles are thus polar aggregates (since only the polar head groups come in contact with the bulk solution) of varying shapes and sizes, some of the most common shapes include spherical, rod, elliptical and lamellar aggregates. It should be noted that micelles have a different behaviour compared to the free surfactant molecules, as they have no surface activity and are highly soluble in bulk solution. The exact shape and onset of aggregation is a result of complex interactions combining solution properties (ionic concentration, pH, temperature etc.) and most importantly the exact molecular structure of the surfactant. Aggregation and its control and design in bulk solution has been extensively studied and has resulted in the modelling of self-assembly of structures based on a surfactant's packing parameter (which takes into account the shape and volume of a surfactant's head and tail) to predict its possible aggregation.²⁸ The importance of micelles extends to its possible applications such as solubility of hydrophobic molecules. Solubility increases when the CMC is reached and thus surfactants can be used to help solubilise hydrophobic molecules within their micelle's hydrophobic environment. Thus ways of lowering the CMC can be of high value for encapsulation of hydrophobic molecules such as dyes and drugs without excessive use of surfactants.

The most common method of determining the CMC is by measuring the surface tension of a surfactant solution over a wide concentration range. As can be seen in Figure 1.2, as the surfactant concentration increases the surface tension falls until it reaches a drastic change in the slope of the curve at the CMC. Other techniques such as conductivity, osmotic pressure and turbidity can also be used to find the CMC in a similar manner.

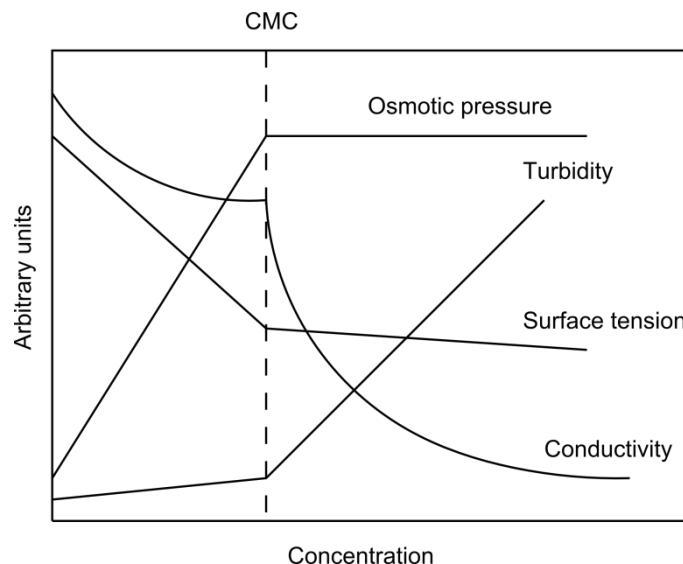


Figure 1.2 Determination of CMC by different experimental techniques.²⁹

On the other hand, adsorption studies are widely and commonly used to help characterize surfactant behaviour and its interactions at an interface. Adsorption at the interface has traditionally been undertaken to determine the surfactants interfacial coverage (adsorbed amount), evolution over time and molecule orientation. The coverage gives a good indication of the surfactant performance in many processes ranging from foaming, detergency and emulsification. The surface adsorbed amount is also known as the surface excess, Γ , and is measured in mg/m^2 or mole/m^2 . The surfactant orientation is particularly important as it determines how the surfactant will change the surface properties by determining which chemical moieties will be exposed and the mechanisms of interaction such as by making the surface more or less hydrophilic/hydrophobic or charged.³⁰ Consequently adsorption studies have also been undertaken to study such interactions in the presence of other molecules. For example, in paint systems, mixtures of surfactants are used, each serving a different purpose, such as emulsifying, stabilising pigment molecules and helping their dispersion etc. In such systems, competitive adsorption can be an issue as surfactants can interfere with each other and cause the paint to become unstable. On the other hand, mixed surfactants are also used in applications in order to

exploit any synergistic activity which may lead to greater adsorption efficiency and effectiveness. Therefore, careful investigation of the adsorption behaviour of surfactants is highly valuable for the advancement of many surfactant applications.

1.2.1 Key electrostatic and hydrophobic effects

There are two forces which play a key role and are fundamental in understanding the self-assembly and adsorption of molecules from solutions, they are the electrostatic interactions and the hydrophobic effect. The hydrophobic effect has been mentioned before, with regards to the ordering of water molecules around hydrophobic moieties, thereby both self-assembly and adsorption at an interface is thermodynamically favourable as it results in increased entropy. Electrostatic interactions are a result of charged species found on the surfactants molecules as well as some interfaces such as silica. In many cases electrostatic interactions are the driving force for interaction between molecules as well as other surfaces and are thus very important. Counterions found in the solution play an essential role in mediating electrostatic interactions. This is because charged surfaces result in counterions binding to the surface. This binding results in a lower entropy and self-assembly and adsorption at interfaces causes the release of these counterions and thereby an increase in entropy.

In order to understand the importance and prevalence of these forces its common practise to probe the interaction through changes in pH, ionic strength as well as adding other molecules or using different surfaces. For example, the addition of a non-ionic surfactant or an oppositely charged surfactant to an ionic surfactant solution will generally result in a lowering of the CMC. This is a result of a reduction in the charge density of the micelle surfaces being formed due to incorporation of the non-ionic or oppositely charged

surfactant. This also results in lower counterion binding to the newly formed surface. Much in the same way, adsorption at an oppositely charged interface can result in improved self-assembly.

This phenomenon can be further probed by the addition of salt into the bulk solution. Increasing salt concentration can result in shielding of electrostatic based interactions and hence ionic surfactants will behave similar to non-ionic surfactants and have a lower CMC. However, when an oppositely charged surfactant is added to such a solution, the CMC will now not decrease as much as favourable attraction is now hampered, this is also valid for adsorption to oppositely charged surfaces. Similarly, to the above, changes in the pH result in changes to the strength and charge of pH dependant chemical species and hence will reveal interaction in the same way as mentioned for the addition of salt.

An additional force which is very common in self-assembly and is worth mentioning is the formation of hydrogen bonds. Hydrogen bonds are not very strong, they form and break continuously but are able to impart stability to aggregates and help in the adsorption and aggregation process.

1.2.2 Adsorption at the air-liquid interface

Adsorption at the air water interface lowers the entropy of the system by removing the hydrophobic moieties from the bulk and as such operates in the same way as was discussed for micelle formation in the bulk solution. However, the adsorbed surfactant molecules at the interface will also lower the free energy per unit area (surface tension) at the surface. For more information regarding surface tension and its measurements please refer to section 2.3. Surfactant adsorption generally increases at the interface up to the CMC, at which point the maximum adsorbed amount is reached as the concentration

of free surfactants in solution no longer increases. This results in the typical surface tension curve for pure surfactants shown in Figure 1.3.

The relationship between the adsorbed amount and the surface tension can be quantified by applying the Surface Tension-Gibbs equation. In its simplest form, the Gibbs equation can be applied to calculate the surface excess of dilute solutions of non-ionic-surfactants in the following form:

$$\Gamma = -\frac{1}{RT} \frac{d\gamma}{d\ln C}$$

(1-1)

Where R is the gas constant (8.314 J mol⁻¹K⁻¹), T is the temperature, C is the molar concentration of the surfactant, and γ is the surface tension. Therefore, the slope of a surface tension curve is directly related to the surface excess, Γ .

Adsorption of surfactant solutions has been thoroughly studied over the years using surface tension. Systematic studies which evaluated the effects of head or tail size, head group charged species, ionic concentration, pH etc. have been carried out.^{31, 32} More recently however the focus has moved on to investigating the effects of mixed surfactant solutions. Especially surfactant interactions with polymers, polyelectrolytes and proteins. Such studies have significant value for many industrial processes and applications. In most such systems the adsorption at the interface can take the routes of synergistic (cooperative) adsorption, which results in both component's adsorbed amount increasing at the interface or competitive adsorption, where they adsorb independently and compete for adsorption at the interface. Surface tension measurements in such cases have the added advantage that interactions in the bulk can be inferred as well as the adsorption at the interface.

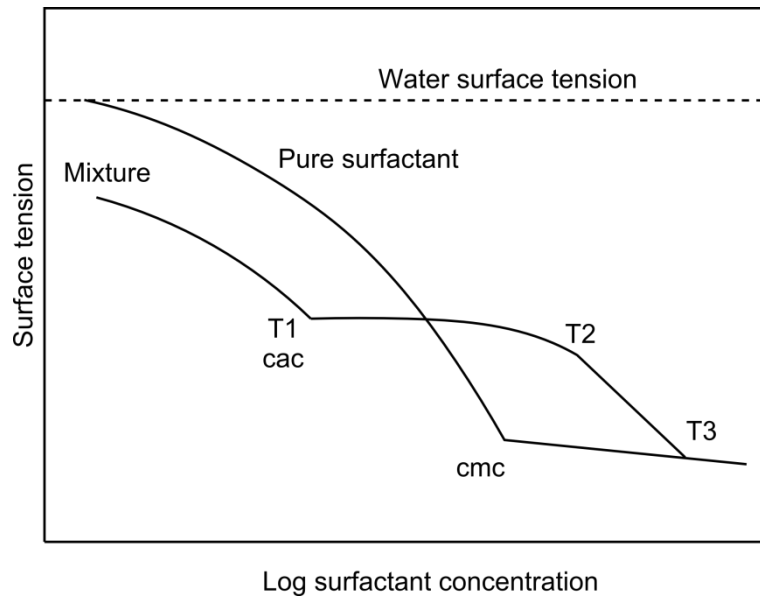


Figure 1.3 Model surface tension curve for the typical interactions between a polymer and a surfactant.³³

A typical surface tension curve for a polymer-surfactant system is shown in Figure 1.3. It shows the presence of a critical aggregation concentration (cac), at T1, which is found below the CMC, where polymer molecules and surfactant molecules cooperatively bind in solution. Increasing the surfactant concentration beyond the cac results in close to no decrease in surface tension. This is because surfactant binds to the polymer and forms aggregates in the solution. As surfactant concentration is increased further the surfactant-polymer binding in solution reaches a saturation level (T2) and no more surfactant binds to the polymer and instead is free to adsorb at the interface and further reduce the surface tension. Eventually a new CMC is reached (T3) for the pure surfactant molecules in the bulk solution and this results in a constant surface tension and no more adsorption at the interface.

It should be noted that whilst the shape and trends in surface tension curves can reveal important interactions in the system, quantitative information through the use of the Gibbs

equation becomes increasingly difficult and prone to inaccuracies. Recently, a number of papers have been published by Menger et al.³⁴⁻³⁶ raising the issue of the accuracy in determining surface excess from surface tension data from the Gibbs equation on a range of surfactant systems. Most of these inaccuracies stem from the fact that surface tension measurements are not always accurate enough, due to high sensitivity to wetting, viscoelastic properties, impurities and other disturbances. This is excellently explained in a number of papers dealing with cationic, anionic and non-ionic surfactant systems with the help of neutron reflection to directly measure the surface excess.³⁷⁻³⁹ Indeed the use of neutron reflection for quantification of adsorbed layers should be preferred when possible. In recent years the body of work which has used neutron reflection for the study of adsorption at the air-water interface has significantly increased. Especially with complex mixtures involving proteins or polymers, neutron reflection has been used to reveal not only surface excess but also, thickness, orientation and structures at the interface. For more information regarding the theory and use of neutron reflection please refer to section 2.1.

1.2.3 Adsorption at solid-liquid interface

The study of adsorption at the solid-liquid interface is relevant to a number of applications and industries such as recycling of paper and plastic, herbicide dispersion, detergency and mineral/particulate floatation to name a few. Paria et al.³⁰ has reviewed these applications alongside a thorough discussion of important adsorption mechanisms and kinetics of surfactants and their mixtures. Adsorption of surfactants at the solid-liquid interface has also been extensively studied and reviewed by others.^{30, 40-44}

Generally, for these adsorption studies mineral oxides and silica surfaces are used as model substrates (example of other common surfaces include quartz, mica, graphite).⁴⁵ Studies range from the characterisation of adsorbed structures, such as assembly of a C₁₂E₆ defective bilayer at the solid silica-water interface,⁴⁶ to the study of C₁₆TAB adsorption on cellulose surfaces and its evolution over time.⁴⁷ In the studies the surface can be carefully selected and tailored to help best mimic a surface and conditions of interest. Hence, surfaces can be used to model fabric surfaces, implant surfaces, biosensors, filter membranes etc.^{42, 47, 48}

Many studies however use silica due to its extensive surface characterization and its locally flat surface which can also be easily modified and is thus ideally suited for study by surface characterization techniques such as neutron reflectivity, as explained in more detail by Fragneto-Cusani et al.⁴⁹. Common surface modification methods include chemical modifications, such as silanization of surface hydroxyl groups with octyltrimethoxysilane resulting in a hydrophobic surface,⁵⁰ or physical modification through coating (spin coating, Langmuir-Blodgett etc.) with appropriate compounds such as cellulose or other proteins or lipids as required.^{47, 49, 51} Silica is thus an excellent surface to make initial characterisation of a surfactant system and can be subsequently tailored or substituted as necessary to model more specific conditions.

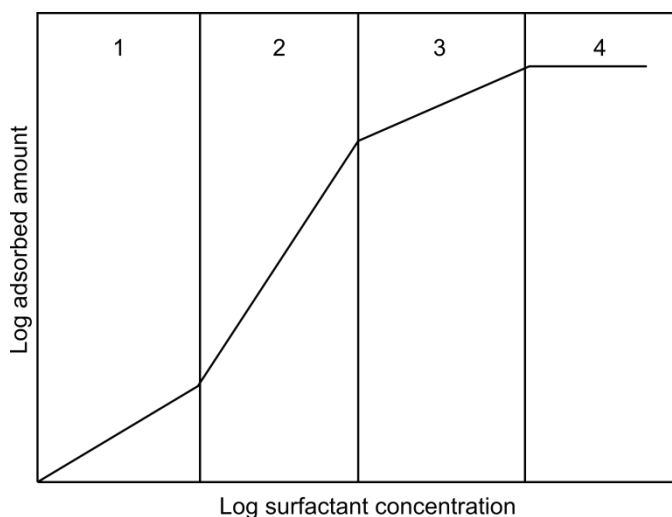


Figure 1.4 Adsorption at the solid-liquid interface adapted from Paria et al.³⁰

The general adsorption process for most surfactant systems on oppositely charged surfaces has been shown to follow the adsorption curve in Figure 1.4 and can be broken down into distinct adsorption steps. Initially, as shown in region one adsorption obeys Henry's law, i.e. the adsorbed amount is linearly proportionate to the concentration. In this region adsorption is thought to be driven by any electrostatic interactions between the surface and surfactant monomers. Region two has a much steeper gradient as a result of favourable lateral interactions between the adsorbed monomers resulting in surface aggregates. Region three has a less steep gradient as the full surface coverage approaches followed by the plateau region. Adsorption beyond CMC levels is usually negligible, as the monomer concentration will be constant in the bulk solution.⁵²

Factors affecting adsorption include the hydrocarbon chain length, functional group, salt, pH, etc.^{52, 53} For example addition of salt to an ionic surfactant at a hydrophobic surface would shield charges and reduce the entropy loss from counterion binding which results in higher adsorption with increasing salt concentration. Similarly, changes in pH can also be used to modulate the adsorbed amount at the interface.

Furthermore, surfactants which contain hydroxyl, carboxylic or amine groups can stabilise its structures at the interface via hydrogen bonding.⁴⁰ The formation of structures at the interface has attracted much research. Since adsorption of surfactants at solid-liquid interfaces can yield complex structures, from monolayers, cylinders, fibrils, spheres and bilayers which could then be used to pattern surfaces.⁵⁴

More recently, the study of mixed surfactant systems, as well as surfactant polymer (or other compounds) is attracting significant attention due to its relevance to many industrial applications where surfactants are formulated and interact with other molecules. Such adsorption studies are usually carried out by either addition of surfactant to a pre-adsorbed layer or adsorbing from a mixed solution.^{30, 40, 55} An important question is whether a system will exhibit cooperative adsorption at the interface or competitive adsorption as it is of great importance to many applications such as coating of surfaces and immobilisation of molecules at a surface. Especially in mixed systems, neutron reflection has become an important tool which is capable of differentiating and quantifying adsorption of each component. Neutron reflection has now established itself as an ideal tool for the study of such buried interfaces and the work and use has been amply reviewed.^{49, 56, 57}

1.3 Peptides

Peptides are biological compounds which are made from short chains of amino acids (discussed in detail in section 1.3.1). Briefly, there are 20 naturally occurring amino acids which act as the building blocks from which peptides can be created. These amino acids are analogous to monomers in a polymer. The term peptide is specifically used when describing amino acid chains containing less than 50 amino acid residues, whilst the term

protein is used for anything longer. In nature peptides are very common and have a range of activates. For example, they form part of the human innate host defence system, where their role is help attack foreign pathogens. They are also found in lung secretions and have an important role in stopping the lung surface from collapsing on itself through its surfactant action.⁵⁸ They are also secreted by microorganism as well as fungi and creatures such as frogs or even bees, their role in nature spans from wetting, stabilisation of biomolecules, foaming and surface tension lowering properties to venom and antibacterial effects.^{23, 59-61}

1.3.1 Amino acid structure and characteristics

The basic structure of an amino acid consists of a carbon atom attached to a variable side chain known as the R group, an amino group ($-\text{NH}_2$) and at the other end a carboxyl group ($-\text{COOH}$). The presence of the amino and carboxyl group gives amino acids an amphiphilic character. In addition, each amino acids unique R group further contributes to its physiochemical and biological properties. Based on these R groups, amino acids can be divided into several categories such as polar, hydrophobic, charged as shown in Figure 1.5. Amino acids can be joined to each other through the formation of a peptide bond (amino bond), between the carboxyl group and the amino group of two amino acids, with the release of a water molecule. Such a chain of amino acid residues is known as a peptide.

interactions from the R groups can then affect the structure adopted by the peptide. For example, in an aqueous solution, the hydrophobic amino acids found in a peptide will favour a structural conformation in which they are shielded, minimising unfavourable interactions with the bulk aqueous solution. Whilst polar amino acids would face the bulk solution, maximising favourable interactions. Charged amino acids, will play an important role in determining the kind and strength of interactions with other molecules and surfaces. Amino acids can therefore interact with other amino acids and molecules or surfaces through hydrogen bonding, electrostatic interactions, hydrophobic interactions etc. and some of these interactions will be more or less affected by solution conditions. This is especially true with the electrostatic interactions since they arise from the charged species which are pH dependant and will also be affected by ionic strength of the solution. This richness of interactions only grows with increasing number of amino acids and results in a delicate and complex interplay of forces which builds all the way up to how proteins fold and their eventual structure and function. Hence the overall structure and conformation of peptides is a direct result of both its primary structure and the solution conditions which together result in what is known as a secondary structure. Some common secondary structures include alpha helices and beta sheets which arise from hydrogen bonding within specific regions in the primary structure.

1.3.2 Designer peptides

The development of the technique known as solid phase peptide synthesis (SPPS) gave scientists the access to a potent tool which allowed for the synthesis of personalised amino acid sequences and could then be used to study structure-function relationships. Researchers now synthesize peptides with relative ease in the lab and have the option of

developing peptides inspired by known structures found in nature (biomimetic peptides) or develop entirely new sequences (*de novo* designed). They can then systematically alter the sequences to gain a better understanding on their design and function. A number of reviews have now covered some of the strategies used to design peptide based nanomaterials and the tremendous amount of structures which can now be created.⁶²⁻⁶⁷ Most of the advances were the result of carefully designed amino acid sequences inspired by natural motifs which could self-assemble into larger structures. The possibility to control and dictate self-assembly of molecules into larger structures is highly sought in the fields of nanotechnology. Self-assemble into supramolecular structures is an especially attractive bottom up approach for the creation of nanotechnology and nanomaterials. The potential application of peptides spans from cell culture and tissue engineering scaffolds, antimicrobial agents, drug and gene delivery and microfabrication of circuits.⁶⁴ The self-assembly is generally induced by designing peptides which will exhibit a strong amphiphilic character in its secondary structure thus also making them highly surface active. Surfaces can be coated with antibacterial peptides, such as nisin a cationic peptide 34 amino acid residues long, and impart a significant antibacterial activity to the surface and can hence be used for implants or catheter materials, which are prone to high levels of infection.^{68,69} Cell adhesion on surfaces can be controlled by using self-assembling peptides designed to expose amino acid sequences which promote cell adhesion or alternatively which inhibit non-specific adsorption of proteins and cells through changes in the surface's physical properties.⁷⁰ This remarkable range of application is a result of the highly specialised structures and sequences that have been developed to suit each situation.

1.3.3 Surfactant-like peptides

Zhang's group were one of the first to investigate the design and self-assembly properties of a subclass of designed peptides dubbed surfactant-like peptides.⁷¹⁻⁷³ The rationale for their development stemmed from curiosity in trying to discover some of the simplest amphiphilic peptide sequences which could self-assemble. Incidentally, the structures developed mimicked linear surfactant like structures with a hydrophobic tail and a polar head. However, they are far more complex in terms of their molecular chemistry compared with conventional alkyl tail bearing surfactants. The amino acid R groups which decorate the polypeptide backbone of such peptides give them a rich physio-chemistry.

The designed peptides were generally no more than 12 amino acid residues long, with the polar head having a maximum of two polar amino acids (such as lysine, arginine, histidine, aspartic acid or glutamic acid) and a sequence of hydrophobic amino acids (such as valine, isoleucine leucine or alanine). These surfactant-like peptides self-assemble much the same way as other surface active biomolecules such as lipids, but they can form nanostructures which are many times smaller in size.

Initially self-assembly studies of the peptides were conducted in the bulk solution. Some of the negatively charged surfactant-like peptides studied included A₆D, V₆D, V₆D₂ and L₆D, and have been shown to form nanotubes and nanovesicles.⁷⁴ Positively charged surfactant like peptides studied, include sequences such as A₆K, V₆K, and L₆K and have also been observed to form nanotubes and nanovesicles.^{72, 75, 76} Their structures and potential applications have been recently reviewed.^{64, 67, 77, 78} The applications ranged from antibacterial use, drug gene delivery, nanofabrication templates and use in cosmetics.

More recently, studies had also worked on elucidating the adsorption behaviour and mechanisms of adsorption at different interfaces. Much like the studies conducted on conventional surfactants at the solid-water and air-water interface, the peptides adsorption behaviour was characterised with regards to changes with solution conditions such as pH and ionic strength.⁷⁹⁻⁸¹ The behaviour of these surfactant-like peptides does resemble that of conventional surfactants with their high propensity to adsorb at interfaces and self-assembling into structures both in solution and at the interface. However, so far their surfactant properties have not been investigated alongside conventional surfactants. Adsorption studies involving mixed solutions, such as were done with surfactant studies, outlined earlier in section 1.2, are also lacking and would be highly beneficial in order to expand their use into applications from mixed formulations.

1.3.4 Alternative peptide sources

Although the design and synthesis of peptides with specific amino acid sequences and structures has become more easily available with the advance of SPPS, this method is not feasible in terms of cost and yield for large scale production. The alternative method for peptide synthesis is by recombinant peptide production through bacterial expression.⁸² However, even though in recent years costs have fallen and yields have increased its still relatively lengthy and costly, and SPPS has a better yield and speed of production for peptides below 20 amino acid residues

If the design aspect of peptides is forgone, natural peptide sources can be considered as a valid alternative. For example, a new category of protein surfactants known as bio surfactants is gaining significant attention. Researches have now identified several classes of biosurfactants originating mostly in bacteria. These have the advantage of being

naturally occurring surfactant-like protein/peptides produced by microorganisms. The microorganism can be sustained on renewable resources as their feed making the process bio sustainable.²⁵ This is an attractive option and many industries including food, cosmetics and biotechnology are researching its potential.⁸³⁻⁸⁵

Finally, another such alternative are hydrolysates of large proteins which contain functional peptide motifs in their structure. Hence these peptides can be liberated at the fraction of the cost, especially if produced from proteinaceous waste materials. Protein hydrolysates are generally achieved from either enzymatic digestion or by chemical processing (acid hydrolysis). Enzymatic digestion is more attractive, especially for use in food products, and there is a wide range of enzymes which have been reviewed for this purpose.⁸⁶ Ultrafiltration of products into separate molecular weight fractions has also been used to help improve the functional properties of the hydrolysate product.⁸⁷ A recent review has covered the potential for the release of biofunctional peptides from the processing of waste fish and shellfish. They have identified a range of protein hydrolysate peptides with biological activities such as antihypertensive, antioxidant, antimicrobial, and anticoagulant effects which can be liberated and recovered.⁸⁸ Hydrolysates have also been studied for their improved surface active properties and as potential as surfactants.^{89,}⁹⁰ As such they are an attractive, relatively cheap, sustainable, green way of producing peptides with a wide range of possible applications depending on the parent proteins primary structure.

1.4 Silk Fibroin

Silk fibroin is the major protein component found in silk filaments produced by living organisms such as silk worms and spiders. One of the most widely studied and used silk fibres comes from the silk worm *Bombyx mori*. Traditionally, silk worms have been the major source of silk for the textile industry, as they are more easily domesticated than spider silk. Silk fibres have been used as suture material for hundreds of years due to their biodegradability and biocompatibility. Processing methods have now allowed for silk fibroin to be regenerated (RSF) from the raw silk fibres and for new biomaterials to be fabricated from it. These include films, particles, coatings, hydrogels, sponges and scaffolds to name a few.⁹¹ Its extreme versatility has helped establish silk fibroin as an exceptional natural polymer which can be used as an alternative to many synthetic polymers and which exhibit weaker properties. As will be discussed in detail in section 1.4.1 silk fibroin amino acid sequence is of great importance to its physiochemical properties and much research efforts have been going into understanding its structure and function.

1.4.1 Molecular structure and composition

Silk fibres are composed of fibroin filaments held together by a glue-like protein known as sericin. The sericin roughly amount to 25-30% of the total silk fibre weight composition. The exceptional mechanical and biocompatible properties of silk are believed to arise from the silk fibroin component found in silk and its unique repetitive molecular sequence.⁹² The full amino acid sequence of *Bombyx mori* silk fibroin has been sequenced and was found to be composed of two main macromolecules, a heavy chain

(390kDa) and a light chain (25kDa) linked together by a disulphide bridge (shown in Figure 1.6).⁹³ The heavy chain is composed of 45.9% glycine, 30.3% alanine, 12.1% serine, 5.3% tyrosine, 1.8% valine, and only 4.7% of the other 15 amino acid types. The heavy chain fibroin contains repeating Gly-Ala-Gly-Ala-Gly-X amino acid sequence where 'X' can either be an Ala>Ser>Tyr>Val>Thr.⁹⁴ This repeating sequence is also known as the crystalline component of silk fibroin. Each of these hydrophobic sequences is then followed by a repetitive length of an amorphous hydrophilic sequence. The above mentioned hexapeptide has a structure reminiscent of the surfactant-like peptides which have been discussed earlier in section 1.3.3. They have a hydrophobic tail like section, formed by the Gly-Ala repeats, followed by a polar amino acid such as Ser, which behave as the surfactant head group. This repeating amino acid motif should thus have the basis for a good surface activity when liberated.

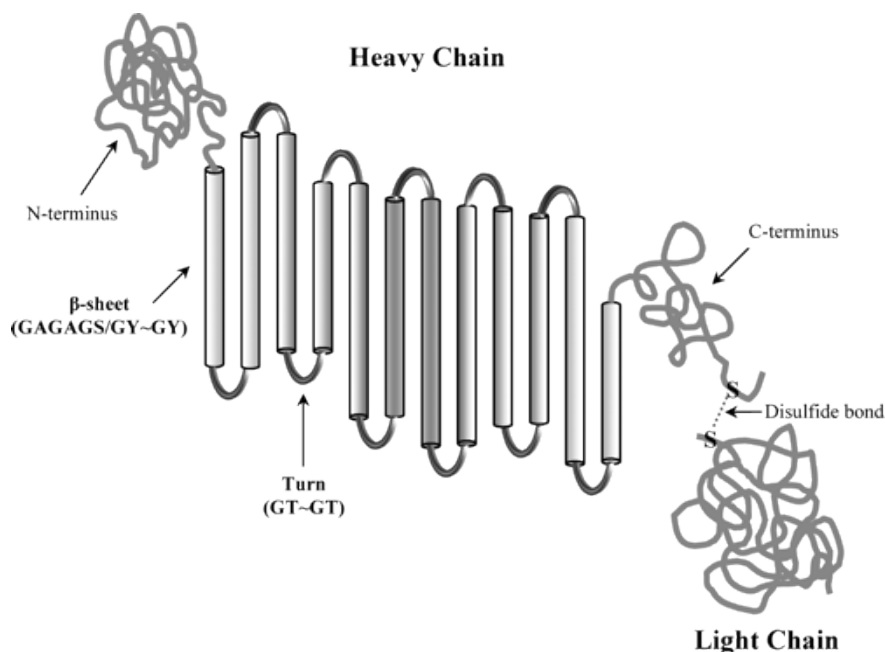


Figure 1.6 Molecular structure of silk fibroin chains from *Bombyx mori*. Reprinted with permission from Ha et al.⁹³ Copyright 2017 American Chemical Society.

1.4.2 Regenerated silk fibroin

The extraction procedure of silk fibroin from raw silk fibres results in regenerated silk fibroin (RSF). The procedure involves a degumming step to remove the sericin and then a dissolution process to solubilise the fibroin which is then dialyzed and filtered. The degumming procedure involves boiling the silk fibres in a salt solution (typically 0.02 M Na₂CO₃ for 30 minutes). This has known to affect the tensile strength of the degummed fibre and is thought to result in the degradation of the amorphous linkers and N- and C-terminus regions.⁹⁵ Consequently the degumming time has been shown to affect the MW of RSF.⁹⁶ The dissolution process involves the hydrolysis of chains by heating in solutions containing chaotropic salts. Many different dissolution protocols exist and have been reviewed for their effects on the RSF stability and MW.⁹⁷ Common dissolution systems include 9.3 M lithium bromide or water: calcium chloride: ethanol (1:2:8 molar ratio). The method of silk dissolution has also been shown to affect the way in which the RSF molecules are hydrolysed yielding significantly different RSF molecular chains. The effect on MW has been reported by many studies.^{96, 98, 99}

It was found that changes to the MW composition of RSF due to different degumming times and procedures appear not to have any significant effect on its inflammatory potential.⁹⁶ It should be noted that silk fibroin does cause a minor immune response but it has been shown that this minor response can help improve wound healing and was not deemed to be an obstacle for its use *in vivo*.¹⁰⁰ On the other hand recent studies have shown that when silk fibroin and sericin are found together they cause significant inflammatory reactions in patients but, unlike previously thought, sericin alone does not cause a strong immune response¹⁰¹⁻¹⁰³ and therefore correct degumming is very important. RSF has found many successful applications as a biomaterial.⁹¹ However the use of RSF peptides has not been explored as much. Studies are limited to investigation

of the solution properties such as its rheology and a few have explored possible protein/peptide structural conformations.^{97, 104-107}

1.5 Research motivation

As discussed in the literature review, steps have been taken in order to mitigate the environmental impact from the use of harsh surfactants derived from the petrochemical industry. The route to more environmentally friendly use of surfactants includes, moving towards the production of surfactants from renewable resources, development of new better designed surfactants, and strategies for reduced consumption or more efficient use of surfactants. Within this framework the use of biological molecules such as peptides for their surface active properties is a promising solution. Studies have shown that peptides can have very good adsorption behaviours both at the solid-liquid and air-liquid interfaces. Synthesis of such peptides can be done by SPPS, but a top-down approach to recover surface active peptides from larger proteins may be more viable. However, currently there are no studies which investigate the use of peptides in conjunction with conventional surfactants. The work presented in this thesis was thus undertaken to firstly investigate the use of surfactant-like peptides with conventional surfactants and then explore regenerated silk fibroin as a potential source of similarly surface active peptides and characterise its adsorption.

1.6 Outline of thesis

Chapter one was designed to firstly introduce the reader to surfactants, their widespread use and the environmental concerns arising from their use. Then the science behind surfactant adsorption at interfaces and an account of the work carried out is discussed, followed by an introduction to peptides highlighting the work that had been carried out to mimic surfactant structures. The chapter ends with the introduction of silk fibroin and its structure highlighting the surface active potential of RSF solutions.

Chapter two gives an account of the use and theory behind the fundamental instruments and techniques that were used to carry out the experiments reported in the thesis.

Chapter three assesses the use of surfactant-like peptide, V₆K, with conventional surfactants, SDS and C₁₂TAB at the solid-liquid interface. Co-adsorption from mixed surfactant-peptide solutions as well as adsorption onto pre-adsorbed peptide layers and their respective adsorbed structures are discussed and evaluated.

Chapter four investigates the adsorption behaviour of RSF at the solid-liquid interface. The adsorption behaviour and adsorbed layer structures are characterised with respect to RSF MW, concentration pH and salt concentration. The chapter ends with adsorption of SDS and C₁₂TAB onto pre-adsorbed layers of RSF.

Chapter five reveals the adsorption behaviour and surface adsorbed layer structures of RSF at the air-water interface. Particular attention is then given to the surface tension reduction caused by small additions of RSF to surfactant solutions. Some foaming studies are also carried out to help identify changes in the adsorbed layer at the air-water interface of the mixed solutions.

Chapter six summarises the work reported in the thesis and gives ideas for future work.

2 EXPERIMENTAL THEORY

2.1 Neutron reflection

2.1.1 Overview

Neutron Reflection is an ingenious technique used to help reveal detailed information regarding structural features of thin films found at interfaces. These include structural information such as thickness, area per molecule, orientation, and composition at an interface. Its usefulness spans many different scientific and technological disciplines, from soft matter studies involving biological membranes and proteins to material sciences involving thin films and magnetic structures. Briefly, the technique involves the reflection of a beam of neutrons from an interface and upon reflection changes to the beam's intensity are measured by a neutron detector. In essence the technique is not too different from certain analogous techniques which utilise X-rays, electrons or visible light to probe structural features. However, several important features separate neutron reflection and give it a truly remarkable advantage, especially when investigating soft matter systems. With regards to the experiments carried out, four features were identified as most

significant. Firstly, neutrons interact delicately with matter, unlike X-rays or electrons which can be highly ionizing and can easily damage or destroy delicate samples. Secondly, neutrons can penetrate deeper into samples enabling buried interfaces and structures to be studied and allowing for a greater freedom when designing and facilitating complex experimental setups (e.g. for controlling pressure, temperature or applying magnetic fields etc.). Thirdly, a technique known as isotopic substitution can be used to selectively enhance contrast and label parts of molecules or systems making it easier to distinguish and quantify molecules and their relative compositions. Finally, the ability to study structures down to an angstrom level resolution. All of these features have been exploited for the experiments carried out, and in the following sections all the relevant background theory will be discussed.



Figure 2.1 A miniature model of the ISIS neutron facility found at the front entrance to the ISIS control room.

2.1.2 Neutron production and facilities

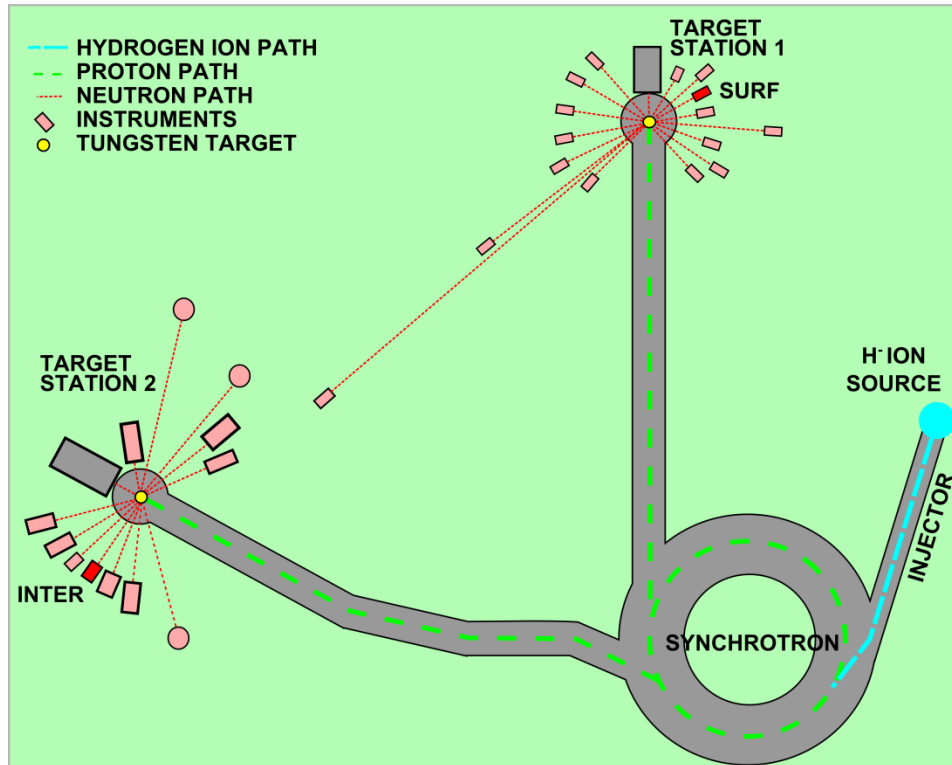


Figure 2.2 Basic spallation source layout for neutron production and instrument facilities at ISIS.

Experiments were carried out at the ISIS facilities (Rutherford Appleton Laboratory, Oxfordshire, UK), which employs a spallation source for the production of neutrons. Neutrons can be produced in a number of ways, but in broad terms large scale neutron facilities depend upon either a spallation source or a nuclear reactor. A complete discussion of neutron production and facilities is beyond the scope of this thesis and only neutron production at ISIS will be outlined (Figure 2.2).

At ISIS the most iconic sight is probably the 800 MeV proton accelerator, with its huge circular structure, it's the heart of the facility and of the process of neutron production. The spallation source can be subdivided into two distinct structures, an injector (linear accelerator) and a synchrotron. The injector's job is to begin the acceleration of the H⁺ ions (two electrons and a proton) produced by the ion source and separate them into

“bunches”. Before entering the synchrotron, the linear accelerator brings up the speed of the H^+ ions to 37% of the speed of light. Upon entering the synchrotron, the H^+ ions go through a thin foil of alumina which strips the electrons leaving a beam of protons. The beam of protons is further accelerated and directed along the 163 m circular synchrotron path with the use of strong magnets and radio frequency electric fields. After completing 12,000 revolutions around the synchrotron the protons reach 84% of the speed of light. At this point the proton beams have gained enough kinetic energy and exit the circular synchrotron and are made to collide with one of the two tungsten targets (located at target station 1 and target station 2). The impact caused by the high energy proton beams cause neutrons to shoot out from the nuclei of the target. Following their ejection from the nuclei, the kinetic energy of the neutrons is too high for their immediate use by instruments and therefore it is necessary to slow them down. To achieve this, the neutron beam is passed through a series of moderator tanks which consist of tanks filled with water, liquid methane or liquid hydrogen. The neutron instruments are scattered along the moderated neutron beams at varying distances and positions according to the neutron characteristics required such as intensity, angle, spin and energy needed by each specific instrument. Experiments were conducted on either SURF (target station 1) or INTER (target station 2), which are two of the five neutron reflectometry instruments found at ISIS. Further details regarding the two instruments and its operation are discussed in section 2.1.4.

2.1.3 Neutron reflection theory

Neutron reflection is a scattering technique used to probe the structures at interfaces. Its advantages over other scattering techniques arise from the fundamental interactions

neutrons have with matter. In order to understand how neutron reflection works some basic physics knowledge regarding neutrons and their scattering behaviour is initially covered.

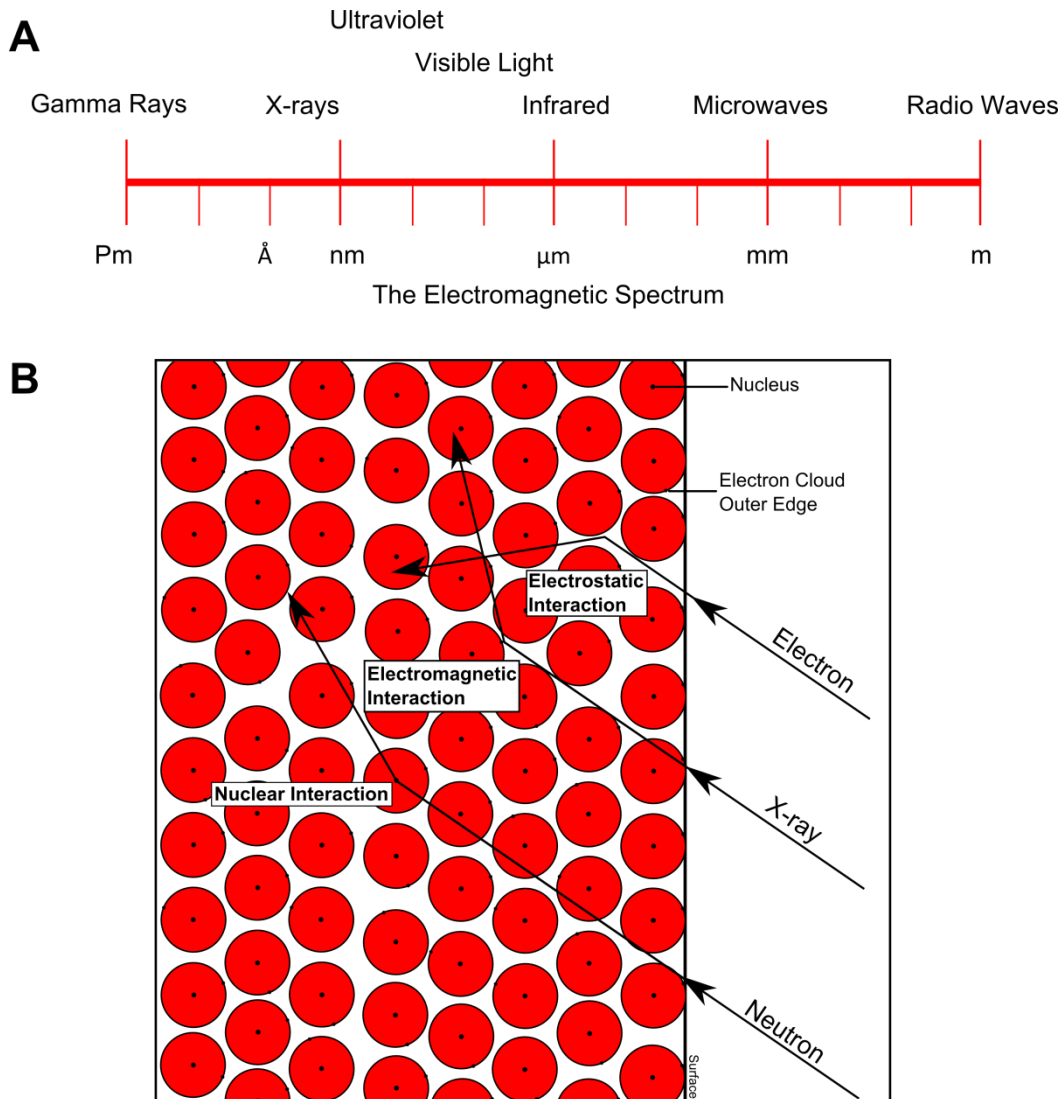


Figure 2.3 A, Wavelengths of electromagnetic waves across the electromagnetic spectrum, B, schematic of the scattering of electron, X-ray and neutron beams at the atomic level.¹⁰⁸

Neutrons have no charge, and alongside protons (positively charged) and electrons (negatively charged) make up the major elements which constitute an atom. Both neutrons and protons reside at the very heart of the atom forming the nucleus. Electrons

on the other hand surround the nucleus forming an ‘electron cloud’ and give the atom its overall size. However, it’s important to note that the nucleus of the atom (which holds the vast majority of the mass) occupies only a fraction of the space (in the order of 10^{-4} to 10^{-5} of the overall size). This has fundamental implications on the scattering behaviour of a beam of particles as discussed below and shown in Figure 2.3.

For example, a beam of electrons would interact with the outer electron cloud of an atom and will be deflected by strong electrostatic interactions. This stops electrons from penetrating deeper than less than a fraction of a micrometre of any given sample, and hence its scattering will yield information only of a sample’s outermost surface.

X-rays are part of the electromagnetic spectrum and possess both oscillating electric and magnetic fields. Compared to visible light, X-rays have a much shorter wavelength and can penetrate deeper into a sample than electrons (as X-rays do not possess a fixed charge). However, the oscillating magnetic and electric nature of X-rays causes weak interaction with the electron cloud which will eventually cause it to scatter (generally, a few millimetres of aluminium will completely stop X-rays).

Neutrons on the other hand, do not possess a charge and thus are unaffected by electrostatic repulsive forces and can therefore penetrate all the way into an atom, past the electron cloud, and scatter only upon interaction with the nucleus. It should be noted that if the sample has magnetic properties, magnetic scattering of neutrons will also occur but will not be considered as it’s beyond the scope of the discussion. Unlike the electrostatic force, the strong nuclear force responsible for the scatter of neutrons, acts only over a minute distances of 10^{-15} m. This adds to the notion that an atom is mostly empty space, resulting in neutrons scattering very poorly. The poor scattering can be considered a double edge sword, as it allows for unprecedented penetrating ability (several centimetres of aluminium) and therefore the opportunity to study interfaces

buried deep in a system but with the drawback of requiring large sample quantities/surface area for a reasonable scattering signal to be detected.

Another important characteristic of neutrons is its wave like behaviour. As discussed earlier neutrons are subatomic particles. They have a mass and apparent volume but they can also be described in terms of wavelength (wave-particle duality).

Classical mechanics assigns a particle with mass, m_n , and speed, v , a momentum, p , through

$$p = m_n v$$

(2-1)

On the other end De Broglie's proposal (1923), building up upon Planck's work, relates a particle's momentum, p , with a wavelength, λ :

$$\lambda = \frac{h}{p}$$

(2-2)

Where $h = 6.626 \times 10^{-34}$ Js and is known as Planck's constant.

The two can then be linked through the kinetic energy equation to give

$$E = \frac{1}{2} m v^2 = \frac{h^2}{2m_n \lambda^2}$$

(2-3)

Hence a neutron's energy and wavelength can be determined.

In scattering theory its convention to refer to neutrons by its wavenumber, k , where $k=2\pi/\lambda$ or its vector, wavevector \mathbf{k} , who's modulus is equal to k . Using the above notation, a scattering event can be described in terms of its momentum transfer, Q , and energy transfer, E

$$Q = \mathbf{k}_i - \mathbf{k}_f$$

(2-4)

$$E = \omega_i - \omega_f$$

(2-5)

Figure 2.4 shows this in terms of an incident neutron particle with wavevector, \mathbf{k}_i , and angular frequency ω_i , which upon scattering has a wavevector \mathbf{k}_f and angular frequency ω_f , where $\omega=2\pi f$.

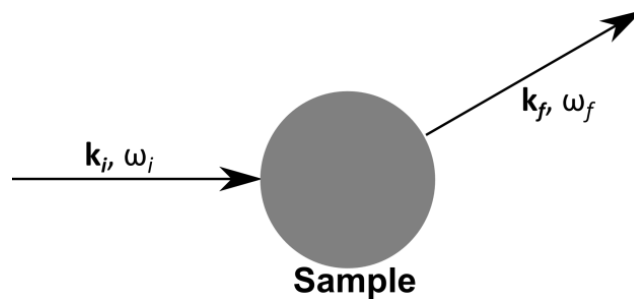


Figure 2.4 Wavevector and angular frequency of a neutron scattering event.¹⁰⁸

In the special case of elastic scattering, as is neutron reflection, there is no exchange of energy, hence $E=0$ and there will be no change in the wavelength, λ , following scattering.

Which means $|\mathbf{k}_i|=|\mathbf{k}_f|=2\pi/\lambda$, thus the momentum transfer describing the scattering event as determined by the vector diagram shown in Figure 2.5, can be solved to give:

$$Q = \frac{4\pi \sin\theta}{\lambda}$$

(2-6)

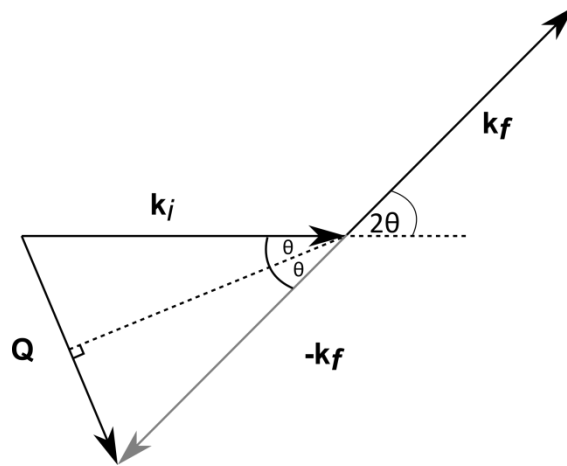


Figure 2.5 Vector diagram for a neutron reflection event.¹⁰⁸

We can use the above relationship relating momentum transfer to angle of incidence and neutron wavelength to control the range of Q values over which we can create an intensity profile of specular reflection to help reveal structures found at the interface.

This is described well in equation (2-7) below, known as the Kinematic (or first Born) approximation which was applied to specular reflection by Crowley.¹⁰⁹ The equation shows reflectivity as a function of Q with the reflectivity falling sharply with increasing Q but also that reflection of neutrons from a surface is influenced by changes in the scattering length density (ρ) perpendicular to the surface.

$$R(Q) \approx \frac{16\pi^2}{Q^2} |\hat{\rho}(Q)|^2$$

(2-7)

Where $\hat{\rho}(Q)$ is the one dimensional Fourier transform of ρ

$$\hat{\rho}(Q) = \int_{-\infty}^{\infty} \exp(-iQz) \rho(z) dz$$

(2-8)

And ρ is the scattering length density of an element or material, and can be calculated from the sum of the number density n of an element i with scattering length b

$$\rho = \sum b_i n_i$$

(2-9)

As shown above, the scattering of neutrons by a specific elements is given by the scattering length, b_i , which is determined experimentally and can then be used to calculate the SLD for specific molecules or a material found at an interface. Hence changes in the SLD are a direct indication of the molecular composition found at the interface and result in measurable changes to the $R(Q)$ profile and is the basis for neutron reflection experiments.¹¹⁰

However, it's important to note that equation (2-7) is an approximation and is not sufficient to describe the full range of reflectivities which may be needed. This is due to the failure to account for the critical angle at which total reflection occurs and consequently becomes a bad approximation at capturing the effects at reflectivities greater than $\sim 10^{-3}$ (approaching the critical angle). Instead a more exact and preferred solution for the calculation of reflectivity profiles can be obtained by applying standard optics with the use of Fresnel's equations.¹¹¹

To do this an analogous definition of refractive index is applied to neutrons in such a way that Snell's law can be used to define the critical angle at which total external reflection occurs and then be incorporated into the Fresnel equations.¹¹²

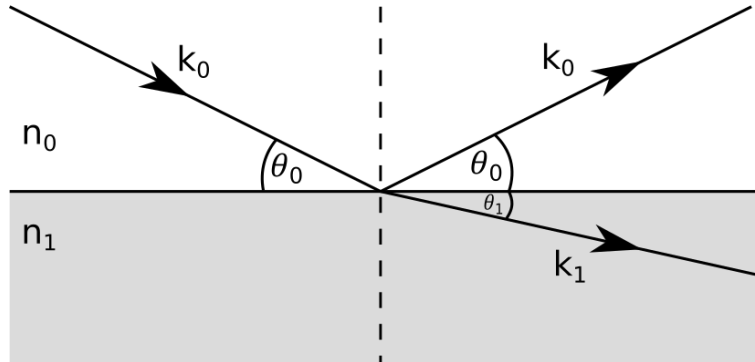


Figure 2.6 The interface between two bulk media with refractive indices n_0 and n_1 , with transmitted and reflected wavevectors k_0 and k_1 , at angles θ_0 and θ_1 .

The neutron refractive index at a boundary between two media is defined as

$$n = \frac{k_1}{k_0}$$

(2-10)

Where k_0 and k_1 are the wavevectors in the first and second medium respectively.

Furthermore, for a medium i the neutron refractive index can be shown as,

$$n_i = 1 - \frac{\lambda^2 \rho_i}{2\pi}$$

(2-11)

Where ρ_i is the scattering length density of the medium and from which we can then find the critical angle, θ_c , below which total reflection occurs for neutrons at the interface between mediums , n_1 and n_0

$$\cos\theta_c = \frac{n_1}{n_0}$$

(2-12)

When $\theta \leq \theta_c$ reflectivity from the Fresnel equation will be unity and when $\theta \geq \theta_c$,

$$R = \left| \frac{n_0 \sin\theta_0 - n_1 \sin\theta_1}{n_0 \sin\theta_0 + n_1 \sin\theta_1} \right|^2$$

(2-13)

The above equation is for a single interface but the Fresnel reflection can also be applied to multilayers (as shown in Chapter 2.2.2, Theory of light reflection for Ellipsometry, but with angles measured to the normal), where the equation accounts for neutrons which are reflected back and refracted at the interface of each layer.¹¹² Furthermore, it should be noted that the above equations assume that the interface is completely smooth. In experimental setting however, changes in the surface topography (roughness) which are in the same length scales as the neutron wavelength used are likely to affect the reflection of neutrons. Changes to the surface roughness in that length scale generally result in a change to in the reflection similar to when a diffuse interface is present. Névot and Croce¹¹³ found that such diffuse layers or roughness, can be modelled by applying a Gaussian roughness factor such as Debye-Waller factor. Cowley and Ryan¹¹⁴ then extended its application to Fresnel coefficients for use at the interface of thin films. Inclusion of such a factor allows control over an SLD gradient across the modelled layer. Most reflectivity software packages are capable of calculating all of the above (reflection

from multilayers and roughness factor) through the use of matrix calculations known as optical matrix methods. The use of optical matrix methods, such as the Born and Wolf¹¹⁵ optical matrix method, makes calculations computationally more efficient. The work outlined in this thesis was carried out using a software, Motofit¹¹⁶, which uses Abeles method¹¹¹ which allows for a roughness factor to be included in the calculations.

2.1.4 Experimental method

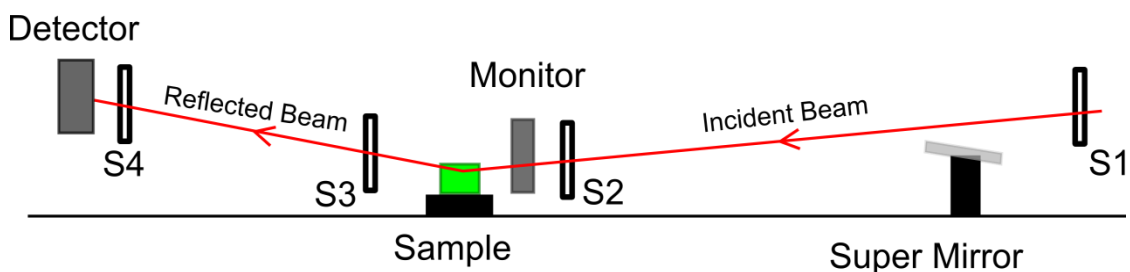


Figure 2.7 Setup of neutron reflectometry instrument chamber.

Experiments were conducted at either INTER or SURF reflectometry instruments. INTER is the most recently built instrument (completed in 2008) of the two. Both instruments have very similar setups resembling

Figure 2.7. The only major differences are in the neutron wavelengths, flux and angle of incidence entering the instrument. INTER uses neutron wavelengths between 1-17 Å with angle of incidence of 2.3°, as opposed to 0.5-7 Å and an angle of incidence of 1.5° on SURF. From equation (2-6) it is then possible to infer that a larger wavelength range results in a much broader Q range available for measurement. This can have practical implications on the running of experiments, as more angles are necessary on SURF to achieve a full Q range. Also the neutron flux is 10x greater on INTER than SURF which significantly improves acquisition times but essentially won't make a difference to the

quality of the results as experiments are conducted with a predetermined neutron exposure (neutron count) as the end point. In Figure 2.7 the slits prior to the sample position (S1 & S2) are used to adjust the beam area that will illuminate the sample. Illuminating a larger area allows for faster and better acquisition of reflectivity from the sample. Whilst the slits found after the sample (S3 & S4) can be used to help reduce any background noise from the scattering reaching the detector. The sample stage can be moved in the x, y and z directions and is mounted on a goniometer which allows for the stage to be tilted to control the precise angle of incidence reaching the sample and consequently the detector position will be adjusted to receive the reflected beam. Since the sample stage cannot be tilted when measuring air/liquid experiments the neutron beam is deflected instead to the desired angle by using a supermirror found prior to the sample stage.

Samples for solid/liquid experiments were conducted using polished silicon blocks (1.2 x 4.0 x 6.0 cm) which were treated with Piranha solution (6:1 ratio of 98% H₂SO₄ to 35% H₂O₂) to yield a clean hydrophilic oxide layer. Sample adsorption on these blocks was achieved with the use of Perspex troughs of matching size which could hold 2ml of sample solution in its lumen. The Perspex trough was clamped onto the silicon blocks with the aid of two rectangular aluminium plates which could be screwed together. The silicon block and the Perspex trough were thus sandwiched in between and adhered tightly to each other. The troughs were designed with a side inlet and outlet tube which was used to inject the sample solutions for adsorption. Upon completing each experiment, the setup was dismantled and cleaned with Deacon 90 (Decon Ltd., Hove, UK), rinsed with plenty of UHQ water and blow dried with nitrogen gas. For air/liquid experiments the samples were allowed to equilibrate on Teflon troughs which were secured to the neutron reflection stage on an anti-vibration table inside of a closed chamber which maintained environmental conditions stable. Once experiments were conducted the troughs were cleaned with Deacon 90 and rinsed with plenty of UHQ water.

2.1.5 Contrast variation

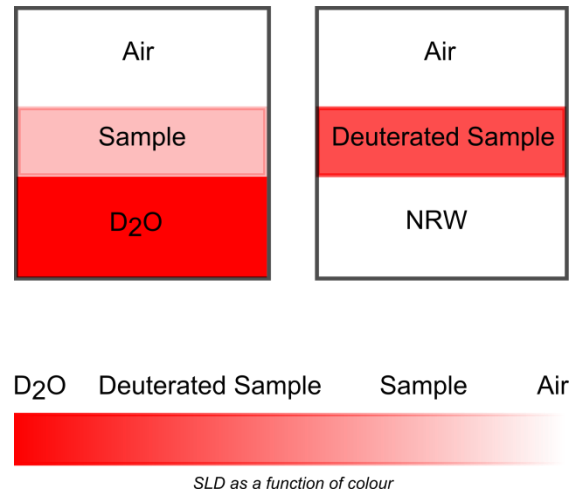


Figure 2.8 Contrast variation at the Air/liquid interface.

Contrast variation is a very useful technique that can be applied to neutron reflection experiments to gain improved scattering or selective scattering of layers in order to enhance the reflectivity. For example, if neutron reflection were to be carried out at the air/water interface, the very low SLD of H₂O ($-0.56 \times 10^{-6} \text{ \AA}^{-2}$) would result in very poor scattering making the interface difficult to detect. Hence contrast variation by using D₂O, which has a much higher SLD ($6.35 \times 10^{-6} \text{ \AA}^{-2}$) would give a very strong scattering signal from the interface. Furthermore, in the case of an adsorbed sample, which doesn't have a very strong scattering (as shown in Figure 2.8), isotopic substitution of H with D can be used to improve its scattering. In addition, Figure 2.8 illustrates a possible use of contrast matching, in this case the SLD of the subphase was made to match that of air by using a mixture of H₂O and D₂O yielding null-reflecting water (NRW). In the example the signal in Figure 2.8 arises exclusively from the adsorbed deuterated sample

2.1.6 Neutron data analysis

Neutron reflection experiments result in a reflectivity curve, in order to extract meaningful information from the reflectivity data regarding the layer structures an appropriate model which fits the data needs to be produced. To do this MOTOFIT was used as a data fitting software.¹¹⁶ The software allows the user to divide an interface into any number of layers and assign values for thickness, SLD and roughness. The user can therefore create an appropriate model by assigning all known values whilst leaving other values free for the software to fit. The software will calculate a reflectivity curve and compare it with the experimental data and evaluate their similarity in terms of chi squared,

$$\chi^2 = \sum_n \left\{ \frac{(R_f - R_e)^2}{\sigma^2} \right\}$$

(2-14)

Where n is the number of data points, R_f and R_e are the reflectivities for fitted and experimental data and σ is the standard error. The software will attempt to minimise the value of χ^2 by least square iterations of the values that need fitting. To improve this procedure, values which need fitting are kept to a minimum and constrained within specific ranges (so that unrealistic but mathematically possible fits are excluded) and the overall number of layers is also kept to a minimum so as to avoid overfitting. In addition to that, the best way to validate a model is to have multiple runs which make use of isotopic substitution to yield different reflectivities which need to then fit the same general model.

Once a good fit is achieved, through the use of some simple equations the fitted values for thickness and layer SLD can be used to reveal more detailed information regarding volume fraction, area per molecule and surface excess.

For example, if a two component adsorption was being studied, such as surfactant and peptide in water, the volume fraction and scattering length density of a layer can be expressed using the following equations:

$$\rho = \rho_p \varphi_p + \rho_s \varphi_s + \rho_w \varphi_w$$

(2-15)

$$\varphi_p + \varphi_s + \varphi_w = 1$$

(2-16)

where ρ is the total scattering length density of a layer and ρ_p , ρ_s , and ρ_w are the known individual scattering length densities of peptide, surfactant and water, and φ_p , φ_s and φ_w , are the respective unknown volume fractions of the components found in the layer which add up to one. In this case, since there are three unknowns, the volume fraction of each component cannot be solved directly. In order to solve such an equation, contrast variation or isotopic substitution with a deuterated version of the surfactant or peptide can yield two independent equations allowing for the volume fraction for both components to be solved. Once the volume fractions have been calculated the surface area per molecule (A) can be calculated using

$$A = \frac{V_p}{\tau \varphi_p}$$

(2-17)

where V_p is the volume of the peptide. The surface excess (Γ) can then be calculated by

$$\Gamma = \frac{MW}{6.02A}$$

(2-18)

where MW is the molecular weight of the molecule.

2.2 Ellipsometry

2.2.1 Overview

Ellipsometry is an optical technique which uses visible light to probe optical properties of materials by measuring two quantities known as Δ and Ψ (discussed in section 2.2.2). These quantities are then used alongside an assumed model of the interface to calculate material properties such as film thickness and layer composition. Ellipsometry is widely used to study thin films and surfaces and has been used in fields ranging from microelectronics to materials science and chemistry¹¹⁷, Tompkins gives an excellent review of its versatile uses¹¹⁸. The technique is ideally suited for studying the adsorption of soft matter at surfaces as it does not perturb the surface and does not damage the soft matter. Additionally, it has the advantage of measuring real time data so that kinetics of adsorption can be studied with a high degree of accuracy and with angstrom level resolution. The following sections will give a solid background on the theory behind the use of Ellipsometry and how the equipment was used to carry out experiments and make reliable conclusions on soft matter adsorption.

2.2.2 Theory of light reflection for Ellipsometry

Ellipsometry measures the changes to the polarisation of a beam of light upon reflection from a surface. To understand better how this is done and what this means it is first necessary to understand a few basic concepts regarding light waves and polarisation.

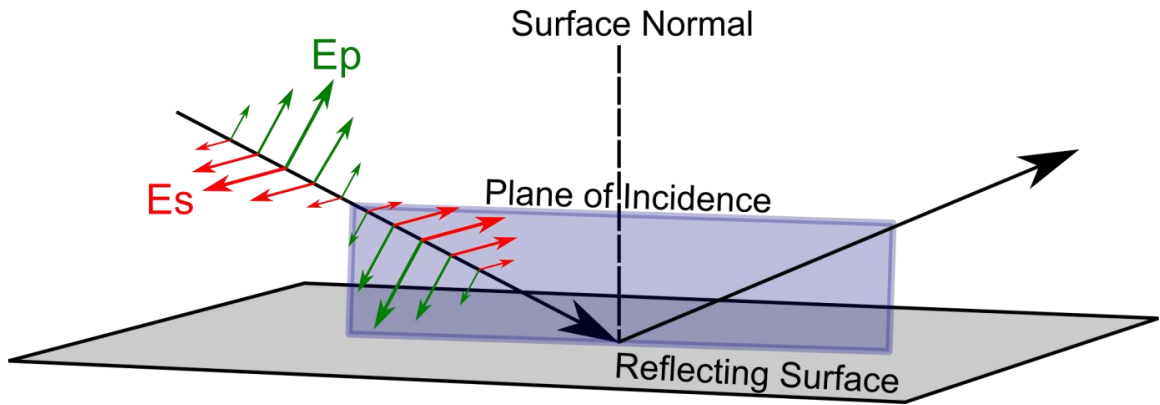


Figure 2.9 P-polarised and s-polarised light reflecting off a surface.

Visible light is an electromagnetic wave and as such it possesses both an electric and magnetic field component which oscillates in the form of a sine wave perpendicular to the direction of propagation. With regards to Ellipsometry and the work carried out the magnetic component of the wave has no influence. Light from an unpolarised source has electric field components oriented in all possible directions perpendicular to the direction of propagation. Polarised light is achieved when the direction of the electric field component is aligned in one specific plane (plane polarised). It is convention to refer to light polarised in the plane of incidence as p-polarised light whilst light polarised perpendicular to the incidence plane as s-polarised light (as shown in Figure 2.9). Also plane polarised light can be referred to as linearly polarised light. This term arises from mentally visualising the trace of the polarised light wave when observed head on, i.e. it will yield a straight line.

Next it's important to understand how two linearly polarised light beams will interact if they are combined along the same path. To keep things simple let's consider two beams which are perpendicular to each other and have the same phase difference (the troughs of both waves are aligned) and same amplitude (same electric field strength), similar to the incident beam in Figure 2.9. When two such waves are combined it will result in a 45° linearly polarised light beam. If the amplitude of the waves were to be changed it would

result in a change in the angle of the resultant polarised light. However, if the two original light beams were made to be out of phase with each other by a set amount, the resulting light beam will result in elliptically polarised light. This term stems from the shape made by the direction of the polarised light when observed head on which has now changed from the previously discussed straight line to an ellipse. The degree by which an elliptic form is achieved is determined by how much the beams are out of phase as well as the amplitude. (for example beams of same amplitude but 90° out of phase result in circularly polarised light) It is in fact the measure of this property of polarised light which gives the technique its name, Ellipsometry.

Reflection of a polarised light beam from a surface will cause changes to the polarised light it is important to understand how polarised light reflected from a surface can be used to reveal information about the surface. To do that the behaviour of light travelling across different mediums/materials must first be examined.

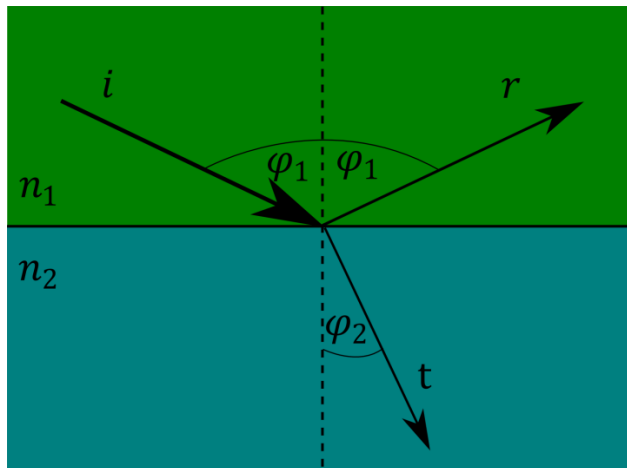


Figure 2.10 Incident light, i , is transmitted into medium n_2 at an angle ϕ .

The physical properties of a medium can affect the velocity of light travelling through it. This characteristic of a given medium can be described by the complex index of refraction given by

$$\tilde{N} = n - jk$$

(2-19)

Where n is the index of refraction, and k is the extinction coefficient of the imaginary part of the equation. For a dielectric material such as glass, which does not absorb any of the light energy, $k=0$, therefore only the index of refraction is considered. The index of refraction refers to the velocity, v , of the light wave travelling through the material relative to the speed of light in a vacuum, such that $n=c/v$, where c is the speed of light in a vacuum. Also it should be noted that both n and k are functions of the wavelength λ , such that when λ increases both n and k fall following the equations

$$n(\lambda) = n_1 + \frac{n_2}{\lambda^2} + \frac{n_3}{\lambda^4}$$

(2-20)

$$k(\lambda) = k_1 + \frac{k_2}{\lambda^2} + \frac{k_3}{\lambda^4}$$

(2-21)

This behaviour is exemplified by the refractive action of a prism capable of separating the component wavelengths of a white light source (blue light experiences a higher refraction index than red light which has a higher λ). The above explains how different λ 's experience different refractive indices but a different equation is needed to describe the change in path of the light beam due to the refractive property of the material. This

behaviour is encapsulated by Snell's law which relates the refracted angle with the refractive indices of the material in which the light travels through

$$n_1 \sin \varphi_1 = n_2 \sin \varphi_2$$

(2-22)

Where φ_1, φ_2 are the angles to the normal of the surface made by the light beam (shown in Figure 2.10). The above equation deals with the trajectory of light transmitted across an interface to another medium, however it does not consider the part of the light wave which is reflected from an interface. The Fresnel reflection coefficient is used at an interface to determine the ratio between the reflected wave amplitude with that of the incident wave amplitude given by

$$r_p = \frac{n_2 \cos \varphi_1 - n_1 \cos \varphi_2}{n_2 \cos \varphi_1 + n_1 \cos \varphi_2}$$

(2-23)

$$r_s = \frac{n_1 \cos \varphi_1 - n_2 \cos \varphi_2}{n_1 \cos \varphi_1 + n_2 \cos \varphi_2}$$

(2-24)

Where r_p and r_s are the p-polarised and s-polarised reflection coefficients. Since the intensity of a light wave is proportional to the square of its amplitude, the reflectance $\mathbf{R} = |r|^2$, for p-polarised and s-polarised light respectively.

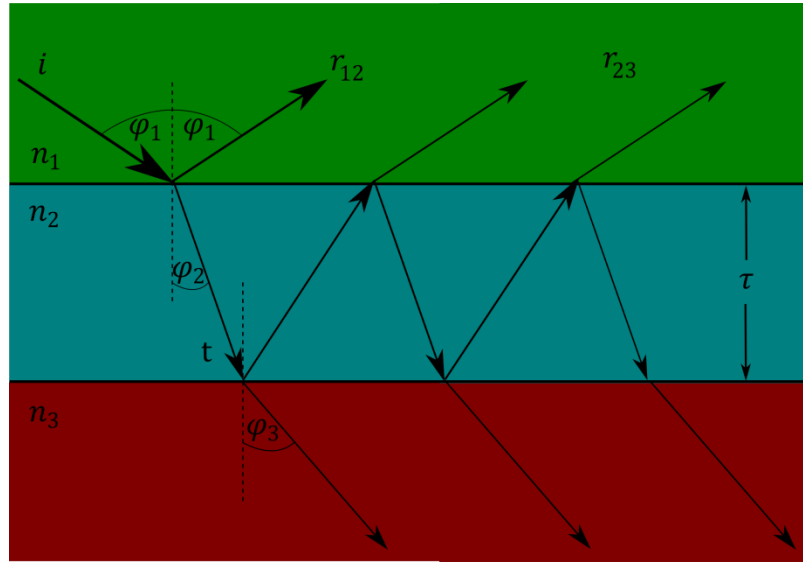


Figure 2.11 Reflection from multiple layers.

However, as it stands, the above Fresnel reflection coefficient is valid only for a single interface, if there are more interfaces a significant component from the transmitted light is also reflected back at each interface and has to be accounted for. The ratio of the reflected amplitude wave to the incident wave, including the reflected component from each transmission across the interfaces, is then given by the total reflection coefficients

$$R_p = \frac{r_{12}^p + r_{23}^p e^{-j2\beta}}{1 + r_{12}^p r_{23}^p e^{-j2\beta}}$$

(2-25)

$$R_s = \frac{r_{12}^s + r_{23}^s e^{-j2\beta}}{1 + r_{12}^s r_{23}^s e^{-j2\beta}}$$

(2-26)

Where r^p and r^s are the Fresnel reflection coefficients between each interface, noted by the subscript number, and β is the film phase thickness given by,

$$\beta = 2\pi \left(\frac{\tau}{\lambda}\right) n_2 \cos\phi_2$$

(2-27)

where τ is the thickness of the layer.

Finally, having now examined the trajectories and reflectivity of a polarised light beam from a surface the changes to the light beam's phase and amplitude upon reflection can be linked together through the fundamental equation of Ellipsometry

$$\rho = \tan \psi e^{j\Delta}$$

(2-28)

Where Δ (Del), is the resulting change in phase upon reflection of the polarised waves and is defined by

$$\Delta = \delta_1 - \delta_2$$

(2-29)

Where δ_1 is the phase difference between the p-polarised wave and the s-polarised wave of the incident beam and δ_2 is that of the reflected wave.

And the quantity ψ (Psi) is the amplitude change upon reflection and is defined through

$$\tan \psi = \frac{|R_p|}{|R_s|}$$

(2-30)

Where $|R_s|$ and $|R_p|$ are the magnitudes of the amplitudes of the total reflection coefficients.

2.2.3 Experimental method

A Jobin-Yvon UVISSEL spectroscopic Ellipsometry (Horiba Ltd. Japan) was used to carry out the experiments. Measurements were taken across a wavelength range of 300 to 600 nm with a fixed incidence angle of 70° . The experiments were carried out in a liquid cell which can hold a maximum volume of ~ 1.2 ml. The liquid cell was placed on the stage in a position which allows for the light beam to enter and leave the liquid cell through the fused quartz windows and reach the detector unobstructed. A silicon wafer with a known oxide layer thickness was placed in the liquid cell and was used to double check that the readings were not affected by misalignment or window position. The liquid cell was then fixed in this position using Blu-Tack or sticky tape and experiments were conducted. After each experiment the cell was cleaned with Decon 90 and rinsed with plenty of UHQ water.

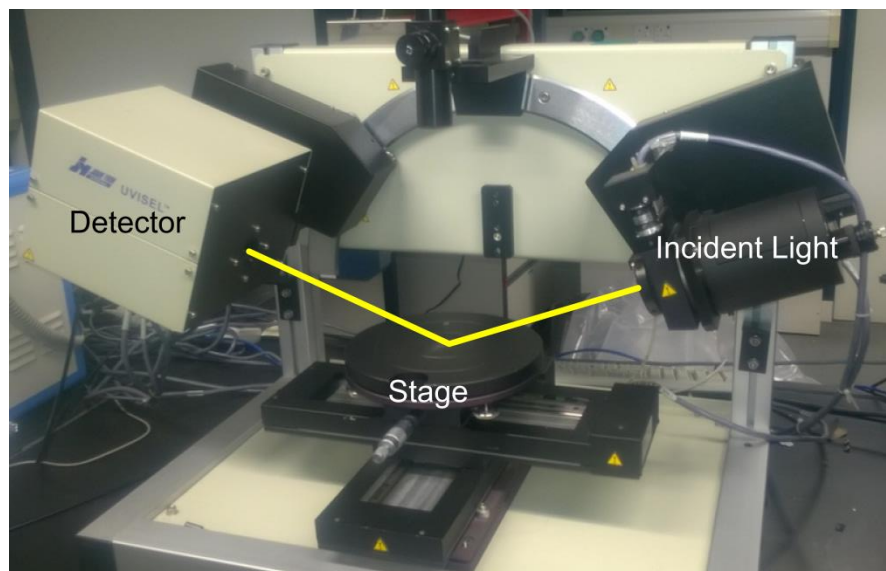


Figure 2.12 Ellipsometer setup used for experiments.

2.2.4 Ellipsometry data

The measurements were analysed using the official software DeltaPsi II provided by Jobin-Yvon. Appropriate models were constructed to reflect the number and type of layers present in the experiments. For example, a model for the adsorption of a peptide on a silicon wafer would include three layers, crystalline silicon as backing, an amorphous silicon oxide layer, and top most a peptide layer. Values for the layers could be found in the software material library or through experimental data. A typical experimental run will firstly involve measuring the bare oxide layer and inputting this information into the constructed model (thus reducing the number of unknowns) and then carrying out the peptide adsorption and then fitting the new data using the model.

For extremely thin films (less than 100 Å) the Ellipsometry cannot distinguish between the contribution from the layer thickness and its refractive index. This is because at that length scale the two values become closely interlinked and therefore calculations of surface excess are considered to be the best output measure. The surface excess is calculated using De Feijter's equation ¹¹⁹

$$\Gamma = \frac{\tau(n_1 - n_2)}{dn/dc}$$

(2-31)

Where n_1 is the refractive index for the sample solution and n_2 is that of the buffer and dn/dc is the change in the refractive index with concentration and has a value of 1.8 cm³ g⁻¹ for peptide solutions.¹²⁰

2.3 Surface tension

2.3.1 Overview

Surface tension is a very simple technique which can be used to measure the surface tension of liquids. It is widely used in surfactant studies, characterisation of formulations for paints and coatings and adsorption studies. Changes in surface tension values give an indication on changes that occur at the interface as molecules adsorb and in some cases they also give an insight into changes occurring in the bulk solution. The following sections will explain the theory behind surface tension and the experimental method for collecting the data.

2.3.2 Theory of surface tension

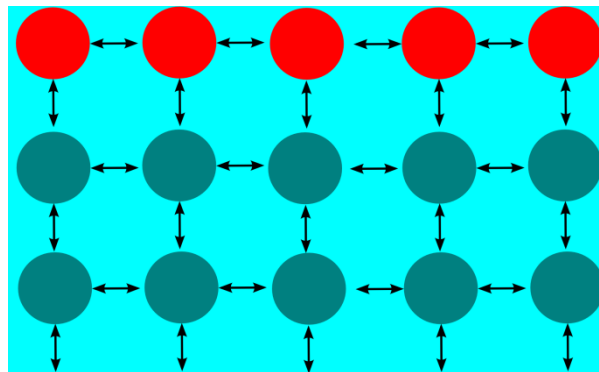


Figure 2.13 Cohesive forces shown acting on molecule in the bulk and at the interface (red).

Surface tension is a measurable force that occurs at the interface between two immiscible liquid phases such as liquid/liquid or air/liquid. Cohesive forces between molecules are

responsible for the manifestation of surface tension. It arises from an imbalance in the forces experienced by a molecule found in the bulk compared to a molecule found at the interface. In the bulk a molecule is surrounded in all directions by other molecules and is able to form attractive interactions which lower its free energy. At the interface, the molecule can only establish cohesive interactions with a limited number of molecules and hence have a higher free energy. At all times the molecules will try to reduce its free energy and therefore will try and assume a minimal area, or in other words work is needed to form a new surface, which leads to liquids forming a drop like shape. Surface tension is thus a measure of a liquids cohesive forces and its resultant effect on the interface and is given by

$$\gamma = \frac{dG}{dA}$$

(2-32)

Where G is the interfacial free energy and A is the interfacial area.

There are several methods for measuring the surface tension which include drop shape/volume analysis, capillary rise and tensiometer. In this discussion we will limit ourselves to explaining the theory behind tensiometer measurements.

Tensiometer measurements rely on measuring the direct force experienced by an object in contact with the interface. There are three main variations in tensiometer methods which rely on different ‘objects’ which are: Wilhelmy plate, Du Nouy ring and Dyne probe. The same physics apply for all three methods and the only difference arises in their geometry and operation which in some special cases maybe preferred over another.

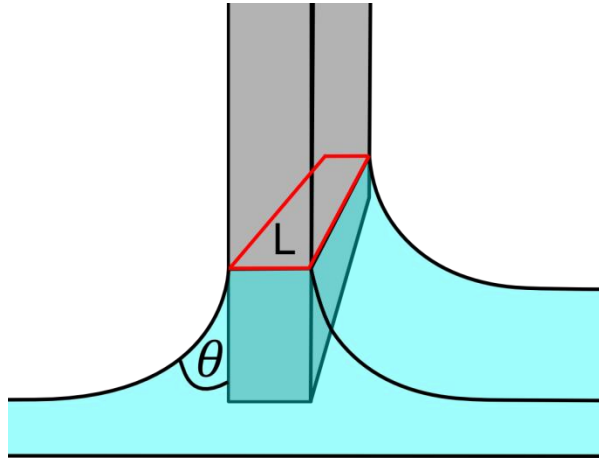


Figure 2.14 Liquid pulling onto a plate, with a wetted perimeter L shown in red and a contact angle θ .

A tensiometer employs a high accuracy microbalance to measure the forces experienced by an object in contact with a liquid's interface. When an object penetrates the interface there are three main forces that affect the tensiometer readings; the surface tension, weight of the object and upthrust. The weight of the object is known and the effect of upthrust is eliminated by bringing the object to the same level as the interface. This leaves the surface tension component which acts on the wetted perimeter of the object as shown in Figure 2.14, thus

$$\gamma = \frac{F}{L \cdot \cos\theta}$$

(2-33)

Where F is the force measured by the tensiometer, L is the wetted perimeter and θ is the contact angle. Most tensiometer can get rid of the contact angle value by using roughened platinum as the contact material since it has optimal wetting and brings the contact angle close enough to zero.

2.3.3 Experimental method



Figure 2.15 Kruss surface tensiometer equipment.

A K11 tensiometer (Kruss, Germany) was used to make surface tension measurements by using a platinum Wilhelmy plate (19.90 x 0.20 x 10.00 mm) with a wetted perimeter of 40.20 mm. Prior to each experiment the Wilhelmy plate was cleaned by rinsing in Decon90 and UHQ and then flame heated until incandescent and then allowed to cool. Samples were pipetted into a small glass beaker which fits into a temperature controlled sleeve (connected to a water bath cooler set at 20°C) positioned directly under the Wilhelmy plate. The sample stage was then raised close enough to the Wilhelmy plate for the instrument to then take control and detect the sample surface and for the measurements to begin. Measurements were stopped when the standard deviation fell below 0.075 mN/m. Before each measurement the cleanliness of the system was checked by confirming a reading of 72.8 mN/m for UHQ.

2.4 Foaming Studies

2.4.1 Overview

Foams are used in a range of applications from food preparation to detergent action and manufacture of materials such as Styrofoam.¹ The ability for a solution to foam and maintain a foam structure over time is closely related to what goes on at the interface. As such changes in the foaming behaviour can help indicate interactions between molecules in the solution and at the interface.

2.4.2 Foaming Theory

There are solid foams and liquid foams. Foams are found in foods (cakes, pastries, bread, meringues and soufflés) as well as personal care and hygiene products and can be used in materials such as metals and ceramics.¹⁸

As mentioned above some foams can be used to create solid structures however in this work we will only focus only on liquid foams which are mixtures of gas inside a liquid phase. Common to all liquid foams, is that they cannot be created in a solution of the pure liquid (unless highly viscous), there has to be a surface active compound or particulate present for a foam to be generated and maintained.^{121, 122}

Foaming theory is thoroughly covered in a review by Pugh.¹²³

There are many methods which have been adopted to create foams, from physical methods which force gas into a solution such as by agitation, to the use of chemical reactions for the production of gas from within the solution itself as in the case of fermentation. All foams are thermodynamically unstable, but can be separated according

to their foam stability into two types - Transient foams and metastable foams, with classic examples of each being champagne and beer respectively.¹²³

The instability of foams is evident in the above mentioned foams, and in most cases it is easily observed to be the result of drainage of the liquid phase and coalescence of neighbouring bubbles. These lead to a thinning of the bubble interface (lamellae) and eventually result in the rupture of the surface and consequent foam collapse. Additionally, a less evident cause of foam collapse is the net diffusion of gases across the thin bubble interface from small bubbles to larger bubbles. This process is known as disproportionation and is a result of the difference in Laplace pressure across the bubbles surface between small and large bubbles and results in the net diffusion of gas to the larger bubbles.¹²³

In the literature, foam stability has been observed to be controlled by two main foam stability mechanisms, the Gibbs-Marangoni effect which counteracts drainage, and the viscoelastic effect which counteracts shrinkage and disproportionation.¹²³ Surfactants such as SDS are believed to stabilise the interface mainly through the Gibbs Marangoni mechanism.¹²⁴ The mechanism relies on concentration gradients forming at the interface relative to the bulk, which result in fast diffusion of surfactant along the interface and dragging some liquid phase with it. High lateral mobility is needed by the surfactants in order to maintain foam stability. On the other hand, the ability of proteins to adsorb at the interface and change the surface rheology of a bubble surface helps create foam stability through a more viscoelastic based mechanism.¹²¹ Disproportionation of bubbles is hindered by the ability of the molecules to adsorb at the interface and change the surface rheology increasing the surface elasticity. Generally, the foaming ability is related with the surface tension.¹²⁵ Therefore, a rule of thumb is that the larger the amount of surface active molecules the greater the foam ability and stability which is generally assessed by foam volume or height. However, when looking at systems with mixed surface active

compounds, the behaviour becomes significantly more complex and many other factors can strongly affect the foam behaviour. For example, surfactants can disturb the viscoelastic protein network which stabilise foams and at the same time the protein can limit the surfactants lateral movement thus compromising the Gibbs-Marangoni mechanism. Analysis of foaming behaviour can hence be an indirect method of gaining insights regarding the interactions occurring at the interface such as displacement of molecules (Orogenic displacement¹²⁶) and interactions in the bulk solution. The literature appears to suggest that a full understanding of foaming behaviour is still elusive and therefore more experimental investigations are needed. For example, Dickinson et al.¹²⁷ tested a range of proteins and found that they had little effect on the rate of disproportionation with bubbles disappearing in less than one hour, whilst Cox et al.¹²⁸ found that hydrophobins remained stable far longer than common proteins.

2.4.3 Experimental method

Foamability and stability are two of the most looked at factors in testing a liquid foam. Several methods have been detailed in the literature.^{18, 129} For stable foams it is common to test foamability by measuring the volume or height of foam generated and then assess stability by observing the collapse of the foam over time. The most common methods are based on variations of agitation in a vessel, Bikerman test and the Ross-miles test.

The Bikerman test consists of a glass column with a sparger at the bottom through which a gas is pumped at a known flow rate.¹³⁰ The Ross-Miles test consists of pouring a fixed volume of the solution from a fixed height onto a fixed volume of the same solution found in a column.¹³¹ Agitation experiments are conducted by controlling agitation of the solution in a closed tube by means such as stirring, whipping and shaking. In all the above

methods the aim, once the foam has been generated, is generally to measure the foam height or volume. Furthermore, the experiments can go on to measure the stability of the foams over a period of time (foam collapse kinetics) as well as characterizing the bubbles found in the foam (shape, size, lamellae thickness etc.) generally through image analysis.¹⁸ For the work carried out in this thesis the agitation method was employed and specific details have been outlined in the Chapter 5.

3 V₆K PEPTIDE ADSORPTION

Part of this work has been published in *Soft Matter*: Jayawardane et al. Co-adsorption of peptide amphiphile V₆K and conventional surfactants SDS and C₁₂TAB at the solid/water interface. **Soft Matter** **2015**, 11, 7986 - 7994.

3.1 Overview

Short surfactant-like peptides are attracting much research attention^{63, 64, 71, 72, 132, 133} in fields such as drug delivery and biotechnology as well as food and personal care applications. They have many attractive biochemical characteristics such as good biodegradability, selectivity and targeting abilities.¹³⁴⁻¹³⁶ A potential route for their widespread use is through formulation with conventional surfactants. Currently there are no studies which have investigated the interactions between surfactant-like peptides and conventional surfactants. This chapter investigates the co-adsorption of the surfactant-like peptide, V₆K, with conventional anionic and cationic surfactants at the solid/water interface. The experiments conducted investigated their combined adsorption process and

the interactions taking place between these molecules and the solid interface. The results highlighted molar concentration dependant changes to the adsorption kinetics and adsorbed layer structure and composition, as well as the ability for V₆K to modulate adsorption of conventional surfactants.

3.2 Introduction

Peptides designed to mimic the basic structural features of common surfactants generally bear distinct hydrophilic and hydrophobic moieties and thus share many common functions to conventional surfactants.^{66, 137, 138} However, the amino acid sequence which builds up a peptide surfactant renders them far more complex than simple alkyl chain surfactants. In addition, the possibility to carefully tune and create very specific amino acid sequences which are fit for purpose is highly attractive. The commercial use of short peptides is still at an early stage and is hampered by a poor understanding of their complex interfacial behaviour. Detailed studies are thus warranted to explore their basic adsorption behaviour and interactions with conventional surfactants. There have previously been several reports on the self-assembling properties and surface adsorption dynamics of a class of short designed peptides (V_mK_n, where m = 3-6 and n = 1-3) at the solid/liquid interface.^{79, 80, 139} Within this class of peptides V₆K exhibited excellent adsorption and stability at the solid/liquid interface as shown in Figure 3.1(A). It was the most surface active peptide with the highest adsorption amount and it reached the steady-state adsorption faster than V₆K₂ and V₃K. Furthermore, Figure 3.1(B) shows V₆K's excellent stability over a wide range of pH. V₆K was thus a good candidate to explore and investigate adsorption and compatibility with other surfactants.

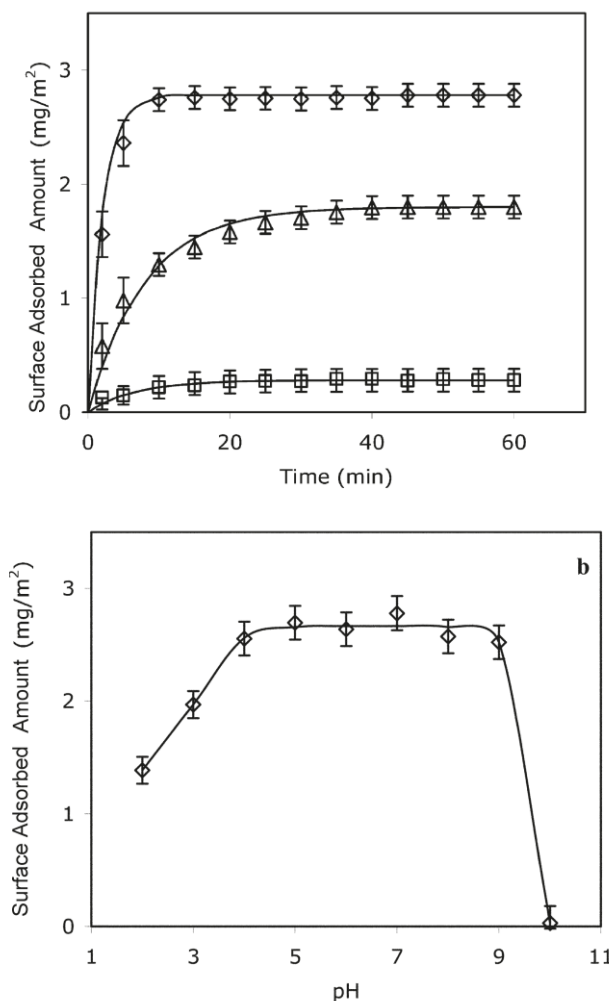


Figure 3.1 (A) Adsorption isotherms of V₆K (◇), V₆K₂ (Δ), V₃K (□) at the silica/water interface, measured at pH 7, 100 μg/ml. (B) Adsorbed amount of V₆K plotted against solution pH. Reprinted with permission from Pan et al⁷⁹. Copyright 2017 American Chemical Society.

Another very interesting feature of V₆K was its ability to self-assemble into nanostructures at the hydrophilic silica/water interface (shown in Figure 3.2). At high peptide concentrations (0.2 mM), it was found that V₆K formed a peptide bilayer that incorporated some defects and peptide stacks or vesicles. At lower peptide concentrations (0.05 mM), V₆K was shown to adsorb onto the silicon oxide interface and formed distinct flat cylindrical micellar structures.¹³⁹ As outlined also in the literature review, the ability to self-assemble and aggregate into

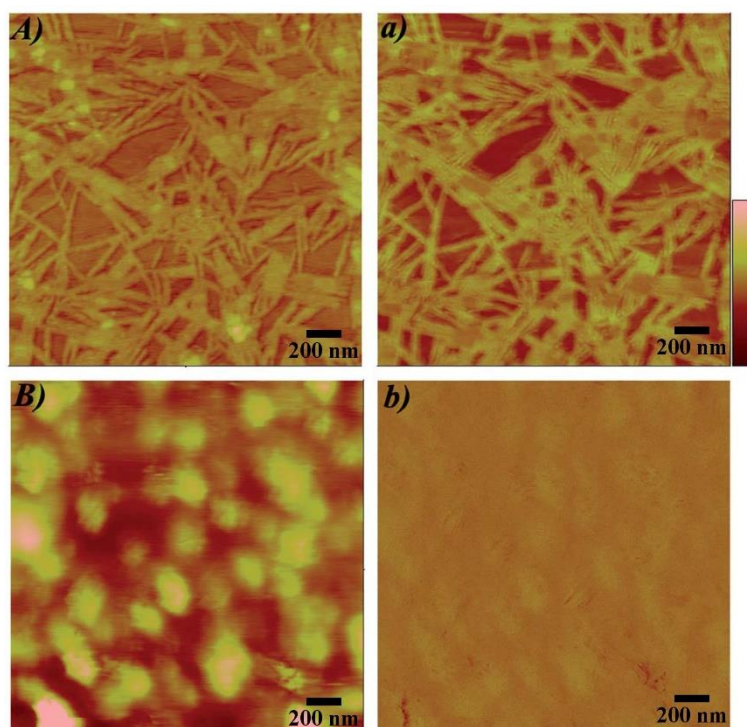


Figure 3.2 *In situ* AFM images ($2 \times 2 \mu\text{m}$) of V₆K at the silica/water interface at pH 6.0. AFM images were collected after 30 min adsorption. (A) height image and (a) the corresponding phase image with the peptide concentration fixed at 0.05 mM. (B) height image and (b) the corresponding phase image with the peptide concentration fixed at 0.2 mM. The Z scale is shown on the right (0 - 30 nm). Reproduced from Han et al¹³⁹ with permission from The Royal Society of Chemistry.

supramolecular structures such as a bilayer arrangement is a common feature of surfactants.^{41, 46} Once adsorbed, the V₆K layer could not be removed by rinsing with water, and the structures also showed good stability across a wide range of pH values and peptide concentrations.⁷⁹ The above discussed studies investigated and demonstrated V₆K's good adsorption. The good adsorption of cationic surfactant-like peptides would be attractive to personal care industry as most conventional cationic surfactants tend to be highly irritant and therefore their formulation into skin care products with other surfactants would be beneficial.¹⁴⁰⁻¹⁴² Similarly they are also attractive in the pharmaceutical industry to help drug solubilisation or delivery.⁷ For the purpose of formulation with surfactants, the basic interfacial behaviour in the presence of

conventional surfactants SDS and C₁₂TAB are examined in this chapter. Selective spectroscopic ellipsometry and neutron reflection measurements are both used in this chapter to elucidate the main interactions taking place between, V₆K and conventional surfactants, SDS and C₁₂TAB, at the solid/water interface.

3.3 Experimental method

3.3.1 Materials

The V₆K peptide had been synthesized using solid phase synthesis and had been twice purified by gel permeation chromatography to purity of >95%. Peptide stock solutions for use in experiments were freshly made by dissolving in ultrahigh quality (UHQ) water (Purelab UHQ, Vivendi Water Systems Ltd) and subsequently diluted to the required concentrations. The solution pH was adjusted using minimal amounts of HCl or NaOH to pH 7. SDS and C₁₂TAB were purchased respectively from Lancaster and Sigma, UK. Both of them were purified by recrystallization more than 3 times, in ethanol + water for SDS and in acetone + absolute ethanol for C₁₂TAB, till the surface tension around their CMC showed no minimum.

3.3.2 Spectroscopic Ellipsometry

Measurements were carried out using a Jobin-Yvon UVISEL spectroscopic ellipsometer across a wavelength range of 300-600 nm. Prior to each experiment run the silicon surfaces were cleaned and its surface thicknesses checked by ellipsometer. The sample

were then injected into the liquid cell with fused quartz windows adjusted to allow an incident light beam of 70° . Upon completion of the experiment the liquid quartz cell was thoroughly rinsed and cleaned with Decon 90 (Decon Laboratories Limited, Hove, UK) and dried out ready for the next experimental run.

3.3.3 Neutron reflection

Experiments were carried out on SURF. The silicon blocks were polished by Crystran Ltd, UK and treated with Piranha solution at 90°C for 1 min. The blocks were fitted with the Perspex trough and 2ml of sample was filled into the lumen. The samples were then left to equilibrate for the required times specific to each experiment. The blocks were then mounted onto the sample holders on the goniometer stage and were correctly aligned with the neutron beam. Each reflectivity experiment was carried out at three incidence angles of 0.35° , 0.8° and 1.8° and the resulting reflectivity profiles combined to cover a Q range between 0.012 and 0.5 \AA^{-1} . Prior to running the adsorption experiments, the oxide layer on each silicon block used was determined using D_2O as the subphase. The thickness of the SiO_2 was highly consistent amongst the blocks and was in the range of 20 \AA and a background scattering in the range of 10^{-6} , both were included in all the calculations of the models but for clarity are not shown in the reported structural parameters. Furthermore, to help aid the fitting procedure, complexity of the models was kept low by using minimum number of layers and zero roughness.

3.4 Results and discussion

3.4.1 Adsorption of SDS/V₆K mixed solution at solid-liquid interface

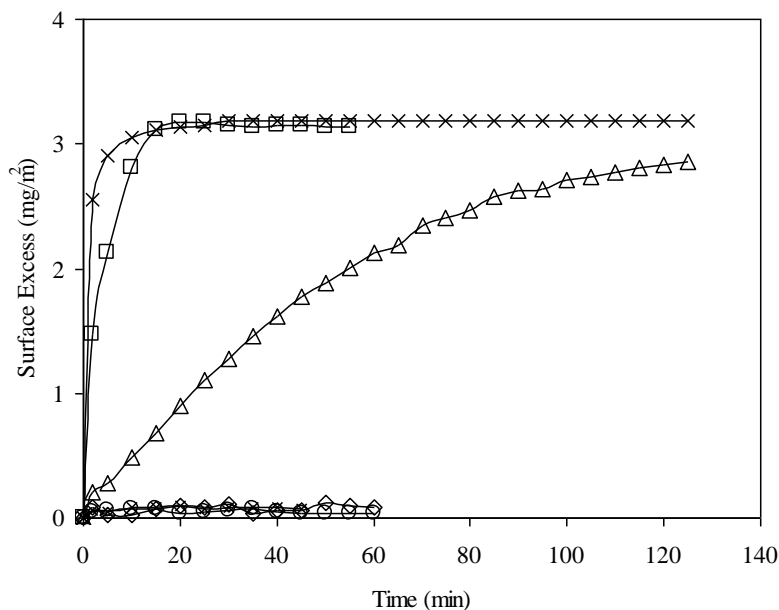


Figure 3.3 The adsorption of V₆K (×) peptide and co-adsorption of SDS and V₆K at the silica/water interface with the molar ratio of SDS: V₆K at 0.5:1 (□), 0.78:1 (Δ), 1:1 (◇), and 3.9:1 (*), 7.8:1 (○). V₆K was fixed at 100 μg/ml, pH 7. (Jayawardane et al ¹⁴³, Published by The Royal Society of Chemistry).

Adsorption of SDS/V₆K Mixed Solution at the Solid/Liquid Interface. The effect of different molar ratios of SDS on the time dependent adsorption of V₆K peptide was explored using SE (Figure 3.3). The peptide itself readily adsorbed onto the silicon oxide surface and reached a stable plateau within 10 minutes with a maximum adsorbed amount of 3.2 mg/m². Addition of SDS significantly changed the adsorption dynamics at the solid/liquid interface. At a molar ratio of 0.5:1 (SDS/V₆K), the adsorption reached the same plateau as V₆K alone but the process was slower, and as the ratio was further increased the adsorption dynamics slowed down further. It took over 100 min to reach a lower plateau, at a ratio of 0.78:1, with a final surface adsorbed amount of 2.8 mg/m².

When the ratio increased to unity and above, only a negligible amount (less than 0.2 mg/m²) of adsorption was detected. The SE results indicated that peptide adsorption was strongly inhibited by the increasing molar ratio of SDS in the solution. As the molar ratio of SDS/V₆K is equal to the charge ratio, the adsorption dynamics in Figure 3.3 is explained by the charge neutralization of cationic V₆K molecules by SDS in the solution. At and above unity, the amount of free peptide was minimal, hence adsorption was negligible. Below molar unity, SDS was not enough to neutralize all the peptide molecules in the solution, thus excess peptides drove the surface adsorption. The adsorbed amount and dynamic process both reduced and slowed down as the ratio was increased, similar to the SE adsorption curves at concentrations below 100 µg/ml reported in previous studies.⁷⁹ SE results alone cannot reveal how much SDS contributed to the total adsorbed amount and whether the presence of SDS in the mixture altered the self-assembling properties of V₆K at the solid/liquid interface. Therefore, NR was carried out for the adsorption of SDS/V₆K (0.78/1) at pH 7, reflectivity profiles are shown in Figure 3.4A for both SDS and deuterated SDS (d-SDS). The fitted data for the curves along with the calculated volume fraction and adsorbed amounts for each layer are shown in Table 3.1.

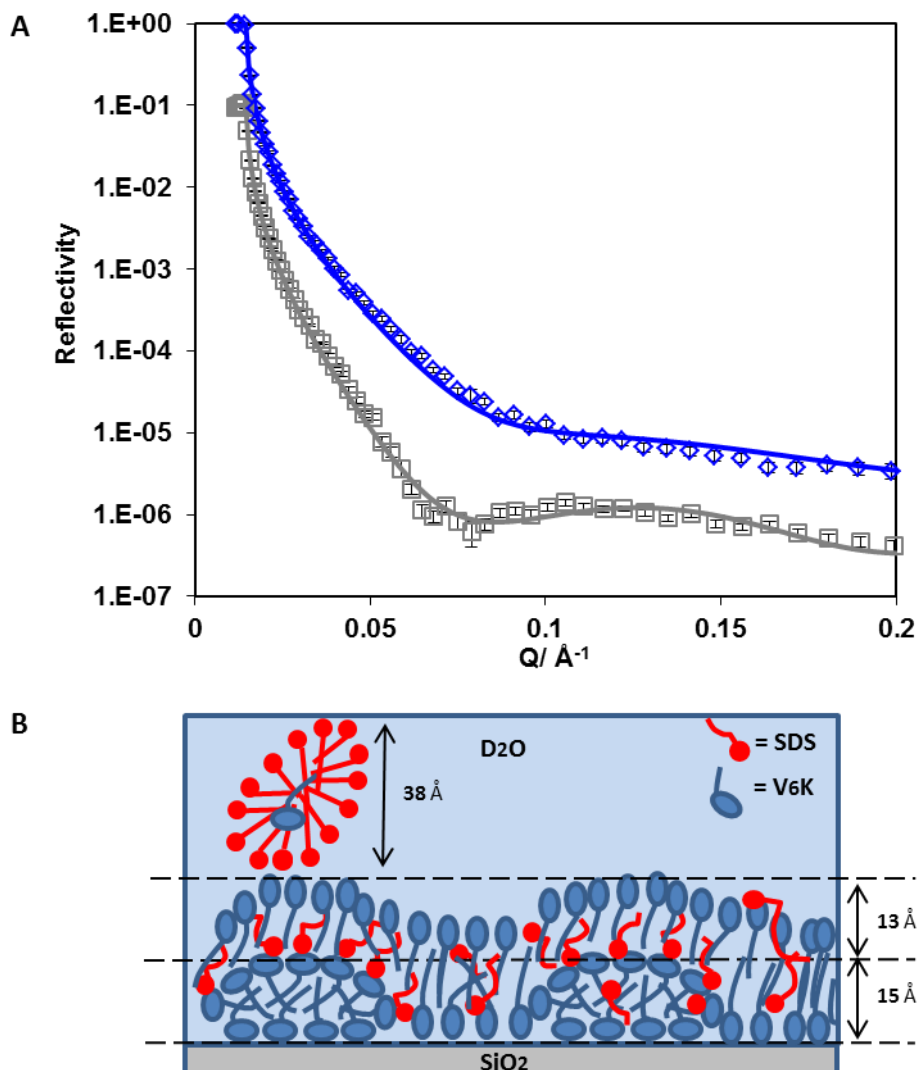


Figure 3.4. (A) Reflectivity profiles for SDS/V6K (0.78/1) mixture (\square) and d-SDS/V6K (0.78/1) (\diamond) at the SiO₂ interface in D₂O pH 7. Solid lines through the data points correspond to the model fits for the corresponding measured reflectivity data points. (B) Schematic diagram showing the arrangement of V₆K molecules (blue), SDS (red), at SDS/V₆K=0.78/1. (Jayawardane et al ¹⁴³, Published by The Royal Society of Chemistry).

Due to the electrostatic repulsion SDS does not adsorb directly onto the hydrophilic SiO₂ surface. However, the presence of cationic V₆K peptides at the SiO₂ interface can aid the subsequent adsorption of SDS through increased hydrophobic interaction and charge reversal of the surface. Careful evaluation and analysis of the NR data revealed that three distinct layers were found at the interface (Figure 3.4B). The innermost layer was 15 Å thick and densely packed, above it a more diffuse 13 Å layer followed by an even more

diffuse SDS layer, as shown by the volume fraction values in Table 3.1. The peptide structures in the innermost layer were reminiscent of the V₆K structures adsorbed at 20 µg/ml (discussed later). The thickness of the outermost SDS layer (38 Å) suggested the formation of surface micelles or lamellar structures which have frequently been reported to occur on positively charged hydrophilic surfaces.¹⁴⁴⁻¹⁴⁷ Since the outermost layer was predominantly occupied by SDS and D₂O, the layer was essentially invisible and cannot be detected by the d-SDS run as both d-SDS and D₂O have similar SLDs. Co-adsorption of SDS was likely aided by a combination of hydrophobic/electrostatic interactions with excess V₆K peptides which had readily adsorbed at the interface.

Table 3.1 Structural parameters obtained from best fits of neutron reflection data shown in Figure 3.4 for the co-adsorption of SDS/V₆K in D₂O pH 7. Fitting of SDS gives a three layer fit whilst fitting of d-SDS curve gave a two layer fit. (Jayawardane et al ¹⁴³, Published by The Royal Society of Chemistry).

Sample/ Contrast	Thickness ±2 Å	Fitted SLD ±0.1×10 ⁻⁶ / Å ⁻²	Sample SLD (V ₆ K/SDS) ±0.01×10 ⁻⁶ / 2 Å ⁻¹	Volume Fraction (V ₆ K/SDS) ±0.005	Γ (V ₆ K/SDS) ±0.1 mg/m ²
SDS/V ₆ K (0.78/1)	15	2.1	1.71/0.37	0.815/0.080	1.4/0.1
/ D ₂ O	13	4.6	1.71/0.37	0.255/0.095	0.4/0.2
	38	5.6	1.71/0.37	0/0.115	0/0.5
					Γ _{Total} 2.6
d-SDS/V ₆ K (0.78/1)	15	2.6	1.71/6.72	0.815/0.080	1.4/0.1
/ D ₂ O	13	5.2	1.71/6.72	0.255/0.095	0.4/0.2
					Γ _{Total} 2.1

The adsorbed SDS reduced electrostatic repulsion between peptides and allowed for a tight packing of V₆K in the inner leaflet of the peptide bilayer. Overall the total adsorbed amount measured by NR, 2.6 mg/m², closely matched ellipsometry results, but V₆K was revealed to have contributed only 1.8 mg/m² (2.3×10^{-3} mM/m²) to the total amount. Significantly less peptide compared to adsorption at the same peptide concentration without surfactant. On the other hand, adsorption from the binary mixture significantly aided SDS adsorption and resulted in 0.8 mg/m² (2.9×10^{-3} mM/m²) at the interface.

3.4.2 Interaction of SDS with pre-adsorbed V₆K peptide

Interaction of SDS with Pre-adsorbed V₆K Peptide. Short surfactant-like peptides have a tendency to self-assemble at the solid/liquid interface. Experiments conducted by Han et al. highlighted the presence of two distinct plateaus in the adsorption isotherms for V₆K corresponding to different structural arrangements of the molecules at the interface.¹³⁹ The effect of SDS addition on pre-adsorbed V₆K peptide layers was investigated at peptide concentrations of 20 and 100 µg/ml which correspond to two different peptide self-assembled structures. Analysis of the reflectivity curves (Figure 3.5A and Table 3.2) from the pre-adsorbed peptide layer, at 20 µg/ml, supports the formation of flattened V₆K cylindrical micelles. The adsorbed peptide layer was very reproducible and had a surface excess of 1.4 mg/m² after 20 minutes' adsorption at pH 7, matching adsorption results from ellipsometry measurements reported by Pan.⁷⁹ The thickness of the peptide layer was found to be 19 Å with a volume fraction of 0.66.

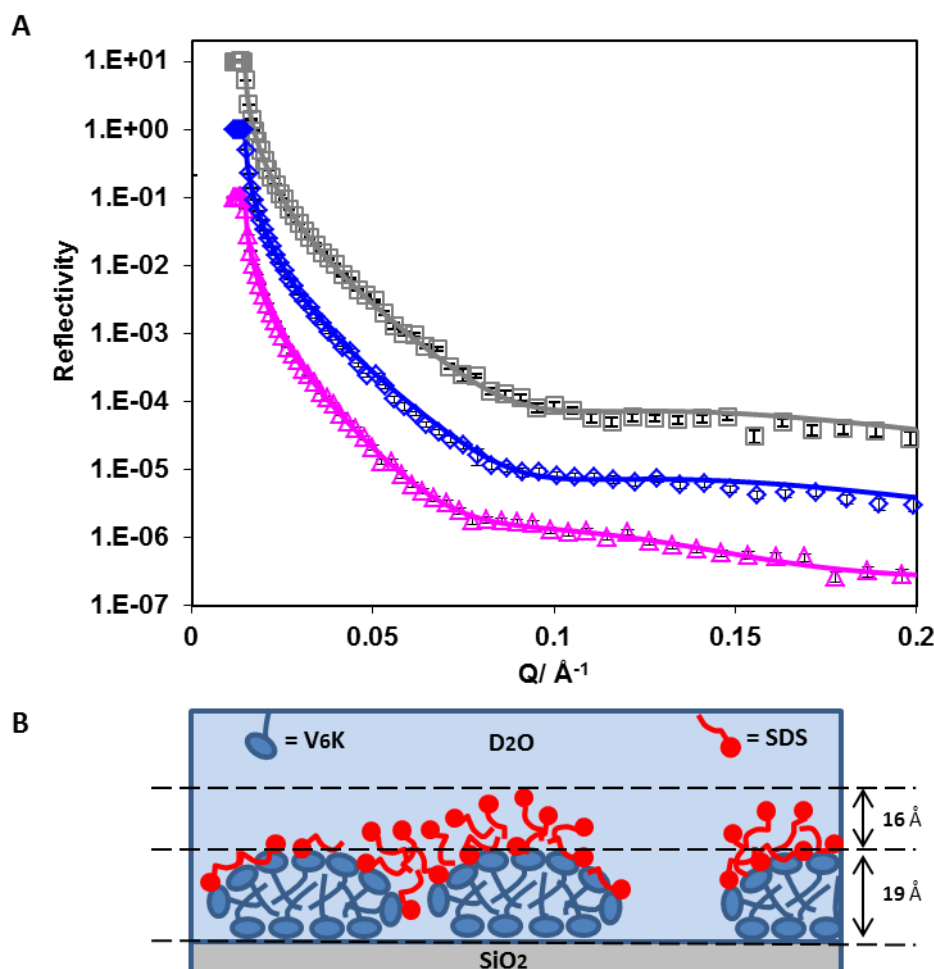


Figure 3.5. A, Reflectivity profiles for $20\ \mu\text{g/ml V}_6\text{K pH 7}$ (\square), $20\ \mu\text{g/ml V}_6\text{K pH 7} + 4\ \text{mM d-SDS}$ (\diamond) and $20\ \mu\text{g/ml V}_6\text{K pH 7} + 4\ \text{mM SDS}$ (Δ). Solid lines through the data points correspond to the best fits for the corresponding reflectivity data points. B, Schematic diagram showing the arrangement of pre-adsorbed V6K peptides at $20\ \mu\text{g/ml}$ (blue) and adsorption of SDS (red) at the $\text{SiO}_2/\text{D}_2\text{O}$ interface at pH 7. (Jayawardane et al ¹⁴³, Published by The Royal Society of Chemistry).

Following the initial adsorption, the peptide solution was carefully rinsed out with D_2O (peptide desorption was negligible) and $4\ \text{mM SDS}$ solution was added. As expected, the addition of SDS resulted in an increased layer thickness at the interface.

To investigate whether SDS adsorption caused any changes to the initial structural arrangement of the pre-adsorbed peptide layer and quantify adsorption, the experiment was repeated using d-SDS (Table 3.2). Addition of $4\ \text{mM d-SDS}$ revealed no significant changes to the pre-adsorbed V6K layer, suggesting that SDS adsorption was limited to the

surface of the peptide structures. If SDS had strongly interfered with the pre-adsorbed peptide structures (e.g. disruption), the d-SDS run would reveal a significant change to the layer SLD and or its thickness. However, in this case, both the subsequent addition of d-SDS and peptide only runs could be fitted with the same model, indicating SDS displaced D₂O and adsorbed onto the peptide layer. On the other hand the changes in SLD between the SDS and d-SDS run (Table 3.2) were used to determine the adsorbed amounts at the interface. Volume fraction values show less than 10% penetration of SDS into the pre-adsorbed peptide layer with a surface excess amounting to 0.20 mg/m² (0.7×10^{-3} mM/m²). A higher proportion of the adsorbed SDS, 0.4 mg/m² (1.5×10^{-3} mM/m²) formed a distinct 16 Å thick layer on top of the peptide structures.

Table 3.2 Structural parameters obtained from the best fits as shown in Figure 3.5 for 20 minute pre-adsorbed V₆K at 20 µg/ml, followed by addition of 4 mM SDS. (Jayawardane et al ¹⁴³, Published by The Royal Society of Chemistry).

Sample/Contrast	Fitted Thickness ±2 Å	Fitted SLD $\pm 0.1 \times 10^{-6} / \text{Å}^{-2}$	Sample SLD (V ₆ K/SDS) $\pm 0.01 \times 10^{-6} / \text{Å}^{-2}$	Volume Fraction (V ₆ K/SDS) ±0.005	Γ (V ₆ K/SDS) ±0.1 mg/m ²
20 µg/ml V ₆ K /D ₂ O	19	3.3	1.71/-	0.660/-	1.4/- <hr/> Γ _{Total} 1.4
20 µg/ml V ₆ K + 4 mM d-SDS /D ₂ O	19	3.3	1.71/6.72	0.660/0.095	1.4/0.2 <hr/> Γ _{Total} 1.6
20 µg/ml V ₆ K + 4 mM SDS /D ₂ O	19	2.7	1.71/0.37	0.660/0.095	1.4/0.2
	16	5.0	-/0.37	0/0.225	-/0.4 <hr/> Γ _{Total} 2.0

Figure 3.5B shows a cross-sectional diagram of the proposed arrangement of pre-adsorbed peptide, highlighting a compact flattened micellar structure with gaps between individual structures and SDS adsorbed around and on top. Similar to ionic surfactant adsorption onto oppositely charged hydrophilic surfaces; individual surfactant molecules are likely to have initiated adsorption onto the peptide structures with their negatively charged heads. Subsequent adsorption of SDS molecules would be through hydrophobic interactions with the alkyl tails of SDS molecules already adsorbed or hydrophobic patches on the peptide structures. SDS molecules extending from the peptide structures in such a manner would indeed stretch to around 16 \AA .¹⁴⁷

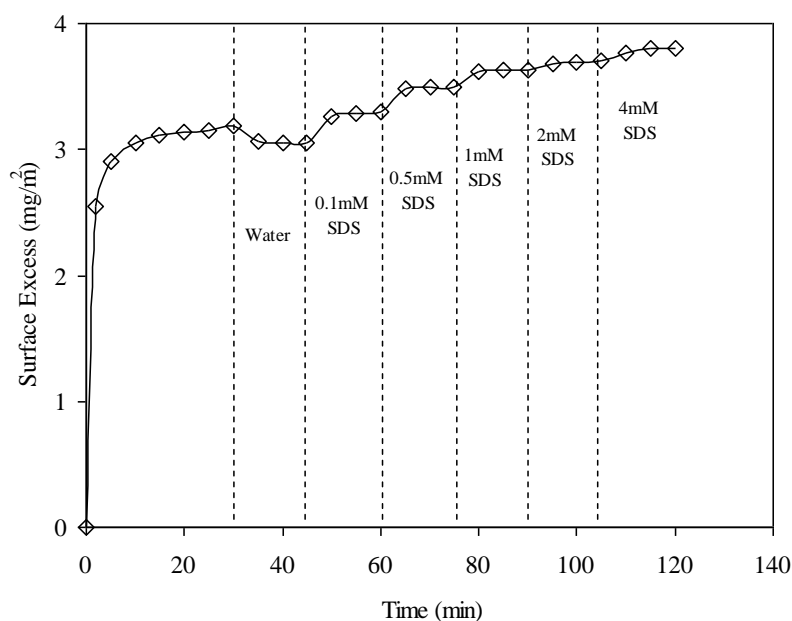


Figure 3.6 Ellipsometry data showing the adsorption of V₆K (100 µg/ml, pH 7) at the silica/water interface and washed by water and different concentrations of SDS (from 0.1 mM to 4 mM). (Jayawardane et al¹⁴³, Published by The Royal Society of Chemistry).

At 100 µg/ml, the resulting adsorbed V₆K layer could withstand UHQ water rinse and a series of rinses with SDS concentrations ranging from 0.1 mM to 4 mM (Figure 3.6). Initially, during the UHQ water rinse, minimal amounts (less than 0.2 mg/m²) of loosely

adsorbed peptide was removed leaving a very stable and firmly adsorbed peptide layer. Subsequent SDS rinses with increasing SDS concentration, up to 4 mM, resulted in increasing surface adsorbed amounts.

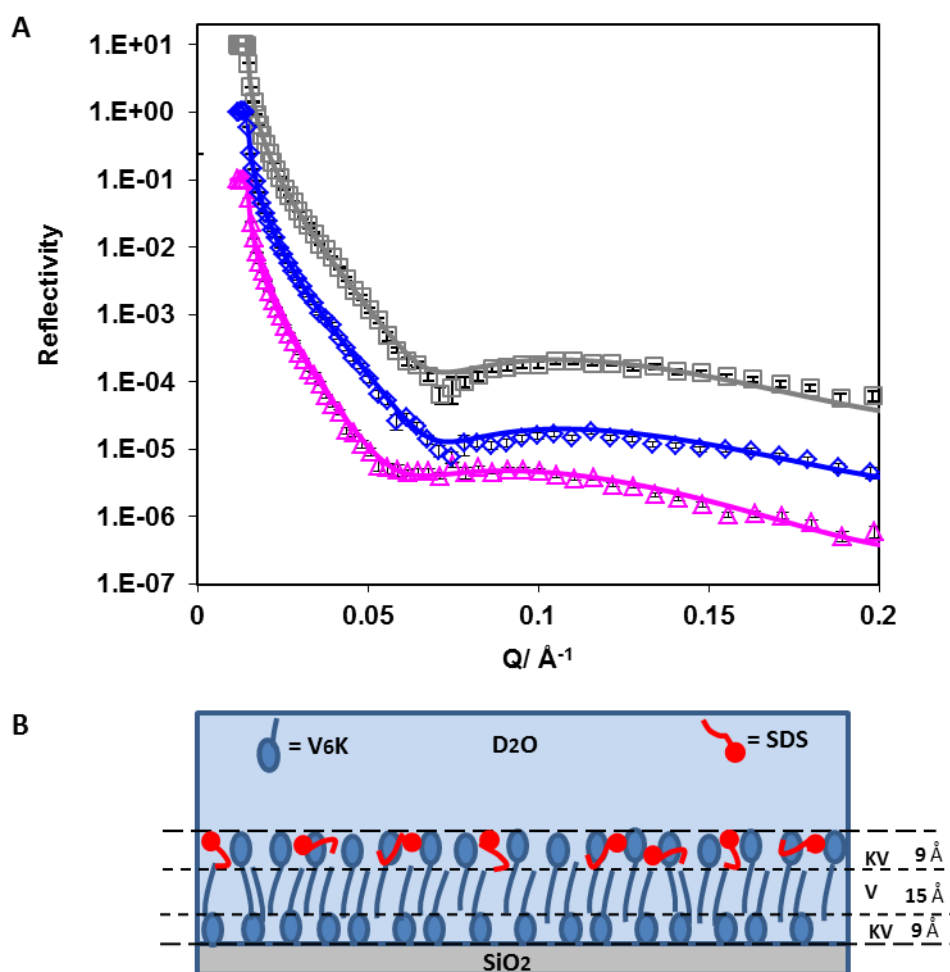


Figure 3.7 A, Reflectivity profiles for: 100 $\mu\text{g/ml}$ V6K pH 7 (\square), 100 $\mu\text{g/ml}$ V6K pH 7 + 4 mM d-SDS (\diamond) and 100 $\mu\text{g/ml}$ V6K pH 7 + 4 mM SDS (Δ). Solid lines through the data points correspond to the model fits for the corresponding reflectivity data points. B, Schematic diagram showing the arrangement of pre-adsorbed 100 $\mu\text{g/ml}$ V6K peptides (blue) and the effect of SDS (red) on its arrangement at the SiO₂/D₂O interface at pH 7. (Jayawardane et al ¹⁴³, Published by The Royal Society of Chemistry).

NR data (Figure 3.7A) confirmed the presence of a bilayer structure of V6K at the SiO₂/water interface. The pre-adsorbed peptide formed three distinctive layers (Table 3.3)

detectable due to the ordering of the lysine heads and valine tails, the latter having a lower SLD than lysine. Due to irregularities in the bilayer structure, the three layers could not be modelled to have perfectly defined K-V-K (lysine head-valine core-lysine head) layers, instead, the peptide layer was fitted by incorporating at least one V in the head region, hence KV-V-KV was used. Similar structure arrangement was found in a previous study of the interfacial structure of V₆K₂ peptide at SiO₂/water interface.⁸⁰

Table 3.3 Structural parameters obtained from model best fits of neutron reflection data shown in Figure 3.7 for the adsorption of 4 mM SDS onto pre-adsorbed V₆K in D₂O pH 7. (Jayawardane et al¹⁴³, Published by The Royal Society of Chemistry).

Sample/Contrast	Fitted Thickness ±2 Å	Fitted SLD ±0.1×10 ⁻⁶ / Å ⁻²	Sample SLD (V ₆ K/SDS) ±0.01×10 ⁻⁶ / Å ⁻²	Volume Fraction (V ₆ K/SDS) ±0.005	Γ (V ₆ K/SDS) ±0.1 mg/m ²	
100 µg/ml V ₆ K /D ₂ O	KV	9	4.7	2.13/-	0.390/-	0.5/-
	v	15	2.7	1.54/-	0.760/-	1.3/-
	KV	9	4.7	2.13/-	0.390/-	0.5/-
					Γ _{Total} 2.3	
100 µg/ml V ₆ K +4 mM d-SDS /D ₂ O	KV	9	4.7	2.13/6.72	0.390/0	0.5/0
	v	15	2.7	1.54/6.72	0.760/0	1.3/0
	KV	9	4.9	2.13/6.72	0.390/0.420	0.5/0.5
					Γ _{Total} 2.8	
100 µg/ml V ₆ K +4 mM SDS /D ₂ O	KV	9	4.7	2.13/0.37	0.390/0	0.5/0
	v	15	2.7	1.54/0.37	0.760/0	1.3/0
	KV	9	2.2	2.13/0.37	0.390/0.420	0.5/0.5
					Γ _{Total} 2.8	

The valine core had a thickness of 15 Å and SLD of $2.7 \times 10^{-6} \text{ Å}^{-2}$ whilst the inner and outer layer were both 9 Å thick with an SLD of $4.7 \times 10^{-6} \text{ Å}^{-2}$. This corresponds to the peptide molecules being tightly packed with a highly interdigitated valine tail core. The total thickness of the pre-adsorbed bilayer was 33 Å, which is in good agreement with the extended length of a V₆K molecule around 2.5-3 nm. The total surface excess value calculated from the VK-V-VK layer was slightly lower than ellipsometry results (3.1 mg/m^2) shown in Figure 3.6, but is in agreement with the values found in literature ranging between $2.5\text{-}3.0 \text{ mg/m}^2$.¹³⁹

Addition of 4 mM SDS solution after careful rinsing of the peptide solution caused a significant change to the reflectivity curves (Figure 3.7A) confirming that SDS strongly interacted with the pre-adsorbed peptide layer. Measurements using d-SDS also showed a change to the reflectivity curve indicating a change had occurred to the pre-adsorbed peptide layer upon SDS addition. Careful evaluation of the reflectivity curves revealed that SDS had penetrated into the outer peptide layer (Schematic diagram shown in Figure 3.7B). The surfactant was able to insert itself in the spaces between adjacent lysine heads by displacing D₂O. However, SDS was not able to penetrate further into the bilayer valine core to a significantly appreciable amount. There was no additional SDS adsorbed on top of the peptide bilayer, suggesting that the adsorbed SDS was enough to cause an overall charge neutralization of the peptide surface and limit any further SDS adsorption. The total SDS adsorbed amount was 0.5 mg/m^2 ($1.6 \times 10^{-3} \text{ mM/m}^2$) and is comparable to the surfactant adsorbed amount found on the top layer of the 20 µg/ml V₆K run.

Surface Effect. It was found that surface charge and hydrophobicity had a strong impact on the adsorption of V₆K. As noted earlier adsorption of 100 µg/ml V₆K resulted in a very stable bilayer. When the surface substrate was changed to a hydrophobic C₈ surface the

total peptide adsorption was less than half of the adsorption on SiO₂ surface, around 1 mg/m² (Figure 3.8). From the surface excess results, the area per molecule was found to be 130 Å² indicating that the peptide molecules formed a flat monolayer on the C₈ surface. At the SiO₂ surface, the adsorption driving force was the electrostatic attraction between the anionic surface and the cationic peptide, whilst at the C₈ surface, the adsorption was driven by the hydrophobic interaction between the C₈ and valine tail, analogous to cationic surfactant adsorption.⁴¹ This led to a change in the packing of the peptide and a bilayer structure could not be formed.

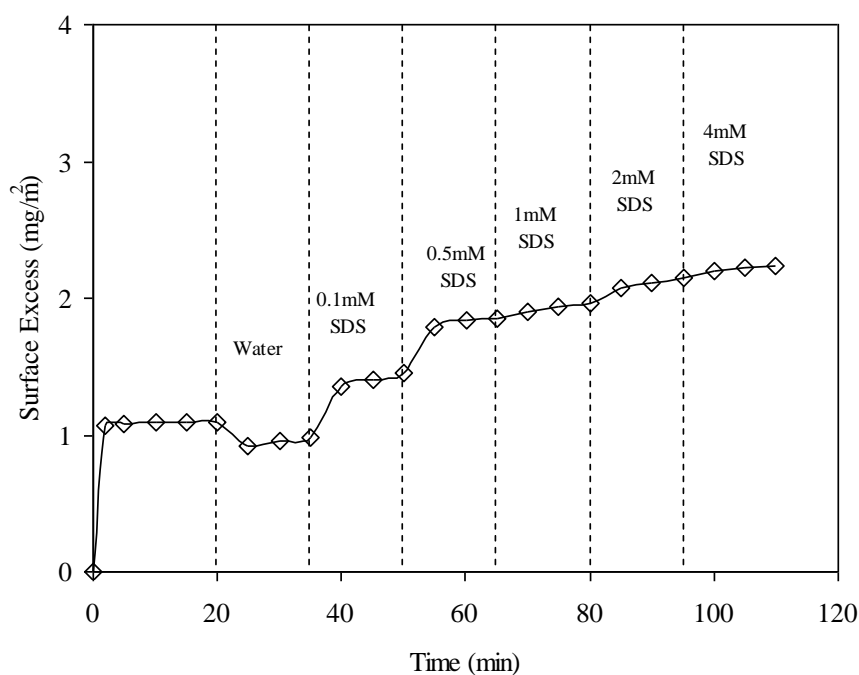


Figure 3.8 Ellipsometry data showing the adsorption of V₆K (100 µg/ml, pH 7) at C₈/water interface and washed by water and different concentration of SDS (from 0.1mM to 4mM). (Jayawardane et al ¹⁴³, Published by The Royal Society of Chemistry).

Subsequent addition of SDS solution (up to 4 mM) onto the peptide monolayer resulted in an additional adsorbed amount of 1.2 mg/m² (Figure 3.8). This is significantly higher than the SDS adsorption onto the peptide bilayer found at the hydrophilic SiO₂ interface

of only 0.5 mg/m² at the same conditions with the same peptide concentration. The increased adsorption of SDS is consistent with the peptide being arranged flat on the hydrophobic surface. In this arrangement, the hydrophobic valine tails of the peptide are more exposed allowing strong hydrophobic interactions with the SDS alkyl chains.

3.4.3 C₁₂TAB/V₆K mixed solution adsorption at the Solid-liquid interface

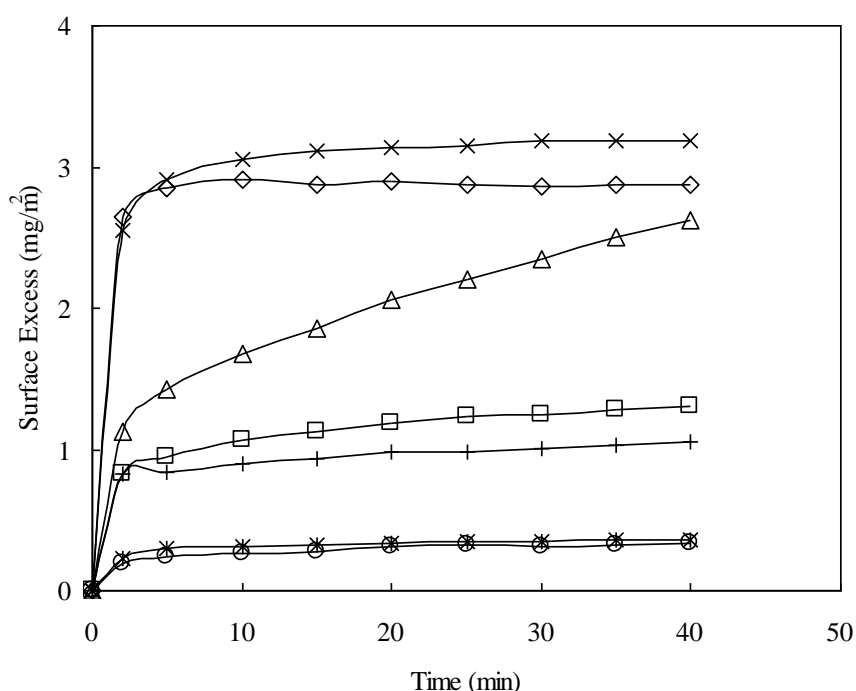


Figure 3.9 The adsorption isotherm of V₆K at 100 μg/ml (×) and C₁₂TAB at 0.128 mM (○); 2.63 mM (*); 12 mM (□). The co-adsorption was at the molar ratio of C₁₂TAB and V₆K of 1:1(◇), 20:1(Δ) and 94:1(+). V₆K was fixed at 100 μg/ml, all at pH 7. (Jayawardane et al ¹⁴³, Published by The Royal Society of Chemistry).

C₁₂TAB/V₆K Mixed Solution Adsorption at the Solid/Liquid Interface. C₁₂TAB was selected to investigate the effect of cationic surfactants on the adsorption of V₆K peptide and to draw comparison with the SDS/V₆K system. The co-adsorption of C₁₂TAB and V₆K at varying molar ratios, as well as the adsorption of pure peptide and pure C₁₂TAB at equivalent molar concentrations, is shown in Figure 3.9. The adsorption dynamics of

C₁₂TAB and V₆K at a ratio of 1:1 was similar to the pure peptide but had a slightly lower surface excess. Increasing the ratio to 20:1 caused the final plateau to reduce further with a noticeable slowing of the adsorption process. Further increase in the ratio to 94:1 resulted in a significant drop of the surface excess. At 94:1, C₁₂TAB had reached its CMC and was highly in excess. Indeed, both the surface excess and the adsorption dynamics closely resembled the adsorption of pure C₁₂TAB at 12 mM (CMC).

The SE results show both the surfactant and the peptide competing for adsorption at the interface. At the highest ratio (94:1) the adsorption was dominated by C₁₂TAB, limiting total adsorption to under 1.3 mg/m². However, it is not clear from the SE results alone how the two components coexisted and arranged themselves at the interface.

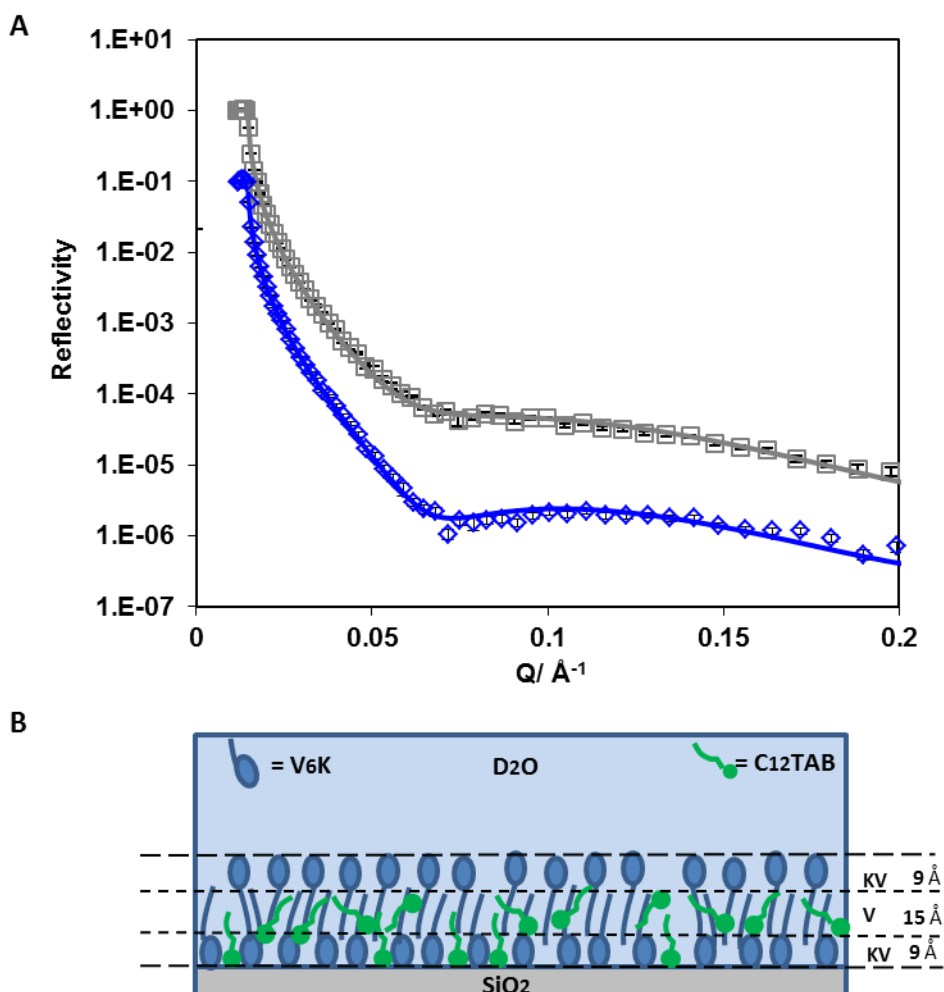


Figure 3.10 A, Reflectivity profiles for: $C_{12}TAB/V_6K$ (20/1) mixture (\square) and $d-C_{12}TAB/V_6K$ (20/1) (\diamond). Solid lines through the data points correspond to the model fits for the corresponding reflectivity data points. B, Schematic diagram showing the arrangement of V_6K molecules (blue), $C_{12}TAB$ (green) at $C_{12}TAB/V_6K=20/1$, at the SiO_2 interface in D_2O pH 7. (Jayawardane et al ¹⁴³, Published by The Royal Society of Chemistry).

NR was used to probe the arrangement of the two molecules at a molar ratio of 20:1. Figure 3.10A shows neutron reflection data and model fits for the adsorption of $C_{12}TAB$ and $d-C_{12}TAB$ with V_6K in D_2O pH 7. Analysis of the data revealed a bilayer structure retained by the V_6K peptide but had significant amounts of $C_{12}TAB$ incorporated within it (Table 3.4).

Table 3.4 Structural parameters obtained from model best fits of neutron reflection data shown in Figure 3.10 for the co-adsorption of C₁₂TAB/V₆K in D₂O at pH 7. (Jayawardane et al ¹⁴³, Published by The Royal Society of Chemistry).

Sample/Contrast	Fitted Thickness ss ±2 Å	Fitted SLD ±0.1×10 ⁻⁶ / Å ⁻²	Sample SLD (V ₆ K/SDS) ±0.01×10 ⁻⁶ / Å ⁻²	Volume Fraction (V ₆ K/SDS) ±0.005	Γ (V ₆ K/SDS) ±0.1 mg/m ²	
C ₁₂ TAB/V ₆ K (20/1)/D ₂ O	kV	9	4.4	2.13/-0.24	0.375/0.055	0.5/0.1
	v	15	1.4	1.54/-0.24	0.750/0.205	1.3/0.3
	kV	9	4.6	2.13/-0.24	0.385/0.020	0.5/0.0
					Γ _{Total} 2.7	
d-C ₁₂ TAB/V ₆ K (20/1)/D ₂ O	kV	9	4.7	2.13/5.13	0.375/0.055	0.5/0.1
	v	15	2.5	1.54/5.13	0.750/0.205	1.3/0.3
	kV	9	4.7	2.13/5.13	0.385/0.020	0.5/0.0
					Γ _{Total} 2.7	

The inner layer was dominated by V₆K and only 0.1 mg/m² (0.3×10^{-3} mM/m²) of C₁₂TAB present. The bilayer core was densely packed and housed the largest amount of C₁₂TAB, 0.3 mg/m² (1.0×10^{-3} mM/m²), and the outer layer had no surfactant present as shown in the schematic diagram Figure 3.10B. Peptide molecules adsorbed faster and in higher amount than C₁₂TAB, allowing the peptide to form a bilayer and in the process trapping C₁₂TAB within its core. Following the formation of the bilayer, electrostatic repulsion stopped additional adsorption onto the co-adsorbed layer. This supports the SE results which suggest competitive adsorption of C₁₂TAB at the interface with increasing amounts of surfactant under increasing molar ratio.

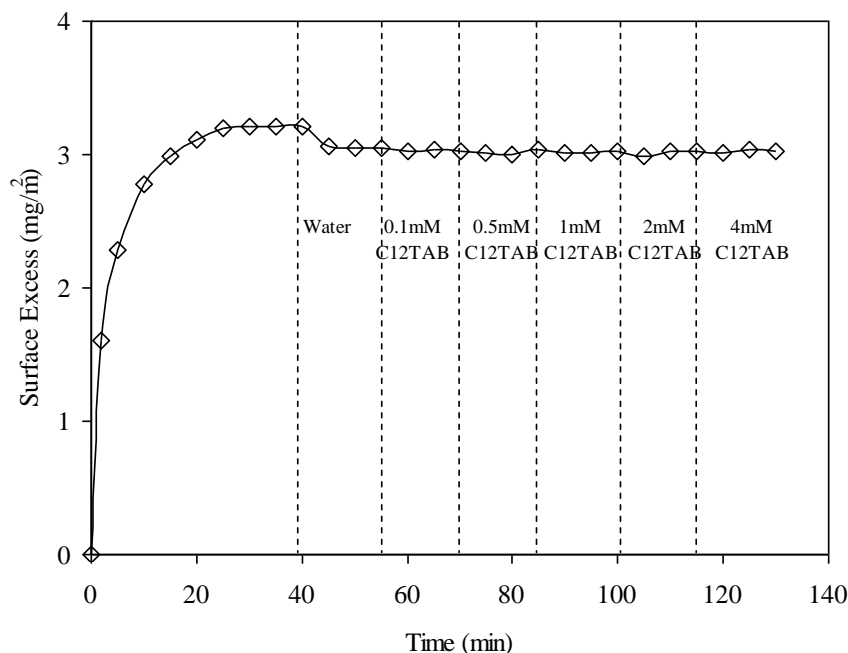
3.4.4 Interaction of C₁₂TAB with pre-adsorbed V₆K peptide

Figure 3.11 Ellipsometry data showing the adsorption isotherm of V₆K (100 µg/ml, pH 7) at silica/water interface and washed by water and different concentration of C₁₂TAB (from 0.1mM to 4mM). (Jayawardane et al ¹⁴³, Published by The Royal Society of Chemistry).

Interaction of C₁₂TAB with Pre-adsorbed V₆K Peptide. Following the adsorption of V₆K, at 100 µg/ml, the adsorbed layer was rinsed with UHQ water. The layer was subsequently subjected to a series of concentrations of C₁₂TAB solution ranging from 0.1 mM to 4 mM (Figure 3.11). As it was outlined earlier for the SDS adsorption results, there was minimal peptide loss during the UHQ rinse, however, in contrast to the SDS system, no increase of surface excess was observed when C₁₂TAB solutions were added. The pre-adsorbed peptide layer prevented any C₁₂TAB adsorbing onto the surface. This is likely an indication of a charge reversal of the surface. A charge reversal of the surface to slightly positive would result in the presence of some bound counterions which would hamper the approach of any C₁₂TAB molecules. Surfactant molecules approaching the

surface would cause an increase of the same counterions already present in the region resulting in osmotic forces pushing the surfactant molecules away.

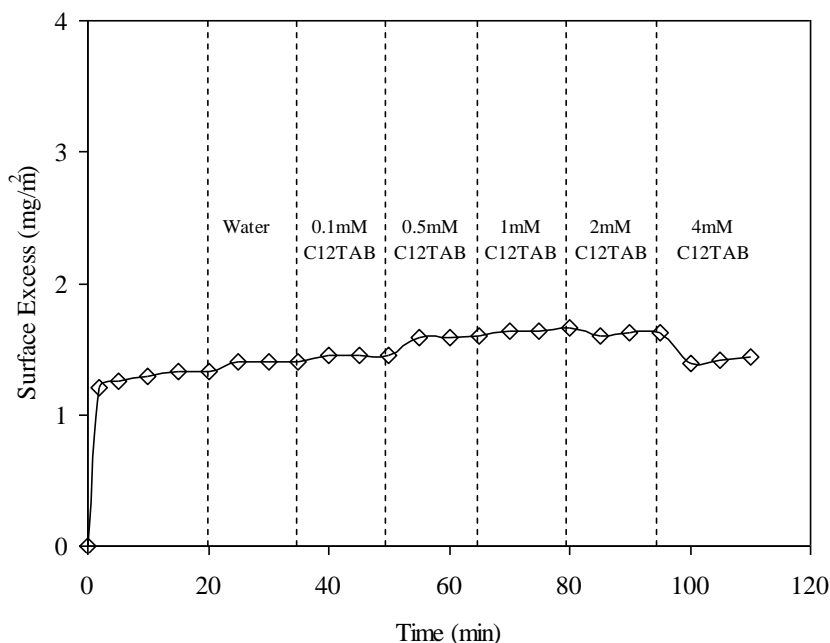


Figure 3.12 Ellipsometry data showing the adsorption of V₆K (100 µg/ml, pH 7) at C₈/water interface and washed by water and different concentration of C₁₂TAB (from 0.1 mM to 4 mM). (Jayawardane et al ¹⁴³, Published by The Royal Society of Chemistry).

Surface Effect. Addition of up to 2 mM C₁₂TAB onto pre-adsorbed V₆K on hydrophobic C₈ surface (Figure 3.12) yielded a maximum increase of less than 0.4 mg/m² (1.3×10^{-3} mM/m²). Similar to the SDS system, the increase in total surface excess upon C₁₂TAB addition was attributed to the hydrophobic interaction between the exposed hydrophobic valine tails and the hydrocarbon tails of C₁₂TAB. This highlights the strength of hydrophobic interactions which enabled the C₁₂TAB to adsorb onto the surface even in the presence of like charges. However, the adsorption of C₁₂TAB was less than that of SDS 1.2 mg/m² (4.2×10^{-3} mM/m²) and further increase to 4mM resulted in a drop in adsorbed amount.

3.5 Conclusion

In this study, spectroscopic ellipsometry and neutron reflection were used to evaluate the adsorption behaviour of V₆K peptide and its interaction with conventional surfactants SDS and C₁₂TAB. When the peptide was pre-adsorbed it was able to form a stable bilayer with good coverage and stability. At the highest concentration of 100 µg/ml, the bilayer formed was very stable against rinsing by UHQ water and adsorption of SDS molecules. The positively charged lysine heads exposed on pre-adsorbed peptide layers facilitated SDS adsorption but hampered C₁₂TAB adsorption. When SDS and V₆K are mixed together in solution, adsorption showed a strong dependence on the molar ratio of the two components. SDS has a neutralizing effect on adsorption and when the molar unity was reached no adsorption was detected. Below molar unity, excess V₆K aided SDS adsorption onto the surface. This behaviour is analogous to several polymer and polyelectrolyte systems which adsorb and cause charge reversal of the SiO₂ surface and increase hydrophobic interactions thus aiding SDS adsorption.^{144, 145, 148, 149} On the other hand, when C₁₂TAB is combined with V₆K in solution, the adsorption became competitive. Above surfactant CMC, V₆K was stopped from adsorbing at the interface but at lower molar ratios V₆K was able to adsorb at the interface faster than C₁₂TAB and could coexist with C₁₂TAB at the interface. These results are also consistent with other studies involving cationic surfactant mixtures.^{144, 149} Overall, the results indicate that V₆K was able to adsorb faster at the solid/liquid interface with the exact amount depending on the ratio and other factors. The fast adsorption and stability of V₆K in the presence of surfactants shows some potential for the peptide to be used as a co-surfactant at the solid interface.

4 SILK FIBROIN SOLID-LIQUID ADSORPTION

Part of this work has been published in *Langmuir*: Jayawardane et al. Interfacial adsorption of silk fibroin peptides and their interaction with surfactants at the solid-water interface. **Langmuir** 2016, 32 (32), pp 8202–8211.

4.1 Overview

Regenerated silk fibroin (RSF) is a FDA approved material and has been widely used in many biomedical applications. Its molecular structure has repeating hydrophobic/hydrophilic segments which are reminiscent of peptides such as previously discussed V₆K, which demonstrated very good adsorption. However, so far, RSF adsorption behaviour has not been characterised at the solid-liquid interface. A better understanding of the adsorption can lead to its potential use as a surface active component for a range of applications particularly in biomedical, cosmetic, pharmaceutical and food

industries. Hence, RSF adsorption is initially investigated with regards to MW, pH and ionic strength, using neutron reflection and spectroscopic ellipsometry to assess its surface active behaviour and structure at the interface. Subsequently adsorption is investigated with conventional anionic and cationic surfactant molecules, sodium dodecyl sulphate (SDS), and dodecyl trimethyl ammonium bromide (C₁₂TAB). In order to assess how RSF interacts with conventional surfactants if it were to be used in formulations with such molecules.

4.2 Introduction

Surfactants are of interest in many fields ranging from bioremediation¹⁵⁰, biomedical applications^{151, 152}, food industry^{6, 153} and personal care.^{25, 26} Current environmental requirements place emphasis on the use of biosustainable and biodegradable surfactant based products pushing industries to search for multi functioning surfactants derived from natural sources.¹⁹ To meet requirements and increase consumer appeal, alternatives to conventional petrochemical derived surfactants are highly sought after. In this landscape, the search for new bio-polymer surfactants derived from proteins has become an important area of research, as they possess desirable physicochemical properties and a biocompatible and environmentally friendly nature.¹⁵⁴ Silk fibroin is a protein which has been extensively studied as a biomaterial⁹¹, attracting much attention for its biodegradable and biocompatible¹⁰⁰ properties as well as other excellent material properties (e.g. strong mechanical strength) making it highly versatile for use in a diverse range of applications from tissue engineering scaffolds to drug delivery vectors.¹⁵⁵⁻¹⁵⁸ However silk fibroin's interfacial adsorption behaviour and its surface active properties are poorly understood

and have not been extensively characterized thus limiting its potential use as a surface active agent and its possible applications.

The molecular structure of native silk fibroin, extracted from the silk worm *Bombyx Mori*, consists of a light chain (25 kDa) and a heavy chain (391 kDa). Repetitive crystalline regions are found in the chain, which is mainly based on a Gly-X sequence as well as a repetitive hexapeptide sequence of Gly-Ala-Gly-Ala-Gly-X, where X is one of Ala>Ser>Tyr.^{93, 94} Hydrogen bonding between these crystalline regions gives rise to insoluble silk II (beta sheet) structure found in fibres. Most dissolution methods employ chaotropic agents to disrupt the hydrogen bonds holding the silk II structure in place. However, the regenerated silk fibroin arising from the dissolution process has been observed to yield a very broad range of molecular sizes (other than 25 kDa and 391 kDa) indicating fragmentation of the native silk fibroin chains into a complex mixture of peptides.^{96, 159} The resulting peptides can resemble common surfactant structures, embodying an amphiphilic nature with a hydrophilic head and hydrophobic tail.⁶⁶ The repetitive nature of silk fibroin's amino acid sequence indicates the presence of hydrophilic segments arising from the hydroxyl side chains present on amino acids such as Ser and Tyr and carboxyl group of the C terminal, and hydrophobic segments from methyl side chains found in Gly-Ala segments. Hence the dissolution process can liberate shorter peptide sequences which possess a stronger amphiphilic character and surfactant properties. Similarly, food proteins such as pea protein and whey have been chemically or enzymatically digested in order to produce low molecular weight with enhanced surface active behaviours.^{89, 90, 160, 161}

A detailed understanding of RSF's adsorption behaviour is necessary in order to exploit desirable surface active properties and compare its adsorption behaviour with other biopolymers and biosurfactants.^{4, 137} Over the years much effort has gone into studying the adsorption of proteins^{42, 48, 162, 163} at interfaces which can have complex adsorption

behaviours, especially in mixed systems.¹⁶⁴ Regenerated silk fibroin is inherently a complex mixed system and filtration of the solution can yield fractions which exhibit distinct behaviours adding value to the product.¹⁶⁵⁻¹⁶⁸ The effect of different bulk solution conditions is investigated and the effect of conventional surfactants on the silk fibroin peptide's adsorption at the SiO₂/water interface. Neutron reflection and spectroscopic ellipsometry are used to study interactions for their combined excellent ability to study buried interfaces, adsorption behaviour and probe the structures found at the solid/liquid interface.¹⁶⁹⁻¹⁷³

4.3 Experimental method

4.3.1 Silk preparation

Silk fibroin peptides with molecular weight cut-offs (MWCO) of 5-30 kDa, 30-300 kDa and over 300 kDa were obtained from Huaian Hongma biotech Ltd, China. For information, *Bombyx Mori* silk was degummed by boiling in 0.02 M Na₂CO₃ for 30 min before being dissolved in Ajisawa's reagent at 75°C for 3 hours.¹⁷⁴ Samples were ultrafiltrated using different membranes to obtain the RSF peptides with different molecular weight ranges and then lyophilized. Fresh solutions of silk fibroin peptides were dissolved in ultra-high quality milli Q water (UHQ) or D₂O (Sigma-Aldrich, UK). Stock solutions of silk fibroin peptides were then diluted to achieve the appropriate concentrations. Sodium chloride (Sigma-Aldrich, UK) was used to adjust salt concentration and pH was adjusted using minimum amount of NaOH (or NaOD) or HCl (or DCl) (Sigma-Aldrich, UK) as appropriate. For both Ellipsometry and neutron reflection experiments, silk fibroin was allowed to adsorb for 1 hour onto the SiO₂/water

interface. Surfactants SDS and C₁₂TAB were purchased from Sigma-Aldrich, UK and their deuterated versions were contributed by Dr R. K. Thomas, Physical & Theoretical Chemistry lab, University of Oxford. All surfactants were purified and dissolved in UHQ (or D₂O) stock solutions ready for dilution and use in experiments.

4.3.2 Spectroscopic Ellipsometry

SE measurements were determined by Jobin-Yvon UVISSEL spectroscopic ellipsometer. The SE measurements were performed over a wavelength range between 300 and 600 nm. A liquid cell with fused quartz windows was used to enable the SE measurement at the solid/liquid interface with the incident light beam at 70°. The experimental data were analysed using software called DeltaPsi II developed by Jobin-Yvon. The ellipsometer measured the change in the polarization state of light reflected from the surface of the sample.

4.3.3 Neutron reflection

NR measurements were carried out on SURF at RAL, Oxford, UK, using a neutron beam of wavelength 0.5 to 6.5 Å. The silicon blocks used were polished by Crystran Ltd., UK and treated with Piranha solution at 90 °C for 1 min. Solution samples (2 ml) were filled into the lumen cell made by clamping a Perspex trough against the polished face of a silicon block with dimensions of 6 × 5 × 1.2 cm³. The sample cell was mounted on a goniometer stage controlled by the computer terminals. The neutron beam entered the small face of the silicon block, was reflected from the solid/solution interface and exited from the opposite end of the small face. The neutron beam was collimated by two sets of

horizontal and vertical slits placed before the sample cell, creating a typical beam illuminated area around $4 \times 3 \text{ cm}^2$. Each reflectivity experiment was carried out at three incidence angles of 0.35 , 0.8 and 1.8° and the resulting reflectivity profiles combined to cover a wave vector (κ) between 0.012 and 0.5 \AA^{-1} . Reflectivity profiles below the critical angle were theoretically equal to unity and all the data measured were scaled accordingly. Constant background was subtracted using the average reflectivity between 0.3 and 0.5 \AA^{-1} . The background was found to be typically around 3×10^{-6} in D_2O .

4.4 Results and discussion

4.4.1 Adsorption of RSF onto SiO_2 /water interface

Ellipsometry experiments were carried out for the adsorption of several concentrations of RSF 5-30 kDa as shown in Figure 4.1A. Neutron reflectivity curves for the same conditions (Figure 4.1B) revealed how the structural arrangement of the peptide changed with concentration at the interface. RSF was adsorbed onto the SiO_2 surface and gradually plateaued over the period of 1 hour. Rinsing of the adsorbed layer with UHQ resulted in minor removal of loosely adsorbed RSF (less than 0.2 mg/m^2 , data not shown), leaving a stable, strongly adsorbed RSF layer behind. The adsorbed amount, following 1 hour adsorption, was seen to increase considerably with bulk solution concentration, from 1.4 mg/m^2 at 0.3 mg/ml up to 3.1 mg/m^2 at 3 mg/ml , further increase in concentration to 10 mg/ml led only to an additional 0.3 mg/m^2 increase in the adsorbed amount, indicating the saturated adsorption was being reached.

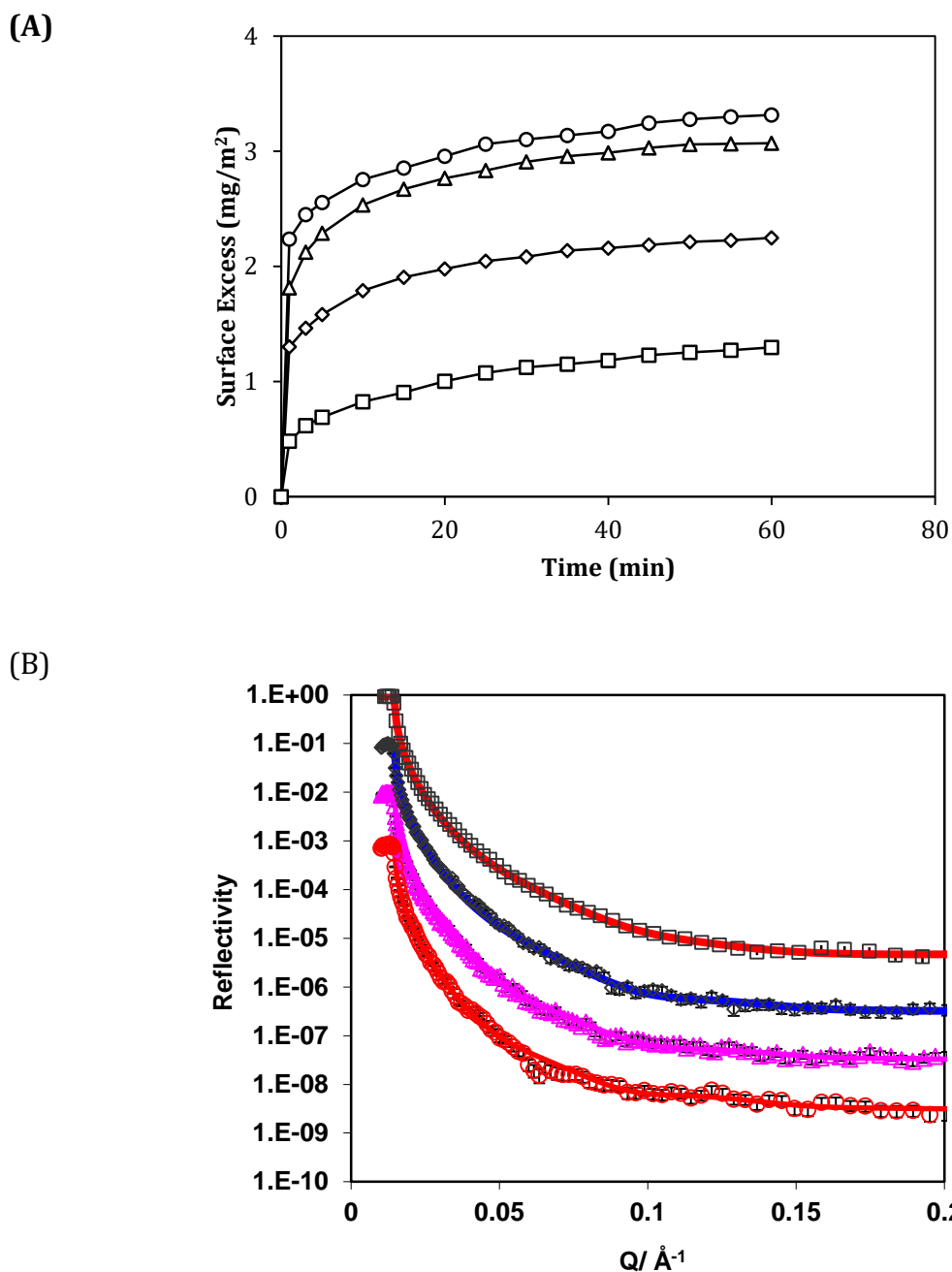


Figure 4.1 (A) Adsorption kinetics for RSF 5-30 kDa at concentrations of 0.3 (\square), 1 (\diamond), 3 (Δ) and 10 (o) mg/ml, pH 7, at the silica/water interface, studied by SE. (B) Reflectivity profiles for RSF 5-30 kDa at concentration of 0.3 (\square), 1 (\diamond), 3 (Δ) and 10 (o) mg/ml, pH 7, at the silica/water interface studied by NR. Solid lines through the data points correspond to the best fits for the corresponding reflectivity curves which are detailed in Table 4.1. Reprinted with permission from Jayawardane *et al.*¹⁷⁵ Copyright 2017 American Chemical Society.

Neutron data fittings shown in Table 4.1 show that RSF 5-30 kDa was fitted using a two layer structure with an overall mean thickness of around 83 Å over the concentration range studied. A single layer fitting could not provide a good fit across the entire Q range. The inner layer was seen to have a lower SLD than the outer layer indicating that most of the peptide was found packed closest to the SiO₂ interface and the outer layer was diffuse with a maximum volume fraction of 14%. Increasing the bulk solution concentration from 0.3 mg/ml to 10 mg/ml caused a gradual lowering of the inner layer SLD from 5.9 to 5.2 ($\times 10^{-6} \text{ \AA}^{-2}$) and a lowering of the outer layer SLD from 6.2 to 6.0 ($\times 10^{-6} \text{ \AA}^{-2}$). The SLD of RSF peptide was calculated to be $3.8 \times 10^{-6} \text{ \AA}^{-2}$, based on its amino acid composition. Hence the lowering of the SLDs was due to RSF peptide adsorbing and packing itself more tightly, as seen by the peptide volume fraction increasing from 17.5% to 45%, at the interface.

Table 4.1 Structural parameters of neutron reflection best fits for 5-30 kDa silk fibroin peptides adsorbed for 1hr at the SiO₂/water interface at pH 7. Reprinted with permission from Jayawardane et al¹⁷⁵. Copyright 2017 American Chemical Society

Concentration (mg/ml)	Layer thickness ($\pm 2 \text{ \AA}$)	SLD $\pm 0.1 \times 10^{-6} \text{ \AA}^{-2}$	Volume fraction ± 0.005	Surface Excess $\pm 0.1 \text{ mg/m}^2$	
				NR	SE
0.3	45	5.9	0.175	1.5	1.4
	43	6.2	0.060		
1	37	5.5	0.335	2.4	2.3
	45	6.1	0.100		
3	37	5.2	0.450	3.2	3.1
	40	6.0	0.140		
10	40	5.2	0.450	3.5	3.4
	43	6.0	0.140		

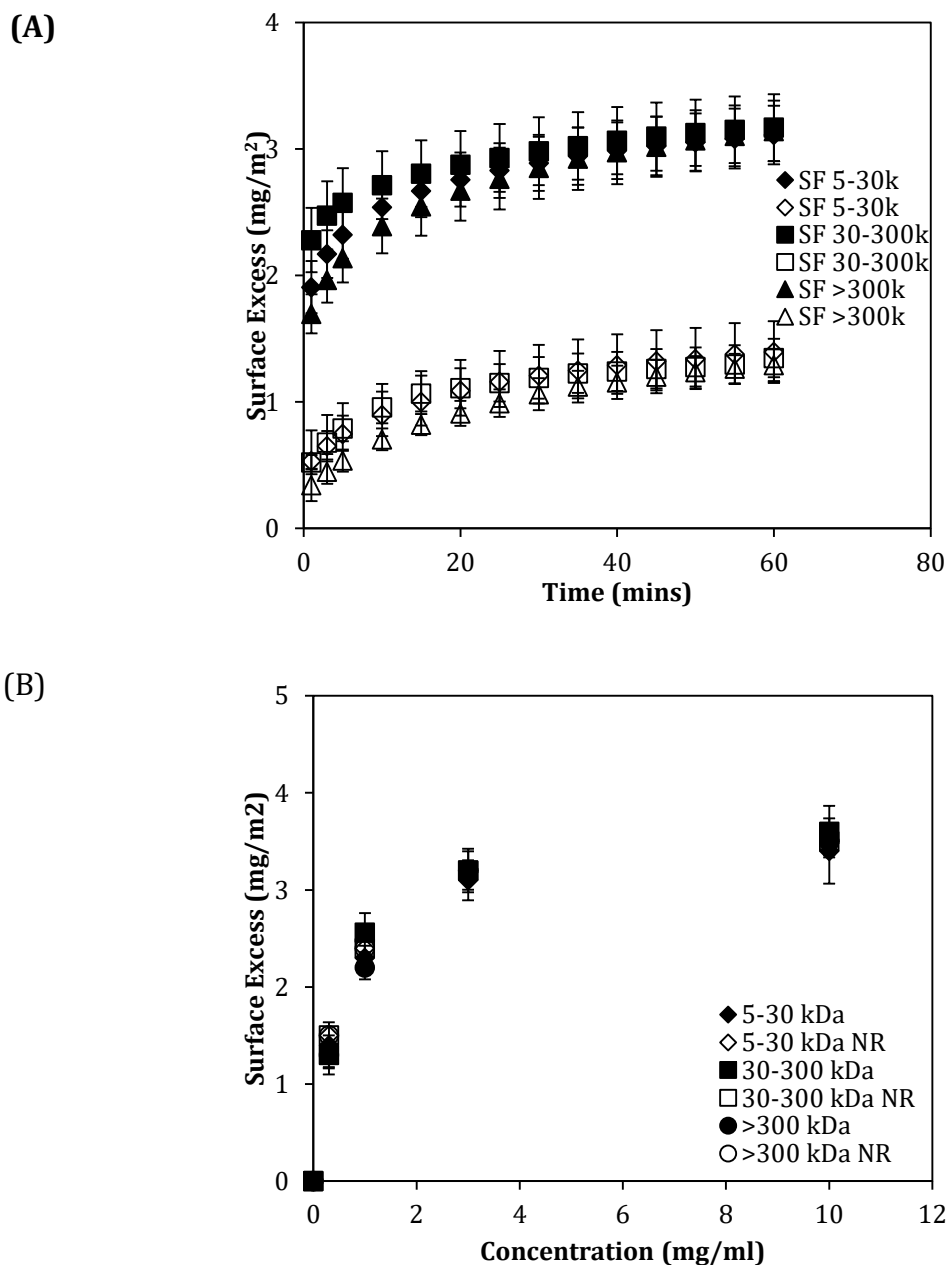


Figure 4.2 (A) Adsorption kinetics (measured by SE) for 0.3 mg/ml (open symbols) and 3 mg/ml (shaded symbols) RSF at the silica/water interface, pH 7. (B) Adsorption isotherms for silk fibroin peptides measured by NR (open symbols) and SE (shaded symbols). Reprinted with permission from Jayawardane et al.¹⁷⁵ Copyright 2017 American Chemical Society.

The surface adsorbed amount obtained from NR was found increased from 1.5 mg/m² at 0.3 mg/ml to 3.5 mg/m² at 10 mg/ml. This finding is highly consistent with the SE results (Table 4.1).

Figure 4.2A shows data comparing the adsorption kinetics between RSF filtered by MWCOs of 5-30 kDa, 30-300 kDa and >300 kDa at concentrations of 0.3 and 3 mg/ml, and Figure 4.2B highlights the agreeing data between the adsorption isotherms measured by SE and NR. There appeared to be no major differences in the absorbed amounts and the structural arrangement of RSF following 1 hour adsorption between the three molecular ranges of RSF fractions at the SiO₂/water interface (shown in Figure 4.3 and Table 4.2, and Figure 4.4 and Table 4.3). However, the adsorption kinetics shown in Figure 4.2A seem to show marginally slower initial adsorption rate by RSF >300 kDa during the first minutes of adsorption at both 0.3 and 3 mg/ml. This would be consistent with a slower adsorption due to slower diffusion resulting from a larger molecular size.

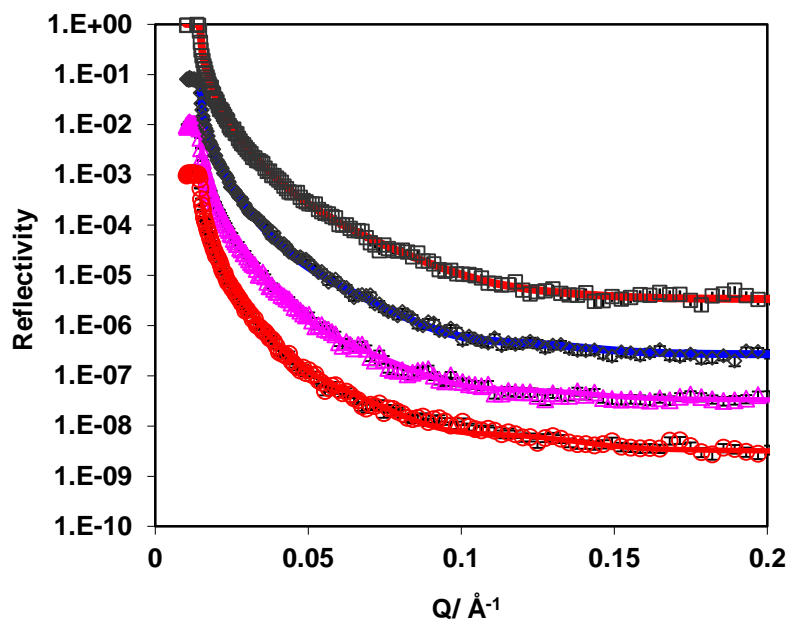


Figure 4.3 Reflectivity profiles for SF 30-300 kDa pH 7 at concentrations of 0.3 (\square), 1 (\diamond), 3 (Δ) and 10 (\circ) mg/ml. Solid lines through the data points correspond to the best fits for the corresponding reflectivity curves which are detailed in **Table 4.2**. Reprinted with permission from Jayawardane et al.¹⁷⁵. Copyright 2017 American Chemical Society

Table 4.2 Structural parameters of neutron reflection best fits for 30-300 kDa silk fibroin peptides adsorbed for 1hr at the SiO₂ interface at pH7. Reprinted with permission from Jayawardane et al.¹⁷⁵ Copyright 2017 American Chemical Society.

Concentration (mg/ml)	Layer thickness (± 2 Å)	SLD $\pm 0.1 \times 10^{-6} / \text{Å}^{-2}$	Volume fraction ± 0.005	Surface Excess ± 0.1 mg/m ²	Ellipsometry ± 0.1 mg/m ²
0.3	36	5.8	0.215	1.5	1.6
	38	6.2	0.060		
1	37	5.5	0.335	2.4	2.5
	45	6.1	0.100		
3	37	5.2	0.450	3.2	3.2
	40	6.0	0.140		
10	40	5.2	0.450	3.5	3.6
	43	6.0	0.140		

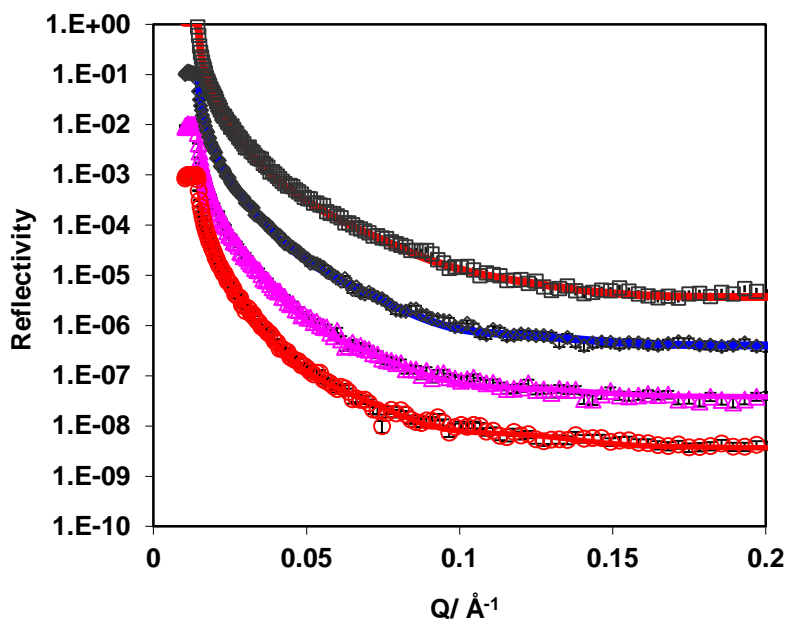


Figure 4.4 Reflectivity profiles for SF >300 kDa pH7 at concentrations of 0.3 (\square), 1 (\diamond), 3 (Δ) and 10 (\circ) mg/ml. Solid lines through the data points correspond to the best fits for the corresponding reflectivity curves which are detailed in **Table 4.3**. Reprinted with permission from Jayawardane et al.¹⁷⁵. Copyright 2017 American Chemical Society

Table 4.3. Structural parameters of neutron reflection best fits for >300 kDa silk fibroin peptides adsorbed for 1hr at the SiO₂ interface at pH7. Reprinted with permission from Jayawardane et al.¹⁷⁵ Copyright 2017 American Chemical Society.

Concentration (mg/ml)	Layer thickness (± 2 Å)	SLD $\pm 0.1 \times 10^{-6} / \text{Å}^{-2}$	Volume fraction ± 0.005	Surface Excess ± 0.1 mg/m ²	Ellipsometry ± 0.1 mg/m ²
0.3	45	5.9	0.175	1.5	1.3
	43	6.2	0.060		
1	37	5.5	0.335	2.4	2.2
	45	6.1	0.100		
3	37	5.2	0.450	3.2	3.2
	40	6.0	0.140		
10	40	5.2	0.450	3.5	3.4
	43	6.0	0.140		

4.4.2 Effect of pH on the adsorption of RSF

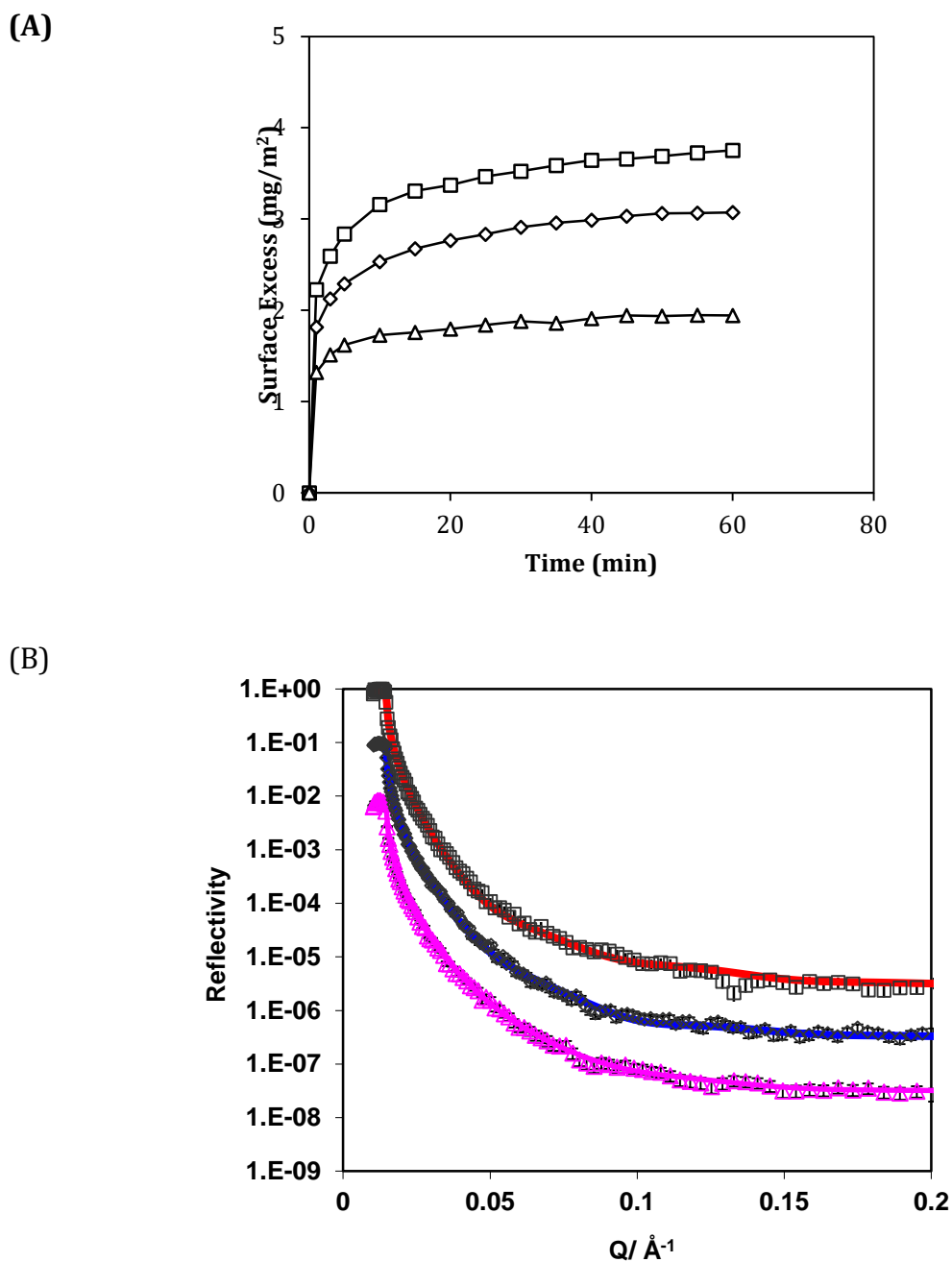


Figure 4.5 (A) Adsorption kinetics for RSF 5-30 kDa at the concentration of 3 mg/ml at pH 5 (\square), pH 7 (\diamond) and pH 9 (Δ) at the silica/water interface, studied by SE. (B) Reflectivity profiles for 3 mg/ml RSF 5-30 kDa at pH 5 (\square), pH 7 (\diamond) and pH 9 (Δ) studied by NR. Solid lines through the data points correspond to the best fits for the corresponding reflectivity curves. Reprinted with permission from Jayawardane et al.¹⁷⁵ Copyright 2017 American Chemical Society.

Ellipsometry and neutron reflection were used to study how changes in the pH solution affected the adsorption behaviour of RSF at the SiO₂/water interface. The solution pH has an effect on both SiO₂ and peptide surface charge density. In the case of SiO₂, the surface charge becomes weakly negative above pH 2, and between pH 5-9 there is a small increase in surface charge density. Silk Fibroin has an isoelectric point of around 4.53,¹⁷⁶ changes in the solution pH above this cause the charge densities on the peptide to increase and consequently affect the adsorption process and adsorbed layer structure at the interface. The results in Figure 4.5A clearly show a pH dependant reduction in the adsorbed amount with increasing pH for a fixed 3 mg/ml solution of RSF 5-30 kDa solution. The surface adsorbed amount reduced from 3.6 mg/m² at pH 5, to 3.1 mg/m² at pH 7, and dropped to 2.1 mg/m² when pH increased to 9 (Table 4.4).

Table 4.4 Structural parameters of neutron reflection best fits for pH effect on RSF 5-30 kDa adsorbed for 1hr at the SiO₂/water interface at a concentration of 3 mg/ml Reprinted with permission from Jayawardane et al.¹⁷⁵ Copyright 2017 American Chemical Society.

pH	Layer thickness (±2 Å)	SLD ±0.1×10 ⁻⁶ Å ⁻²	Volume fraction ±0.005	Surface Excess ±0.1 mg/m ²	
				NR	SE
5	42	5.1	0.490	3.8	3.6
	40	6.0	0.140		
7	37	5.2	0.450	3.2	3.1
	40	6.0	0.140		
9	39	5.5	0.335	2.3	2.1
	42	6.2	0.060		

The results highlight the importance of electrostatic forces on the adsorbed RSF layer. As pH increases the RSF peptide gains a more negatively charged character and thus

experiences more inter and intra-molecular like-charge repulsive forces which combined with the negatively charged SiO₂ surface results in lower adsorbed amounts and a more diffuse adsorbed layer. NR data shown in Figure 4.5B and Table 4.4 reveals the structural changes that occur to the adsorbed layer as pH is increased. The layer SLDs increase in both the inner and outer layers with pH, with a decreasing peptide volume fraction from 49% to 35.5% for the inner layer and from 14% to 6% for the outer layer, indicating a more diffuse layer and a lower surface adsorbed amount. However, the layer thicknesses for both inner and outer layers did not change much with pH (both layers are around 40 Å). The same trend was seen with the other MW fractions (*30-300 kDa and >300 kDa*) of RSF (Figure 4.6 and Table 4.5, Figure 4.7 and Table 4.6).

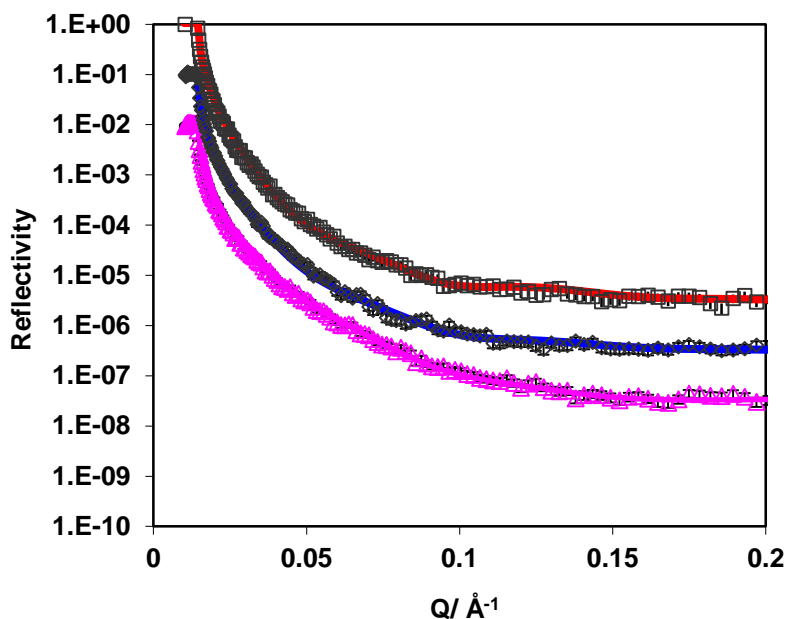


Figure 4.6 Reflectivity profiles for 3 mg/ml SF 30-300 kDa at pH 5 (\square), pH 7 (\diamond) and pH 9 (Δ). Solid lines through the data points correspond to the best fits for the corresponding reflectivity curves which are detailed in **Table 4.5**. Reprinted with permission from Jayawardane et al.¹⁷⁵. Copyright 2017 American Chemical Society

Table 4.5 Structural parameters of neutron reflection best fits for pH effect on 30-300 kDa silk fibroin adsorbed for 1hr at the SiO₂ interface at a concentration of 3 mg/ml Reprinted with permission from Jayawardane et al.¹⁷⁵ Copyright 2017 American Chemical Society.

pH	Layer thickness (± 2 Å)	SLD $\pm 0.1 \times 10^{-6} / \text{Å}^{-2}$	Volume fraction ± 0.005	Surface Excess $\pm 0.1 \text{ mg/m}^2$
5	37	5.0	0.530	3.9
	42	5.9	0.175	
7	36	5.2	0.450	3.2
	40	6.0	0.135	
9	41	5.9	0.180	1.5
	50	6.2	0.045	

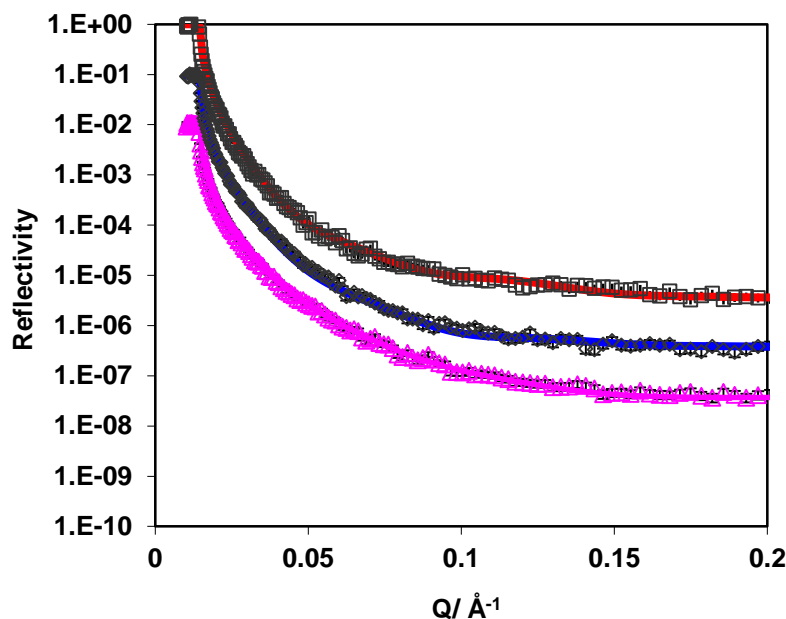


Figure 4.7 Reflectivity profiles for 3 mg/ml SF >300 kDa at pH 5(\square), pH 7(\diamond) and pH 9 (Δ). Solid lines through the data points correspond to the best fits for the corresponding reflectivity curves which are detailed in **Table 4.6**. Reprinted with permission from Jayawardane et al.¹⁷⁵. Copyright 2017 American Chemical Society

Table 4.6 Structural parameters of neutron reflection best fits for pH effect on >300 kDa silk fibroin adsorbed for 1hr at the SiO₂ interface at a concentration of 3 mg/ml Reprinted with permission from Jayawardane et al.¹⁷⁵ Copyright 2017 American Chemical Society.

pH	Layer thickness (± 2 Å)	SLD $\pm 0.1 \times 10^{-6} / \text{Å}^{-2}$	Volume fraction ± 0.005	Surface Excess $\pm 0.1 \text{ mg/m}^2$
5	43	5.1	0.530	4.0
	44	6.0	0.140	
7	38	5.2	0.450	3.3
	42	6.0	0.140	
9	45	5.8	0.215	1.8
	46	6.2	0.060	

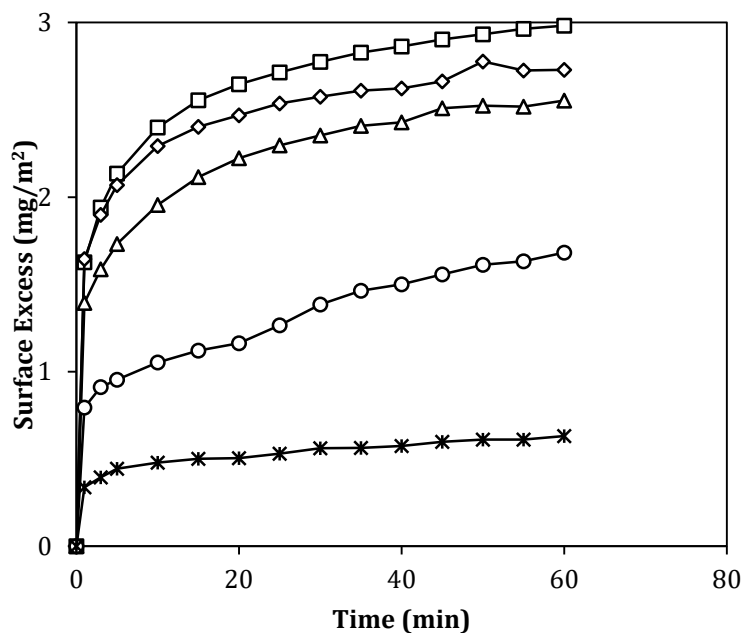
4.4.3 Effect of ionic strength on the adsorption of RSF

To study the effect of solution ionic strength on the adsorption of RSF at the SiO₂/water interface, NaCl was added to RSF solutions of 3 mg/ml and studied by ellipsometer and neutron reflection. Figure 4.8A shows the reduced ability for adsorption by RSF 5-30 kDa with increasing ionic strength. The adsorbed amount was found to be 3.1 mg/m² at 5 mM NaCl and gradually reduced to 0.6 mg/m² when the ionic strength increased to 500 mM. Neutron reflection carried out on the adsorbed layers revealed a falling SLD in the inner layer, from $5.2 \times 10^{-6} \text{ \AA}^{-2}$ (at 5 mM NaCl) to $5.7 \times 10^{-6} \text{ \AA}^{-2}$ (at 150 mM NaCl), and as ionic strength increased a drop in the layer thickness (to 40 Å) in the presence of 500 mM NaCl, as shown in Table 4.7.

Table 4.7 Structural parameters of neutron reflection best fits for NaCl effect on 5-30 kDa silk fibroin peptides adsorbed for 1 hr at the SiO₂/water interface at a concentration of 3 mg/ml, pH 7. Reprinted with permission from Jayawardane et al.¹⁷⁵ Copyright 2017 American Chemical Society.

NaCl (mM)	Layer thickness ±2 Å	SLD ±0.1×10 ⁻⁶ Å ⁻²	Volume fraction ±0.005	Surface Excess ±0.1 mg/m ²	
				NR	SE
5	37	5.2	0.450	2.8	3.1
	44	6.2	0.060		
20	38	5.2	0.410	2.7	2.9
	45	6.2	0.060		
50	40	5.5	0.330	2.5	2.4
	40	6.1	0.100		
150	44	5.7	0.255	1.9	1.8
	36	6.2	0.060		
500	42	6.0	0.140	0.8	0.6

(A)



(B)

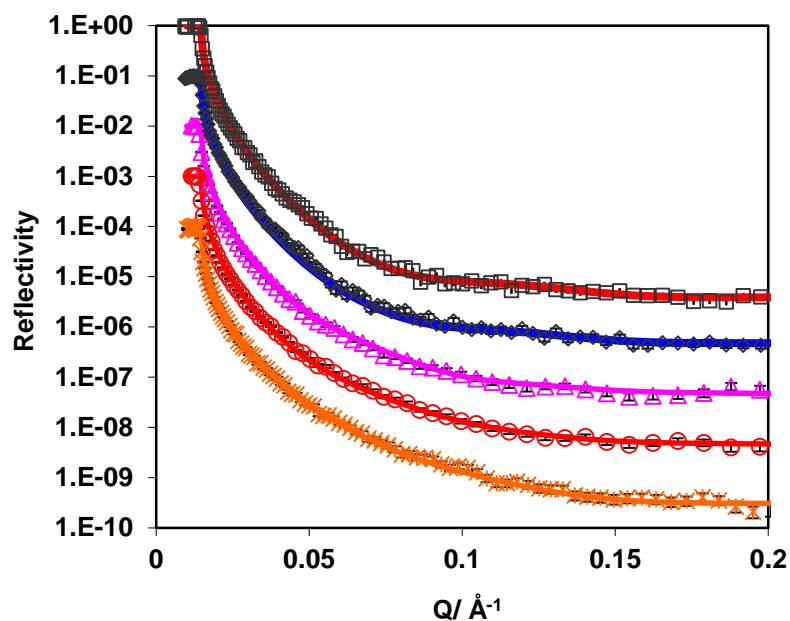


Figure 4.8 (A) Adsorption kinetics for RSF 5-30 kDa 3 mg/ml with NaCl concentrations of 5 (\square), 20 (\diamond), 50 (Δ), 150 (\circ) and 500 ($*$) mM, at the silica/water interface, pH 7 studied by SE. (B) Reflectivity profiles for RSF 5-30 kDa pH 7 with NaCl concentrations of 5 (\square), 20 (\diamond), 50 (Δ), 150 (\circ) and 500 ($*$) mM studied by NR. Solid lines through the data points correspond to the best fits for the corresponding reflectivity curves. Reprinted with permission from Jayawardane et al.¹⁷⁵ Copyright 2017 American Chemical Society.

As the ionic strength of the RSF solution was increased electrostatic charges from both peptide and SiO₂ surface were increasingly flooded with the ions. This impacted on the adsorbed amount by reducing any possible attractive charge interaction between RSF and SiO₂ surface and most importantly it increased peptide-peptide interactions in bulk solution by screening repulsive electrostatic like charges found along RSF chains. Thus preferential peptide-peptide interactions in the bulk solution resulted in lower surface adsorbed amounts at the interface. Increased peptide-peptide interactions at high ionic strengths can result in phase separation or 'salting out' of RSF and the consequent formation of insoluble particles which have potential as drug delivery particles.¹⁵⁷ Similarly, studies with BSA proteins revealed a strong ionic-dependant screening of peptide-peptide repulsive interactions allowing for an enhanced attractive potential between BSA molecules in solution.¹⁷⁷ Adsorptions of other proteins such as β -casein and lysozyme have also been shown to have similar trends when exposed to increasing ionic concentrations.^{178, 179} Figure 4.9, interestingly shows a more stable response by RSF >300 kDa which is able to withstand slightly higher Ionic concentration than the other two RSF fractions. The RSF >300 kDa fraction is likely to have a more stable tertiary structure with less conformational liberty in virtue of its larger size and increased ability to form inter and intramolecular interactions granting it greater stability to changes in ionic strength.

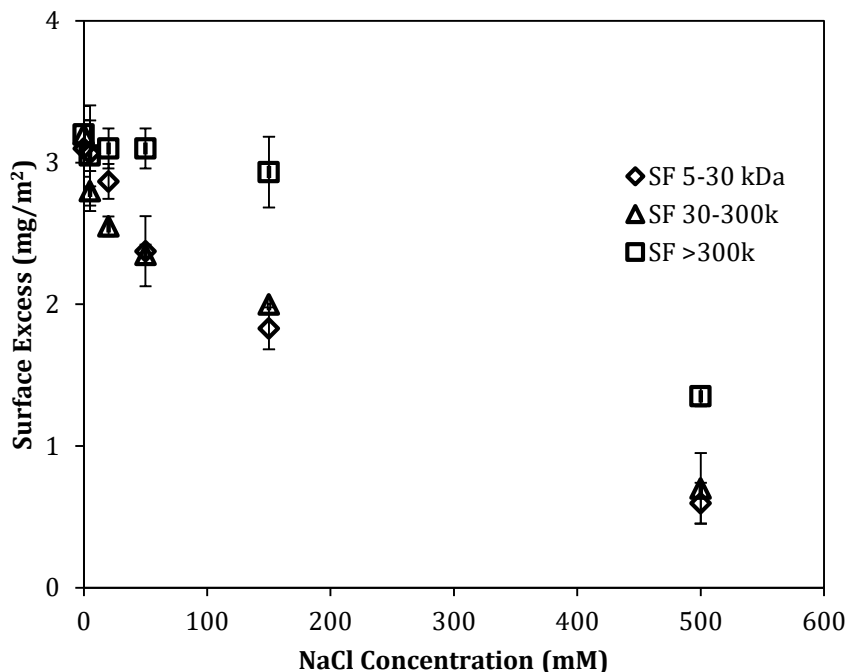


Figure 4.9 Effect of NaCl concentration on the adsorption of 3 mg/ml silk fibroin measured by SE at the silica/water interface, pH 7. Reprinted with permission from Jayawardane et al.¹⁷⁵ Copyright 2017 American Chemical Society.

4.4.4 RSF/SDS interaction at the SiO₂ Interface

RSF at a concentration of 3 mg/ml was initially pre-adsorbed onto the SiO₂ /water interface for 1 hour and then the sample was rinsed with UHQ and then surfactant solution was added. Ellipsometry data shown in **Figure 4.10A** indicates an increase in the overall surface adsorbed amount when increasing surfactant concentration up to a concentration of 0.3 mM SDS, further concentration increases resulted in a gradual reduction in surface adsorbed amount. Anionic surfactants such as SDS do not usually adsorb onto hydrophilic SiO₂ interface due to like charge repulsion. However following the adsorption of a peptide such as RSF the presence of hydrophobic patches can facilitate the adsorption of SDS to the interface causing an increase in the surface adsorbed amounts measured as seen in **Figure 4.10A**.

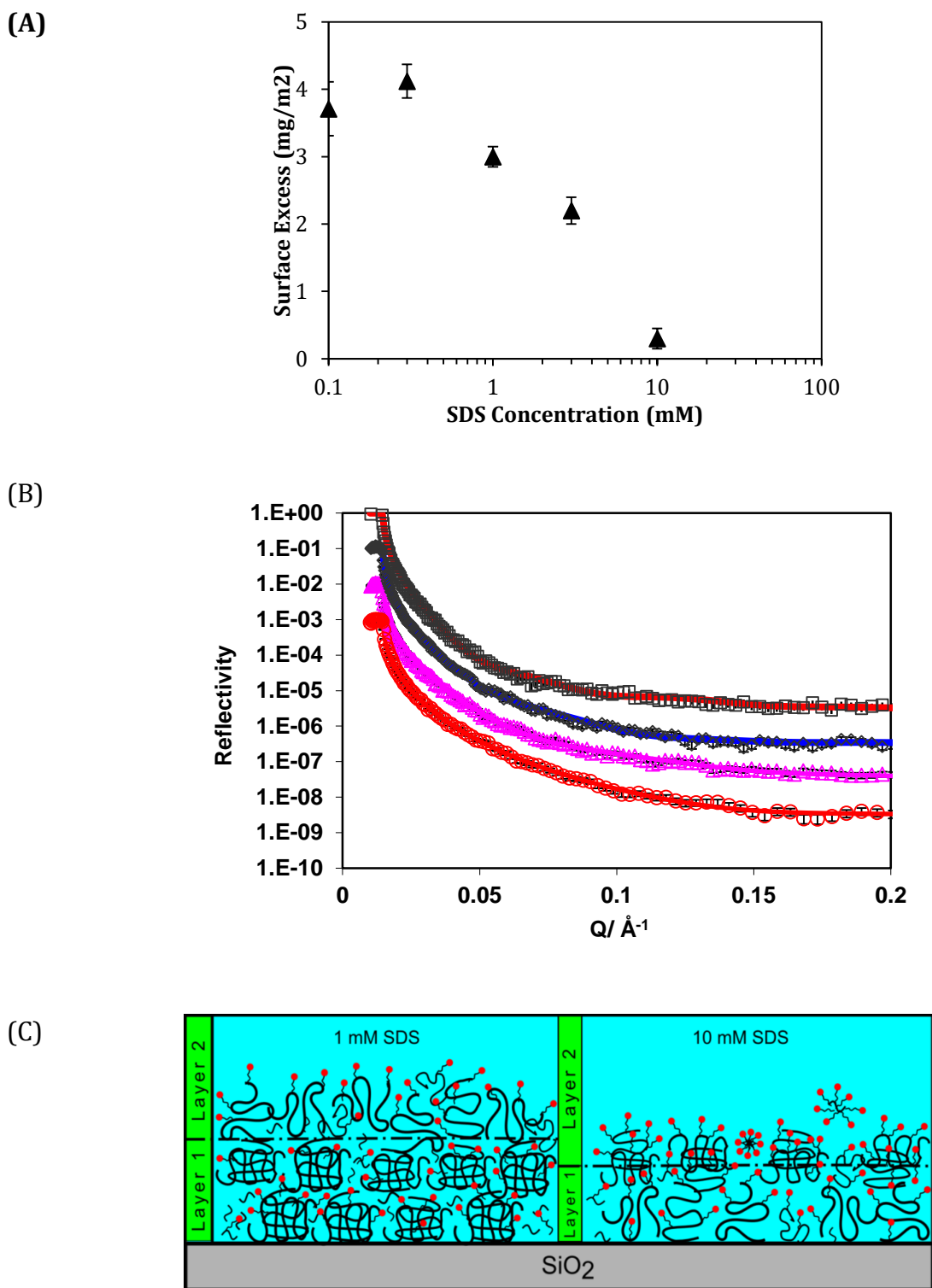


Figure 4.10 (A) Final adsorption values following sequential adsorption of 3 mg/ml silk fibroin (1 hr) and different concentrations of SDS measured by SE at the silica/water interface pH 7. (B) Reflectivity profiles for RSF 5-30 kDa pH 7 with 1 mM SDS (\square), 1 mM d-SDS (\diamond), 10 mM SDS (Δ) and 10 mM d-SDS (\circ). Solid lines through the data points correspond to the best fits for the corresponding reflectivity curves. (C) Schematic model showing the arrangement of RSF molecules (black), SDS (red) at 1 mM and 10 mM SDS. Reprinted with permission from Jayawardane et al.¹⁷⁵ Copyright 2017 American Chemical Society.

Above concentrations of 0.3 mM SDS the surface adsorbed amount is seen to decrease, indicating that it is more energetically favourable for the surfactant-peptide complexes formed at the interface to desorb from the interface and enter the bulk solution. At a concentration of 10 mM SDS, which is above its CMC (8.2 mM), RSF is close to being completely removed from the interface. It was possible to calculate the exact adsorbed amounts of surfactant and RSF adsorbed by running neutron reflection experiments using a deuterated version of SDS (with an SLD of $6.72 \times 10^{-6} \text{ \AA}^{-2}$), and non-deuterated SDS (with an SLD of $0.37 \times 10^{-6} \text{ \AA}^{-2}$). The variation in the SLD layer caused by the isotopic variation of H/D allows to confidently quantify each component at the interface. Neutron reflection fitting shown in Table 4.8 confirmed the presence of SDS in the adsorbed RSF layer and the gradual removal of RSF from the interface. At 1 mM SDS, the surfactant molecules had penetrated into the innermost layer (thickness 34 Å) where most of the peptide resides and where it is able to maximise its hydrophobic interactions most likely with its acyl tail buried into the RSF layer and its hydrophilic head pointing towards the bulk solution. The inner layer SLD in Table 4.8 falls to $4.9 \times 10^{-6} \text{ \AA}^{-2}$ from $5.3 \times 10^{-6} \text{ \AA}^{-2}$ found when SDS is present and the overall layer thickness falls indicating a slightly more compact layer. It was found, at 1 mM SDS, that the inner layer (thickness 34 Å) contains 42% of RSF and 6.5% of SDS while the outer layer (thickness 35 Å) contains 14% of RSF and 3% of SDS. Most of the RSF had desorbed at 10 mM SDS. The thickness of both layers had decreased and most of the remaining RSF and SDS was found in the outer layer. The inner layer (thickness 20 Å) was found to only contain 2.5% of RSF and 3% of SDS while the outer layer (thickness 16 Å) has similar RSF (11.5%) and SDS (11%). The shift in adsorbed amount and volume fraction to the outer layer highlights the desorption process of RSF from the interface and back into the bulk solution complexed with SDS (**Figure 4.10C**). The overall adsorption behaviour with an initial increase in

adsorbed amount followed by gradual removal of the peptide and complete removal above CMC is consistent with systems involving SDS adsorption onto pre-adsorbed BSA, lysozyme and hydrophobin.^{169, 171, 173} For example, similarly to RSF, a two layer adsorption was reported for lysozyme adsorption with a thickness of 30 ± 3 Å for each layer and occupying 46% and 32%, respectively.¹⁷¹ However unlike for RSF, SDS was mainly found to occupy the outer layer with significantly less amount found in the inner most layer, indicating difficulty for the SDS to penetrate all the way and likely due to the more rigid globular structures compared to RSF. Nonetheless complete removal of lysozyme was achieved upon increasing SDS concentration.

Table 4.8 Structural parameters of neutron reflection best fits for 5-30 kDa silk fibroin 3 mg/ml adsorbed for 1 hr at the SiO₂ /water interface followed by SDS adsorption. Reprinted with permission from Jayawardane et al.¹⁷⁵ Copyright 2017 American Chemical Society.

SDS Concentration mg/ml	Layer thickness (±2 Å)	SLD $\pm 0.1 \times 10^{-6} \text{ \AA}^{-2}$	Volume fraction ± 0.005		Surface Excess $\pm 0.1 \text{ mg/m}^2$	
			SDS	Peptide	SDS	Peptide
1 mM SDS	34	4.9	0.065		0.4	
	35	5.8	0.030			
1 mM d-SDS	34	5.3		0.420		2.7
	30	6.0		0.140		
10 mM SDS	20	6.1	0.030		0.3	
	16	5.4	0.110			
10 mM d-SDS	20	6.3		0.025		0.3
	16	6.1		0.115		

4.4.5 RSF/C₁₂TAB interaction at the SiO₂ interface

Experiments were carried out as detailed for C₁₂TAB. Similarly to SDS, there was an initial increase in surface absorbed amount at low surfactant concentrations, in this case up to 2 mM, following which increasing concentrations gradually reduced the absorbed amount as shown in Figure 4.11A. Unlike SDS however, C₁₂TAB is known to absorb directly to the silica/water interface due to charge attraction and is therefore likely to be found in higher amounts at the interface. The SLD of C₁₂TAB used was calculated to be $-0.37 \times 10^{-6} \text{ \AA}^{-2}$, whilst its deuterated version had an SLD of $5.13 \times 10^{-6} \text{ \AA}^{-2}$. Fitted neutron reflectivity data shown in Table 4.9 confirmed the presence of C₁₂TAB in the adsorbed RSF layer even at a concentration of 0.2 mM, lowering the SLD of both the layers, especially the inner most layer. The surfactants occupied 9.5% of the inner layer (thickness 30 Å) and only 4% of the outer layer (thickness 40 Å). The surfactant is likely adsorbed with its cationic head onto the SiO₂ due to electrostatic interactions as depicted in Figure 4.11C.^{47, 180} However, it was not possible to elucidate from the limited reflectivity contrasts the exact orientation (position of hydrophilic head and hydrophobic tail) within the adsorbed layer of C₁₂TAB molecules at the interface. The adsorption of surfactant also appears to render the adsorbed RSF layer more compact with an inner layer volume fraction of 52%. At 20 mM, C₁₂TAB is above its CMC (12 mM) and was found coexisting with RSF at the interface. The adsorbed amount of RSF reduced to 1.2 mg/m² from 3.1 mg/m², and the overall thickness also dropped to around 33 Å.

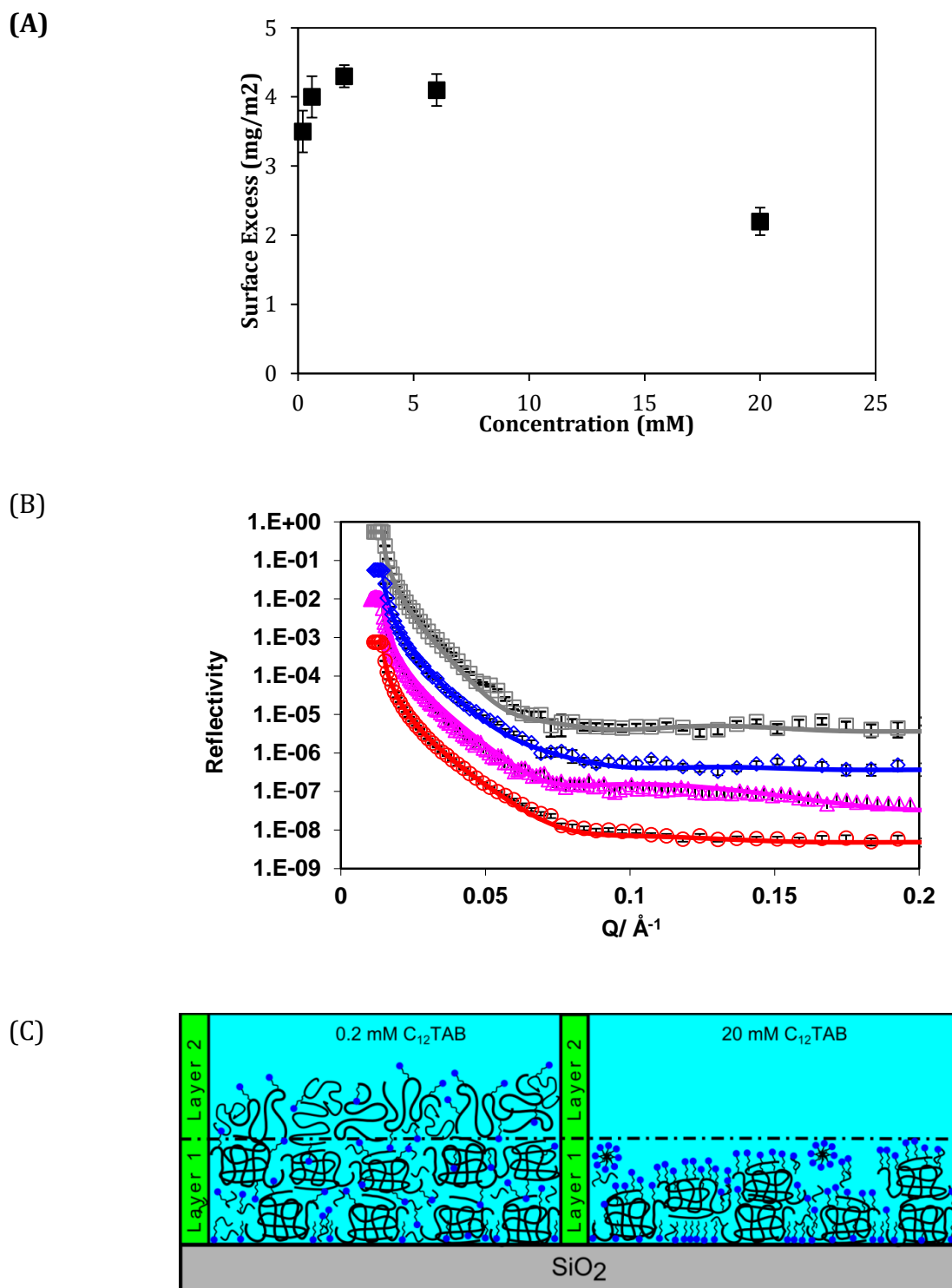


Figure 4.11 (A) Final adsorption values following sequential adsorption of 3 mg/ml RSF (1 hr) and $C_{12}TAB$ measured by ellipsometry at the silica/water interface, pH 7. (B) Reflectivity profiles for RSF 5-30 kDa pH 7 with 0.2 mM $C_{12}TAB$ (\square), 0.2 mM d- $C_{12}TAB$ (\diamond), 20 mM $C_{12}TAB$ (Δ) and 20 mM d- $C_{12}TAB$ (o). Solid lines through the data points correspond to the best fits for the corresponding reflectivity curves. (C) Schematic model showing the arrangement of RSF molecules (black), $C_{12}TAB$ (blue) at 0.2 mM and 20 mM SDS. Reprinted with permission from Jayawardane et al.¹⁷⁵ Copyright 2017 American Chemical Society.

This is consistent with reports of C₁₂TAB forming a uniform layer around 22 Å thick when allowed to adsorb at a hydrophilic SiO₂/water interface,¹⁷² and the layer is consistent with our measurements indicating a thicker layer of 33 Å accounting for the presence of RSF at the interface. C₁₂TAB occupies 33.5% of the adsorbed layer, and RSF only occupies 25%. This sharp reduction in RSF at the interface was forced by the dominating adsorption affinity of C₁₂TAB to the SiO₂/water interface displacing RSF from the interface, but unlike with SDS the surfactant was not able to remove RSF to the same extent. This is also fairly consistent with model adsorption studies involving C₁₂TAB with proteins such as lysozyme and hydrophobin which showed some initial removal from the interface but were able to coexist at the interface even above the surfactants CMC.^{172, 173} Interestingly, unlike RSF, hydrophobin was shown not to adsorb irreversibly onto the hydrophilic SiO₂/water interface, however addition of cationic surfactant was described by the authors as acting as ‘glue’ making the adsorption partially irreversible.¹⁷³

Table 4.9 Structural parameters of neutron reflection best fits for 5-30 kDa silk fibroin 3 mg/ml adsorbed for 1 hr followed by C₁₂TAB adsorption at the SiO₂ /water interface. Reprinted with permission from Jayawardane et al.¹⁷⁵ Copyright 2017 American Chemical Society

Concentration mg/ml	Layer thickness (±2 Å)	SLD ±0.1×10 ⁻⁶ Å ⁻²	Volume fraction		Surface Excess ±0.1 mg/m ²	
			C ₁₂ TAB	Peptide	C ₁₂ TAB	Peptide
0.2 mM C ₁₂ TAB	30	4.4	0.095		0.5	
	40	5.8	0.040			
0.2 mM d- C ₁₂ TAB	30	4.9		0.525		3.0
	40	6.0		0.120		
20 mM C ₁₂ TAB	26	3.5	0.335		0.9	
20 mM d- C ₁₂ TAB	33	5.3		0.250		1.2

4.5 Conclusion

The adsorption of RSF has been studied in detail with regards to solution pH, ionic strength, peptide molecular fraction, concentration and presence of surfactants at the hydrophilic SiO₂/water interface by ellipsometry and neutron reflection. At the SiO₂/water interface RSF was found to adsorb irreversibly and was modelled with a two-layer fitting. Since RSF is a relatively flexible soft protein its adsorption behaviour is similar to a synthetic block co-polymer or other proteins such as β -casein which lack a well-defined tertiary structure, adsorbed as a random walk or as trains and loops at the SiO₂/water interface. Consequently, the layer closest to the interface was modelled as a denser layer and the outer layer represented a diffuse layer of RSF chains looping into the bulk solution. Changes to concentration, pH and ionic strength all had strong impact on the adsorbed amount found at the interface. Increasing pH or ionic strength caused a reduction in the adsorbed amount. This gave an indication about the importance of electrostatic forces in the adsorption process. When pH was increased RSF become more negatively charged. This has two effects, firstly it caused RSF to assume a more extended less compact structure due to inter- and intramolecular repulsive forces and secondly electrostatic repulsive forces were strong enough to negate any hydrophobic interactions holding the peptide together at the SiO₂/water interface. On the other hand, when the ionic strength of the solution was increased peptide-peptide interactions increased due to electrostatic screening effects and RSF molecules found it more energetically favourable to interact with each other in the bulk solution, hence causing a drastic reduction in the adsorbed amount at the interface. In addition the separation of RSF into different MW fractions by membrane ultrafiltration demonstrated that RSF >300 kDa fraction was more stable to ionic strength changes. Hence fractioning of the RSF peptides into more homogenous solutions affects the adsorption behaviour of RSF. Larger RSF molecules

appear to be more stable to ionic concentration and display slower adsorption. Changes in pH, concentration and ionic strength have a similar effect on the adsorption of short amphiphilic designer peptides which were designed to have systematic tweaks in their amino acid sequence to investigate structure function relationships.^{79, 90, 139} Overall the dominating mode of interaction at the interface appeared to be through hydrophobic interactions of the RSF molecules. The presence of these hydrophobic interactions allowed anionic SDS to adsorb at the interface alongside RSF. However, increasing the SDS content above its CMC caused the near complete removal of RSF from the interface. On the other hand, cationic surfactant C₁₂TAB, removed a small amount of RSF and was found to coexist at the interface with a significant amount of RSF, even above its CMC. Both electrostatic and hydrophobic interactions contributed to the permanence of C₁₂TAB with RSF at the interface allowing for greater stability. The interaction with both surfactants followed the behaviour also observed with short cationic peptides (V₆K), biosurfactants and proteins which interact with surfactants and are seen to be gradually displaced by surfactants approaching the surfactant's CMC.^{143, 171-173} Overall RSF shows a good adsorption affinity with the hydrophilic SiO₂/water interface even in the presence of a cationic surfactant. Ultimately, these results give an important insight into how RSF adsorption can be controlled at the interface and this will have important implications for the development of applications based on interfacial adsorption of biomolecules at solid/water interfaces.

5 SILK FIBROIN AIR-LIQUID ADSORPTION

5.1 Overview

The adsorption of RSF at the solid-liquid interface was examined in the previous chapter highlighting the propensity for RSF to adsorb and form a stable layer at the interface. In a similar manner, this chapter characterises the adsorption of RSF at the air-liquid interface and then investigates its adsorption with conventional surfactants SDS and C₁₂TAB. The interfacial behaviour of RSF is investigated using a combination of tensiometer and neutron reflection. Initially, the structural conformations adopted by the adsorbed RSF are discussed with regards to bulk concentration and the effects of solution conditions as well as RSF MW. Surface tension measurements and some foaming studies are used to evaluate the interactions with conventional surfactants at the interface.

5.2 Introduction

Investigating the adsorption at the air-liquid interface is relevant to a wide range of industries from the pharmaceutical industry^{151, 152} to the food industry^{6, 153}. Moreover, adsorption in large amounts at the air-liquid interface is characteristic to surfactant molecules and they have been exploited in a range of applications, such as floatation, pharmaceutical stabilisation, and formulation in agrochemicals¹⁵⁰. However, such surface activity is not limited to surfactants but is also found in some proteins and peptides too. Their attractiveness over conventional surfactants is largely due to their environmental friendliness, biodegradability and biocompatibility. Silk fibroin peptides have the above mentioned attractive features as well as possessing an amino acid sequence which would indicate good surface activity.^{93, 94} Some studies on silk film formation have investigated adsorption at the air-water interface and examined its interfacial rheology and emulsion behaviour highlighting RSF's propensity to adsorb at the interface and form stable viscoelastic films.^{107, 181, 182} The adsorption process and the structures formed at the interface are important when assessing the suitability for applications dependant on surface activity. Understanding its adsorption behaviour and structure at the interface would hence be beneficial for the use of silk fibroin peptides in a range of applications. Detailed molecular studies have discovered some possible molecular conformations adopted by the RSF peptides, identifying silk I (amorphous), silk II (β -sheet rich) and also a silk III structure (three-fold helix).¹⁰⁴⁻¹⁰⁶ In particular, the silk III structure, in the helix form, would enable the alanine and serine (from the GAGAGS repeats) to be found on separate sides of the helix enhancing its amphiphilicity, and it is therefore likely that RSF would adsorb at the interface in this form.¹⁰⁵ Another study, based on interfacial rheology and adsorption kinetics, speculated RSF to initially adsorb as a train and rearrange to favour hydrophobic and hydrophilic interactions.¹⁰⁷ Furthermore, RSF molecules were

thought to adsorb under the initial layer through hydrogen bonding, forming compact multilayers. At higher concentrations it was then suggested that the molecules adopted a beta hairpin structure with its backbones perpendicular to the interface and with significant portion extending out of the liquid surface.¹⁰⁷ However, so far the adsorbed RSF layer has not been physically characterised. In addition, RSF co-adsorption with conventional surfactants has not yet been studied. A range of studies have looked at other protein-surfactant systems and the studies seem to suggest, mechanisms ranging from formation of complexes at the surface, which can enhance adsorption, to competitive adsorption by surfactant molecules which results in the displacement of the proteins from the surface. For example a study of SDS and BSA solution mixtures showed higher surface tension reading in the presence of the protein than the pure surfactant for much of the concentration range studied.¹⁸³ Whilst a similar study involving lysozyme and SDS showed, lower surface tension readings in the presence of the protein.¹⁸⁴ A clearer understanding of the adsorption behaviour and the structural arrangement of RSF at the interface would be beneficial for the advancement in implementation and utilisation of RSF's surface active properties, especially when in mixed formulations.^{4, 137} As such, the adsorption of RSF peptides, the importance of physiochemical properties such as pH, NaCl and the co-adsorption with conventional surfactants were studied. Neutron reflection and surface tension were both used to study interactions for their excellent abilities to study interfacial adsorption behaviour and probe the structures found at the interface.

5.3 Experimental method

5.3.1 Silk preparation

Fresh solutions of silk fibroin peptides were dissolved in ultra-high quality Milli-Q water (UHQ) or D₂O (Sigma-Aldrich, UK). Stock solutions of silk fibroin peptides were then diluted to achieve the appropriate concentrations needed for experiments. Sodium chloride (Sigma-Aldrich, UK) was used to adjust salt concentration and pH was adjusted using minimum amount of NaOH (or NaOD) or HCl (or DCl) (Sigma-Aldrich, UK) as appropriate. Surfactants SDS and C₁₂TAB were purchased from Sigma-Aldrich, UK and their deuterated versions were contributed by Dr R. K. Thomas, Physical & Theoretical Chemistry lab, University of Oxford. All surfactants were purified and dissolved in UHQ (or D₂O) stock solutions ready for dilution and use in experiments.

5.3.2 Neutron reflection

Experiments were carried out on SURF reflectometer. The samples were loaded onto Teflon troughs and were placed on an anti-vibration table on the sample stage. The troughs were then correctly aligned with the neutron beam without tilting the table. The samples were left to equilibrate for at least 1 hour prior to measurement and each reflectivity experiment was carried out at an incidence angle of 1.5°.

5.3.3 Surface tension

A KRUSS K11 Mk4 (Kruss, Hamburg, Germany) was used to measure the surface tension changes over time. The surface tension was determined using a platinum Wilhelmy plate, which was immersed into the sample (6 ml) which was held in a glass container. Temperature was maintained at 20°C by connecting a water bath cooler to the sample holding sleeve. Measurements were stopped when the standard deviation fell below 0.075 mN/m. Prior to each measurement the platinum Wilhelmy plate was flame heated until incandescent and then allowed to cool and the cleanliness of the system was checked by confirming a reading of 72.8 mN/m for UHQ.

5.3.4 Foaming experiments

Foaming was determined by vortexing solutions for 30 seconds using a lab benchtop vortex. Sample solutions of 10ml were placed in graduated 50ml corning tubes (Corning, UK) with an internal diameter of 25 mm. Following vortexing the solution was allowed to stand for 15s before the foam volume was recorded, this determined the foamability. Foam stability was then measured by monitoring the foam volume over a period of 24h. The experiments were repeated at least 3 times.

5.4 Results and discussion

5.4.1 RSF adsorption behaviour and structure at the interface

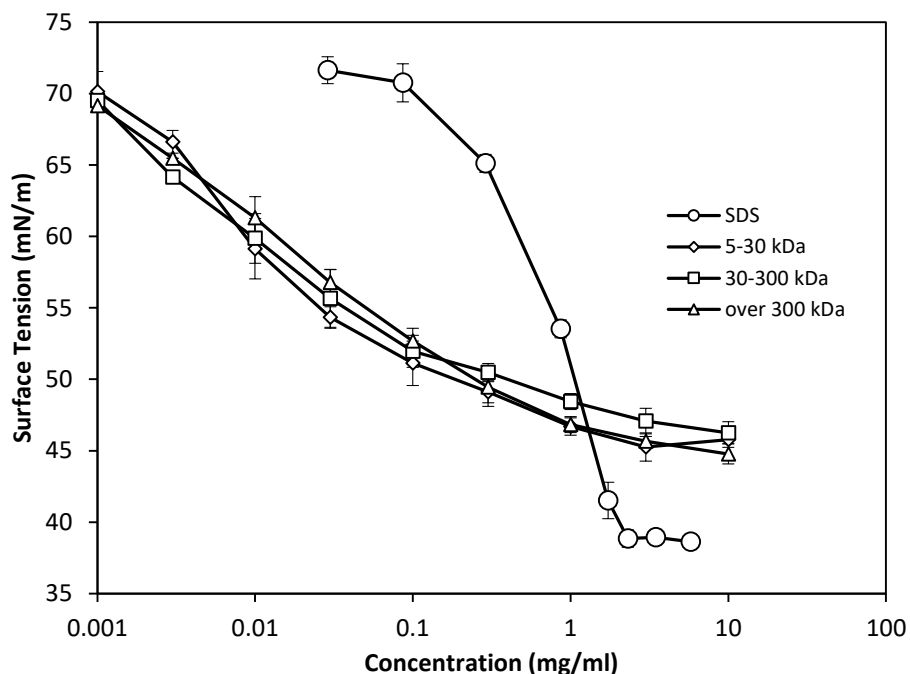


Figure 5.1 Equilibrium surface tension results for RSF peptides with an SDS surface tension curve for comparison.

Surface tension measurements were conducted on RSF solutions ranging in concentration from 0.001 mg/ml to 10 mg/ml. As would be expected, the adsorption of RSF peptides at the interface caused a significant reduction in the surface tension with increasing concentration, as shown in Figure 5.1. Interestingly the surface tension curves for all three MW peptide fractions appear to be almost identical within error. The adsorption of RSF resulted in a minimum surface tension of around 45 mN/m. However, a sharp CMC was not visible as is the case with the surface tension curve of SDS. The absence of the CMC is however typical for mixtures which possess a range of surface active species, in this case the inherent polydispersity of RSF solution results in aggregation occurring over a wide range of concentrations rather than at a specific concentration. The RSF peptides

ability to lower the surface tension is not as good as conventional surfactants (~ 35 mN/m). However, at low concentrations RSF peptides were more efficient at attaining lower surface tension values. As can be seen in Figure 5.1, below 1 mg/ml, RSF peptides resulted in significantly lower surface tension values than SDS. At 0.03 mg/ml RSF peptides achieved a 17 mN/m lower surface tension value than SDS at the same concentration. The ability to reduce the surface tension by RSF is significantly better compared to some other protein systems such as BSA, lysozyme and keratin which have also been studied using surface tension.^{51, 183, 184}

Neutron reflection was then used to try and elucidate whether there was any structural difference between the adsorbed layers between the three MW RSF fractions. Adsorption of the RSF peptides was from NRW solutions, thereby only signal from the adsorbed layer would be detected. Fitted data from the runs are shown in Figure 5.2 and the results of the fits are summarised in Table 5.1

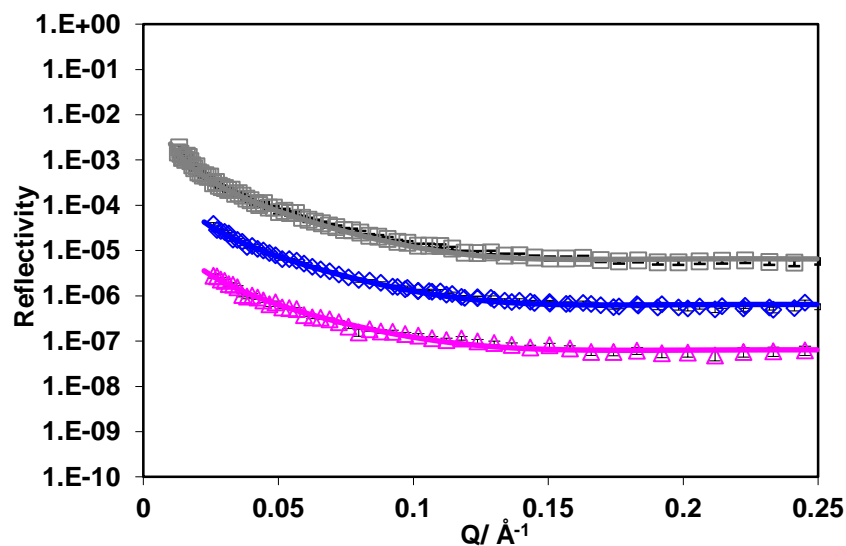


Figure 5.2 Fitted curves of NR data for adsorption of 0.1 mg/ml RSF in NRW: in order from top to bottom, 5-30 kDa (grey), RSF 30-300 kDa (blue), RSF >300 kDa (purple).

Table 5.1 Structural parameters from the best fit of NR curves for adsorbed layers from solutions of 0.1 mg/ml RSF

MW	τ ($\pm 2\text{\AA}$)	SLD $\pm 0.1 \times 10^{-6} \text{\AA}^{-2}$	Φ (± 0.005)	Γ (mg m^{-2})
5-30 kDa	38	1.0	0.410	2.3
30-300 kDa	36	1.0	0.410	2.2
>300 kDa	35	1.0	0.410	2.1

The NR data could be easily fit using a one-layer model. However, the results appeared to show only minor differences between the three adsorbed MW's. The thicknesses and the adsorbed amount were found to be slightly higher using RSF 5-30 kDa compared to RSF >300 kDa, which had the lowest, but only by 3 \AA and 0.2 mg/m^2 . This could be as a result of lower adsorption barrier by the smaller MW peptides compared to the larger MW. Further NR experiments were conducted to characterise how the adsorbed layer evolved with peptide concentration. Fitted data curves for RSF 5-30 kDa covering the concentration ranges from 0.003 to 10 mg/ml from D₂O solutions are shown in Figure 5.3 and Figure 5.4, and from NRW solutions in Figure 5.5 and. Figure 5.6.

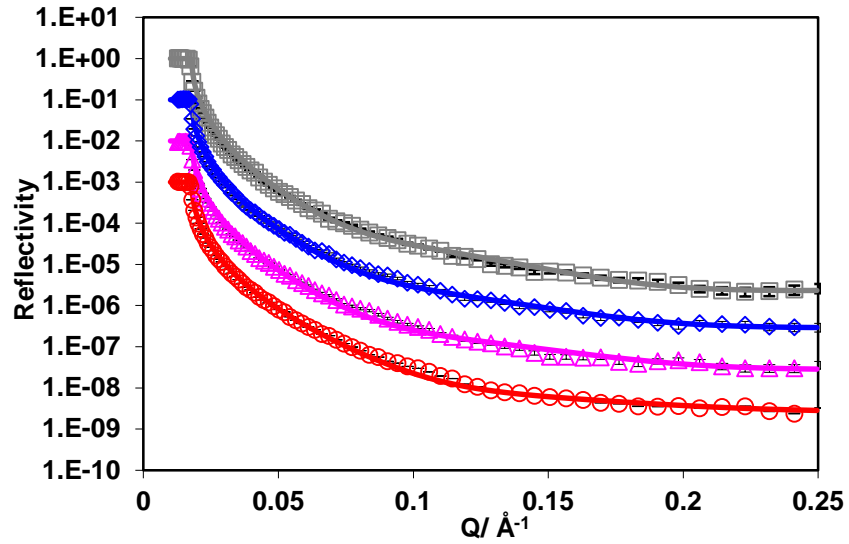


Figure 5.3 From top to bottom: 10 mg/ml, 3 mg/ml, 1 mg/ml, 0.3 mg/ml, RSF 5-30 kDa at the air/D₂O interface

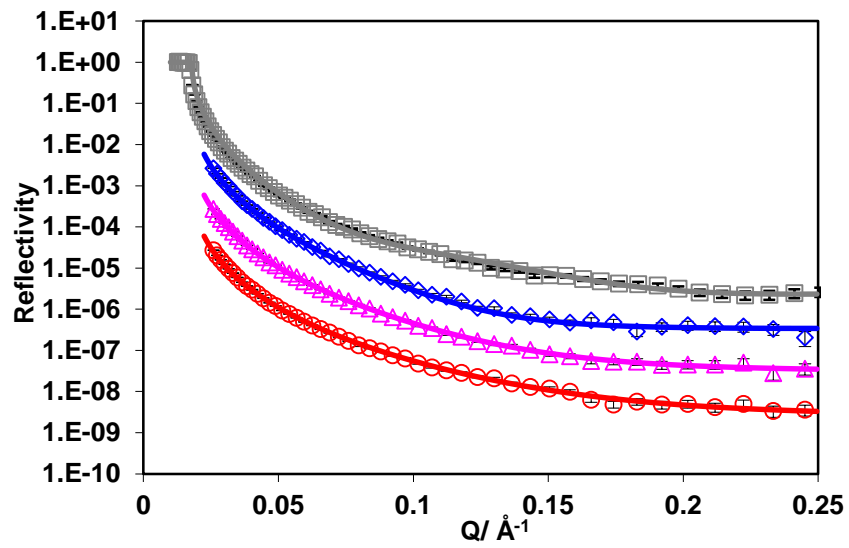


Figure 5.4 From top to bottom: 0.1 mg/ml, 0.01 mg/ml, 0.005 mg/ml, 0.003 mg/ml, RSF 5-30 kDa at the air/D₂O interface

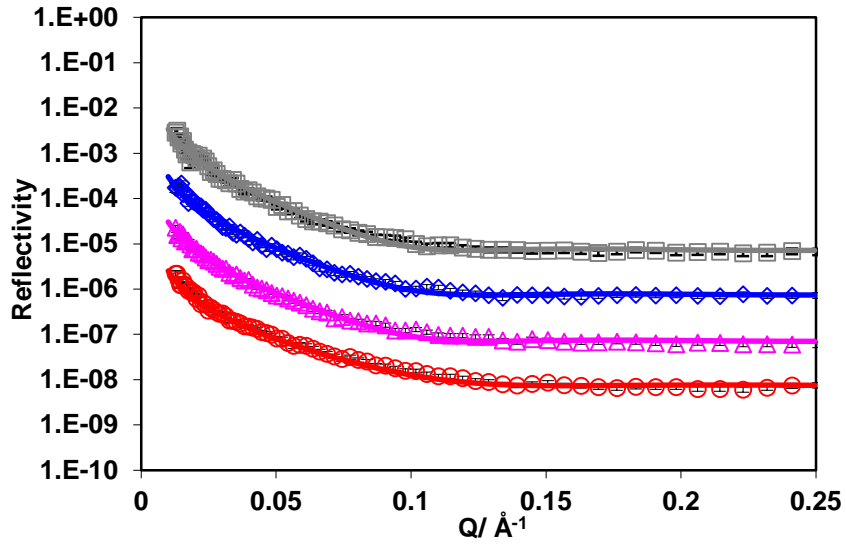


Figure 5.5 From top to bottom: 10 mg/ml, 3 mg/ml, 1 mg/ml, 0.3 mg/ml, RSF 5-30 kDa at the air/NRW interface

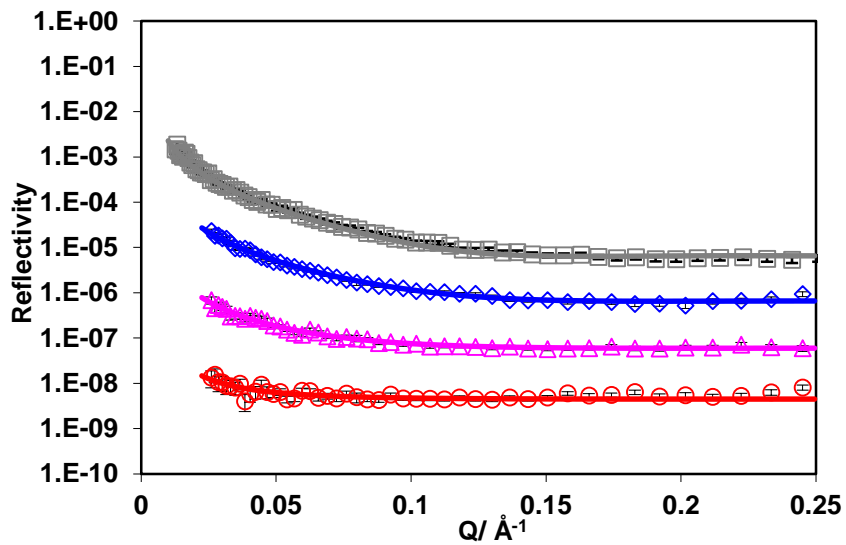


Figure 5.6 From top to bottom: 0.1 mg/ml, 0.01 mg/ml, 0.005 mg/ml, 0.003 mg/ml, RSF 5-30 kDa at the air/NRW interface

Both NRW and D₂O runs were conducted in order to maximise contrast and fit a model which would reveal where and how much RSF was found adsorbed at the interface. NRW runs were initially fitted to give an idea of the adsorbed layer thickness and amount, whilst the D₂O runs gave contrast to identify how much of the layer was submerged and how much extending out into the air phase.

Table 5.2 summarises the structural parameters of the layers as fitted from the NR data. The table shows both the final fitted data from NRW and D₂O runs. The NRW data could be fit using a single layer and shows an increasing layer thickness and SLD with increasing bulk RSF concentration. Subsequently the corresponding D₂O runs were fit using the NRW results as constraints and if necessary the NRW fits were revised. After numerous such iterations the data revealed the presence of RSF extending out into the air phase even at low concentrations. The adsorbed layer in the air did not appear to increase significantly in thickness with increasing concentration, whilst the layer found in D₂O increased from 17 Å at 0.003 mg/ml to 40 Å at 10 mg/ml. The total adsorbed amount was found to increase up to a maximum of 2.8 mg/m² at the maximum concentration investigated and there appeared to be a fairly even packing between the two layers as indicated by the volume fraction values in the table.

Table 5.2 Structural parameters of RSF 5-30k layers adsorbed at the air/water interface

Concentration (mg/ml)	Layer	Thickness (± 2 Å)	SLD 0.1×10^{-6} (Å ⁻²)	Φ (± 0.005)	Γ (mg/m ²)
10	Air	15	1.5	0.395	2.8
	D ₂ O	40	5.5	0.330	
10	NRW	52	0.9	0.370	2.8
3	Air	14	1.5	0.395	2.6
	D ₂ O	37	5.5	0.335	
3	NRW	49	0.9	0.370	2.6
1	Air	13	1.6	0.420	2.6
	D ₂ O	34	5.4	0.375	
1	NRW	49	0.9	0.375	2.6
0.3	Air	12	1.6	0.420	2.3
	D ₂ O	26	5.3	0.410	
0.3	NRW	40	1.0	0.410	2.4
0.1	Air	12	1.7	0.450	2.4
	D ₂ O	25	5.2	0.450	
0.1	NRW	38	1.0	0.410	2.3
0.01	Air	14	1.4	0.370	1.8
	D ₂ O	19	5.4	0.375	
0.01	NRW	33	0.9	0.370	1.8
0.005	Air	12	0.7	0.185	1.0
	D ₂ O	18	5.7	0.255	
0.005	NRW	31	0.5	0.205	0.9
0.003	Air	12	0.4	0.105	0.5
	D ₂ O	17	6.0	0.140	
0.003	NRW	29	0.2	0.100	0.3

The data summarised in Table 5.2 has been graphically shown in Figure 5.7. The thickness can be seen to increase across the entire concentration range whilst the surface excess appears to be plateauing from a concentration of 0.1 mg/ml onwards. This behaviour gives indication that the RSF peptides adsorbed at the interface are likely found in a different conformation at the higher bulk concentrations and thereby explain the increasing layer thickness without significant increase in adsorbed amount.

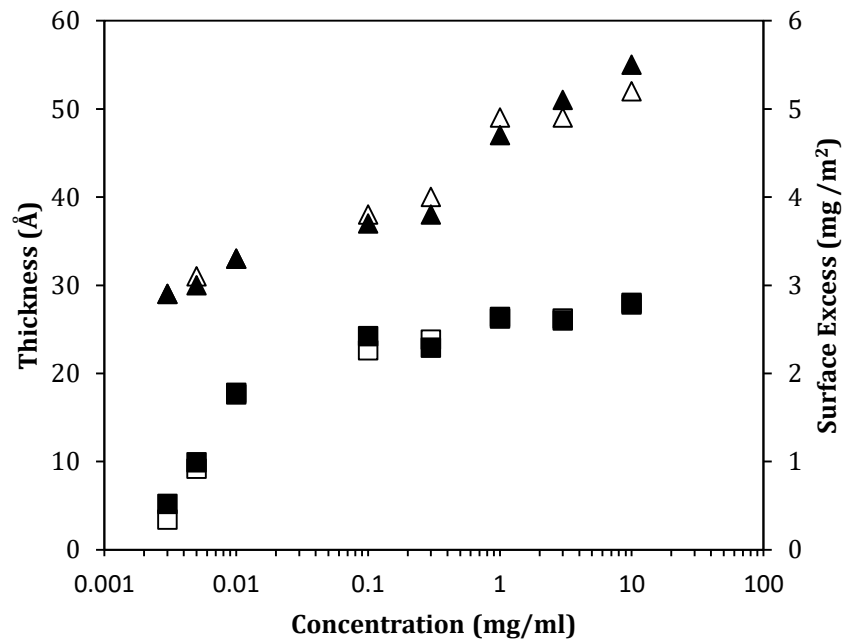


Figure 5.7 The total adsorbed layer thickness and adsorbed amount as a function of bulk RSF concentration as measured from NRW (open symbols) and D₂O (closed symbols) runs. Squares for the surface excess and triangles for the layer thickness.

Based on the above results a structural model of the evolution of the adsorbed RSF layer with bulk concentration is suggested and shown in Figure 5.8. At low concentration the RSF peptides are adsorbed with 12 Å above the surface and 17 Å submerged. This would fit neatly with the literature which suggests the formation of silk III structures upon adsorption at the air-water interface. As mentioned earlier the silk III structure results in

the alanine (hydrophobic) and serine (hydrophilic) residues to be found on opposite sides of the helical structure. As such, part of the helix would be found above the surface of the water and the rest submerged. Furthermore, the layer thickness increased by about 10 Å as the concentration is increased up to 0.1 mg/ml and the adsorbed amount reached 2.4 mg/m². Hence RSF was adsorbing more and tighter at the surface and additional adsorption was found below the surface increasing the submerged layer thickness. This supports the claims suggesting additional adsorption occurring via hydrogen bonding with the initial RSF layer made by Yang et. al.¹⁰⁷. In contrast, above 0.1 mg/ml an increase in adsorbed amount of only 0.5 mg/m² resulted in a layer thickness increase of nearly 20 Å. This significant increase in layer thickness fits perfectly with a reorientation of the silk peptide backbones from parallel to perpendicular to the surface. The increased bulk concentration would cause the RSF to pack tightly and the increased pressure result in adjacent chains interacting to form clusters/aggregates with their backbone perpendicular to the surface.

RSF backbones perpendicular to the surface have been previously observed by X-ray diffraction experiments conducted on compressed RSF layers.¹⁰⁴ The same study suggests a beta hairpin structure for the RSF found at the interface. Previously, Yang et. al., have suggested in their model that the RSF peptides would be found mostly above the surface, in beta hairpin conformation. They had made such an assumption based on their results showing a marked decrease in the surface elasticity of the RSF peptides at higher bulk concentrations. They went on to suggest that this was likely because RSF peptides had formed compact, large, loosely interconnected aggregates on the surface which would thus flow more easily under shear and hence cause a fall in surface elasticity. They thus hypothesised beta hairpin structure would be found above the surface thus limiting interactions in the water interface weakening the surface properties. However, according to the analysis of the NR data in Table 5.2 the RSF is yes perpendicular to the surface but

it is also mostly submerged. In this case the explanation would be the formation of aggregates which are water soluble, for example silk III structures grouped together to shield their hydrophobic cores and exposing their hydrophilic sides. This would satisfy the formation of surface aggregates and the consequent fall in surface elasticity as interpreted by Yang et. al. from their experiments. The difference is likely arising from the fact that the study which suggested beta hairpin structures, used compressed RSF layers which had been left to age for up to 24h, until a surface skin had formed. The NR measurements in contrast were carried out with RSF which on average had been analysed within 5h of preparation and therefore did not have any visible skin on the surface. It is hence plausible to think that RSF would eventually form insoluble beta hairpin structures on the surface and the structure measured by NR is a precursor to the creation of an insoluble RSF layer if left to age until a skin is formed.

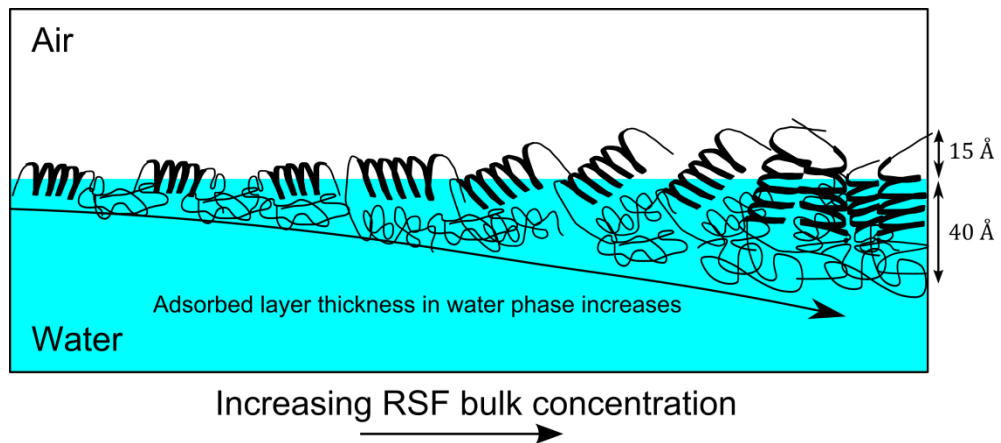


Figure 5.8 Schematic of the suggested RSF adsorbed layer structure as bulk concentration is increased. RSF is shown adsorbed in a silk III conformation parallel to the interface and as bulk concentration increases the RSF peptide is found to orient perpendicular to the interface.

Effect of ionic strength. The formation of the adsorbed RSF layer was then investigated under varying NaCl concentration. NR data is shown in Figure 5.9 and the structural parameters from the best fits are shown in Table 5.3.

The ionic strength of the RSF solution was increased up to a maximum of 1M. The increase in ionic strength did not appear to have a drastic effect on the adsorption of RSF peptides. There only appeared to be a minor increase in the adsorbed amount of around 0.2 mg/m^2 , but there was no trend. Addition of salt is known to cause minor increases in the free energy at the interface and as such make it more favourable for adsorption of amphiphilic molecules. In addition, the salt ions would result in lowered entropic gains by the RSF peptides adopting a compact hydrophilic conformation in the bulk and as a result more hydrophobic aggregates would be found in solution which would readily adsorb at the interface.

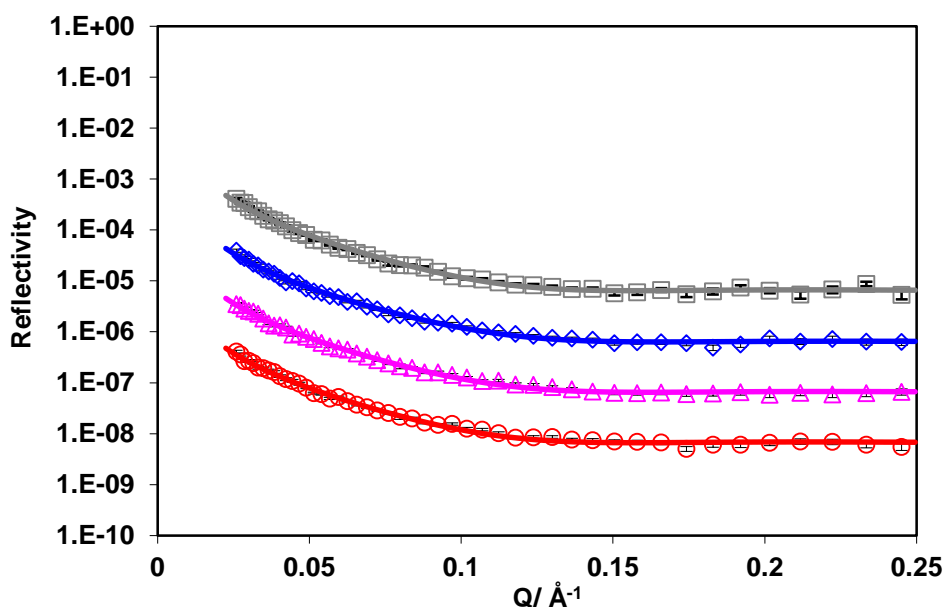
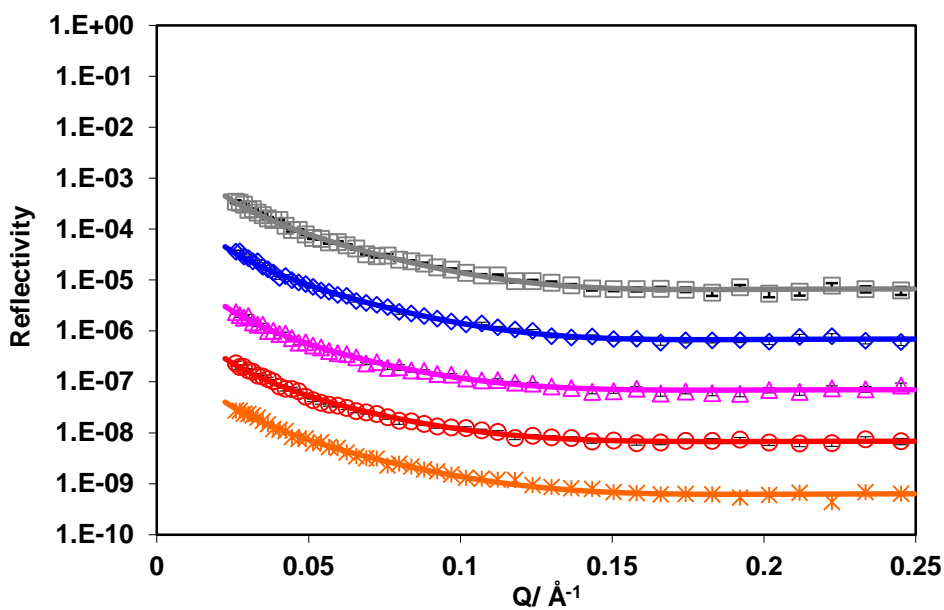


Figure 5.9 Neutron data fitting of 0.1 mg/ml RSF 5-30 kDa adsorption from 10 mM, 30 mM, 300 mM and 1M NaCl solutions (from top to bottom).

Table 5.3 Structural parameters of SF1B 5-30k (0.1 g/L) layers adsorbed at the air/water interface (pH 7) with different NaCl concentrations.

NaCl	τ	SLD	ϕ	Γ
(mM)	(Å)	$\pm 0.1 \times 10^{-6} \text{ \AA}^{-2}$		(mg m ⁻²)
0	38	1.0	0.410	2.2
10	40	1.0	0.410	2.4
30	38	1.0	0.410	2.3
300	39	1.0	0.410	2.3
1000	40	1.0	0.410	2.4

The effect of pH. The adsorption of RSF peptides from solutions of varying pH was explored and the resulting NR data and fits are shown in Figure 5.10. The corresponding parameters from the best fits are listed in Table 5.4

**Figure 5.10** Neutron data fitting for adsorption of 0.01 mg/ml RSF 5-30 kDa at pH's (from top to bottom) 2, 3, 5, 9 and 11

Changes in pH affect the distribution of charges on protein molecules. This consequently affects the electrostatic interactions taking place within the adsorbed layer between adsorbed molecules and also the degree of hydration of the molecules. Changes in pH did not result in drastic changes to the adsorbed layer, indicating stronger dependence on hydrophobic interactions rather than electrostatic ones over the pH range studied. However, changes in solution pH did cause some changes to the adsorbed RSF layer, mainly, that both high and low pH's resulted in a slightly more tightly packed layer and a higher adsorbed amount. At low pH the increased adsorption is explained by enhanced aggregation of the peptides due to reduced charge repulsion allowing for closer packing at the interface. At high pH, the peptides are highly charged and are usually found in an extended conformation in solution and adsorption is therefore driven by increased hydrophobic effect and gain in entropy from adsorption at the interface.

Table 5.4 Structural parameters of SF1B 5-30k (0.01 g/L) layers adsorbed at the air/water interface at different pHs.

pH	τ (Å)	SLD $\pm 0.1 \times 10^{-6} \text{ \AA}^{-2}$	ϕ	Γ (mg m ⁻²)
2	35	1.1	0.450	2.3
3	35	1.1	0.450	2.3
5	35	0.9	0.370	1.9
7	33	0.9	0.370	1.8
9	34	0.9	0.370	1.9
11	33	1.1	0.450	2.2

5.4.2 Co-adsorption with SDS and foaming behaviour

Co-adsorption of surfactant with a milder surface active agent can result in synergistic effects in terms of surface activity and with it a more efficient use of the surfactant (less will be required to achieve the same surface tension). The following experiments attempted to elucidate RSF interaction with SDS when formulated together.

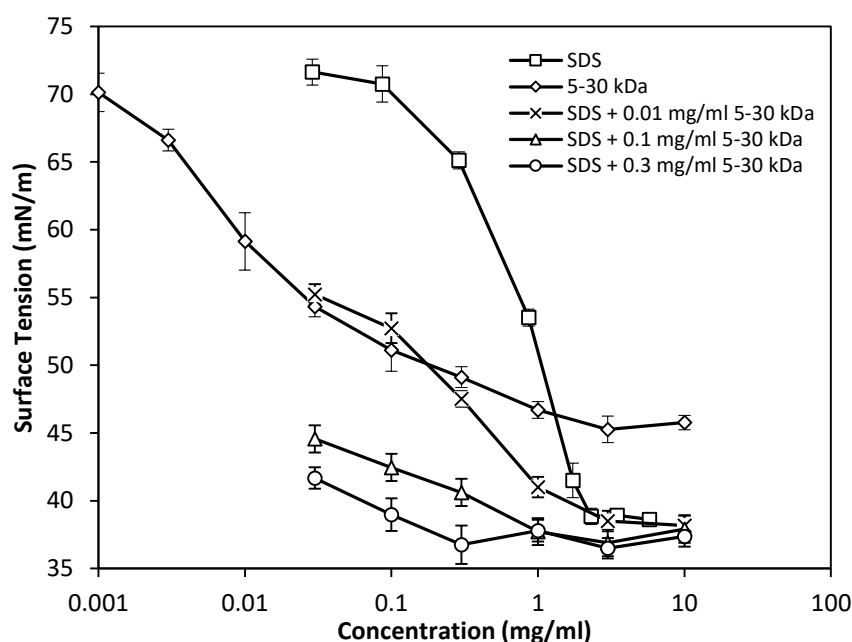


Figure 5.11 Surface tension curves for SDS with the addition of 0.01, 0.1 and 0.3 mg/ml RSF 5-30 kDa.

Three concentration of RSF (0.01, 0.1 and 0.3 mg/ml) were added to solutions of SDS and then surface tension measurements were taken. As can be seen in Figure 5.11, with respect to the pure surfactant, addition of RSF 5-30 kDa resulted in a lower surface tension across most of the concentration range. The analysis can be broken down into the effect of RSF on concentration of SDS above and below its CMC. Below the CMC there was considerable lowering of the surface tension. Whilst above CMC the addition of RSF appeared to cause only a minor fall (~ 2 mN/m) when 0.1 and 0.3 mg/ml RSF 5-30 kDa was added. Below the CMC, the lowering of the surface tension was RSF concentration

dependant, with the higher RSF concentrations achieving lower surface tension values. The CMC of the mixture also appeared to be noticeably lowered in the presence of RSF 5-30 kDa 0.1 and 0.3 mg/ml but remained unchanged with the addition of 0.01 mg/ml.

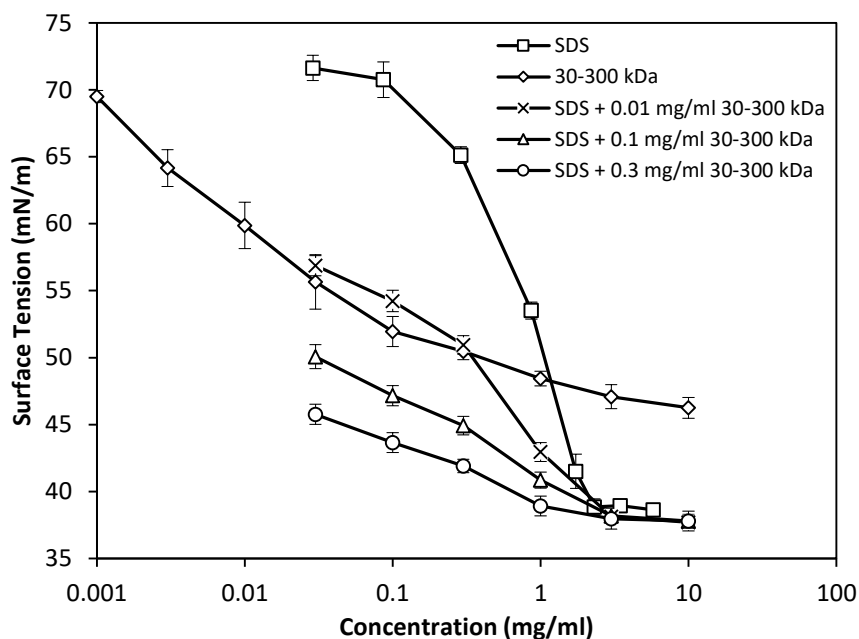


Figure 5.12 Surface tension curves for SDS with the addition of 0.01, 0.1 and 0.3 mg/ml RSF 30-300 kDa.

The addition of RSF 30-300 kDa also caused a significant reduction in the surface tension below the CMC of the pure surfactants (Figure 5.12). Above the CMC, the addition of RSF caused no significant reductions within error (less than 1 mN/m) in the surface tension. There was a RSF concentration dependant reduction in surface tension for mixtures below the CMC. The CMC of the mixture has been lowered with the addition of 0.3 mg/ml RSF (to ~1 mg/ml SDS) the same cannot be said for the other two concentrations of RSF.

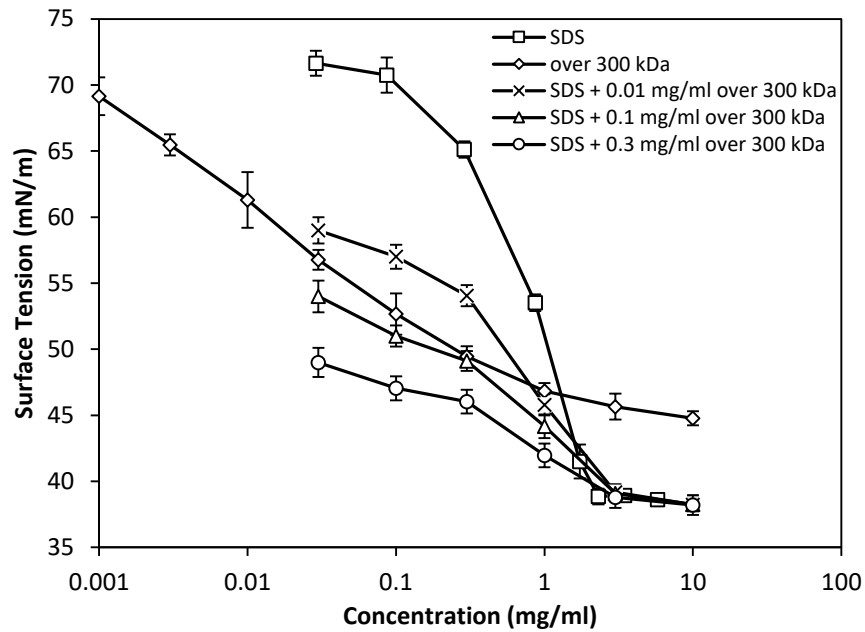


Figure 5.13 Surface tension curves for SDS with the addition of 0.01, 0.1 and 0.3 mg/ml RSF over 300 kDa

Addition of RSF over 300 kDa also resulted in significant reductions in surface tension below the CMC of the pure surfactant (Figure 5.13). Above the CMC, RSF did not cause any further reductions. The reduction in surface tension was dependant on the RSF concentration, where higher RSF concentrations resulted in lower surface tension values. The CMC of the mixture also did not appear to deviate from that of the pure surfactant.

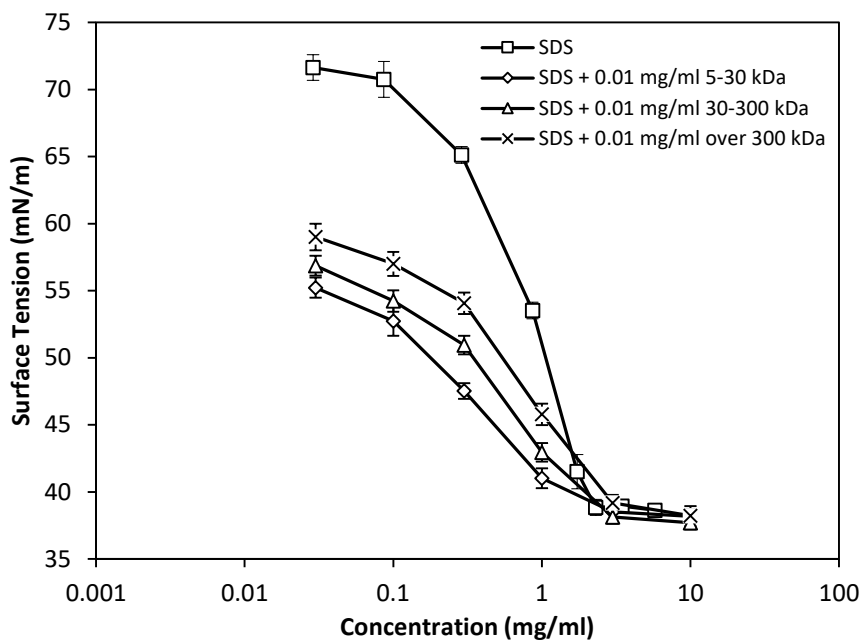


Figure 5.14 Comparison between the additions of 0.01 mg/ml RSF 5-30 kDa, 30-300 kDa and over 300 kDa fraction to SDS.

Overall the addition of RSF to SDS appeared to effectively reduce the surface tension at concentration below the CMC of the pure surfactant. Addition of concentrations as low as 0.01 mg/ml RSF resulted in significant reductions and have been plotted in Figure 5.14.

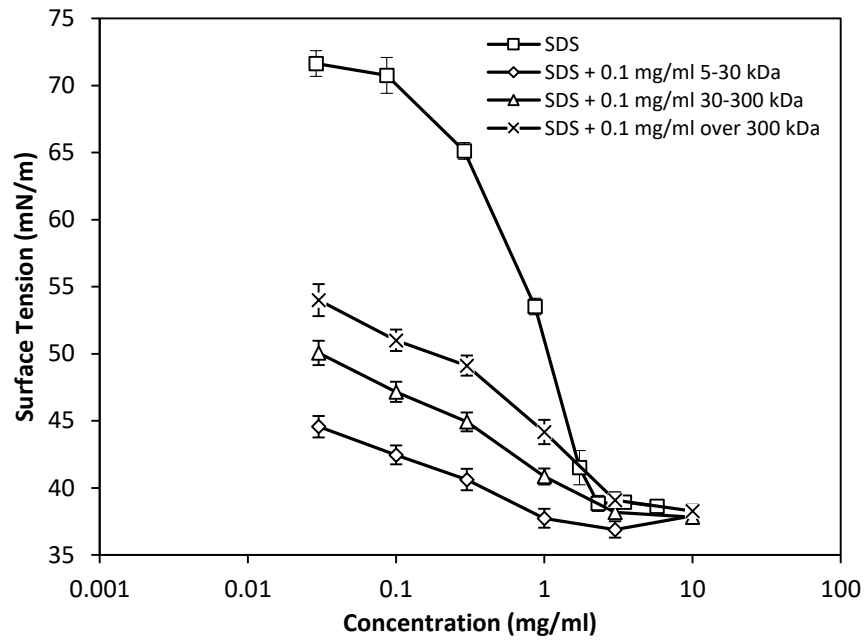


Figure 5.15 Comparison between the additions of 0.1 mg/ml RSF 5-30 kDa, 30-300 kDa and over 300 kDa fraction to SDS.

There is a clear relationship with the MW of the RSF, with the smaller RSF fraction achieving the lowest surface tension values. When the concentration of RSF was increased to 0.1 mg/ml the surface tension reduced further. As seen in Figure 5.15. the curves for each RSF MW is much lower than before.

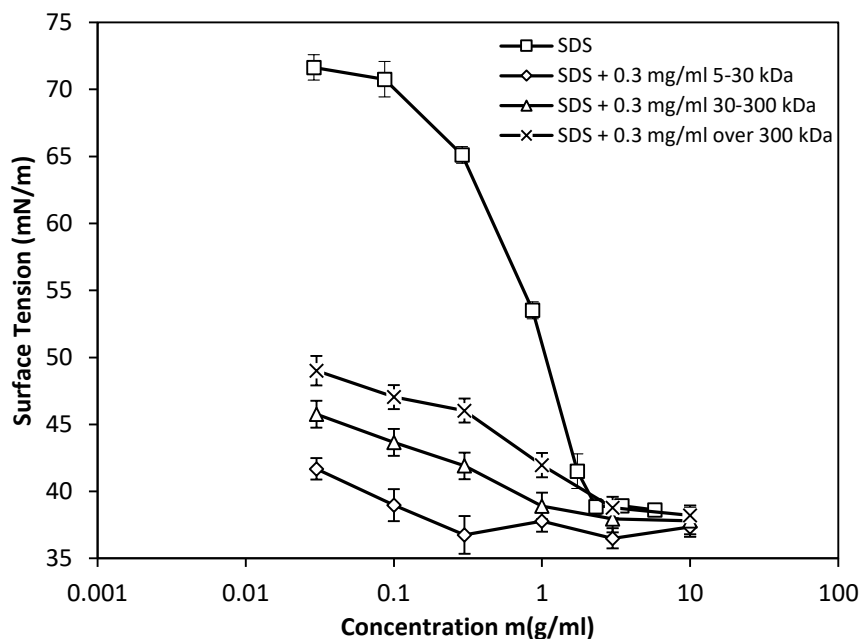


Figure 5.16 Comparison between the addition of 0.3 mg/ml RSF 5-30 kDa, 30-300 kDa and over 300 kDa fraction to SDS.

The same is valid for the addition of 0.3 mg/ml of RSF to the surfactant as shown in Figure 5.16. However, at this concentration, it becomes even more apparent that RSF is able to reduce the CMC of the surfactants to much lower concentrations. The minimum value of the surface tension is very slightly lower than the pure surfactant suggesting that the lowest surface tension might be a result of the formation of surface active SDS/RSF complexes with higher surface activity. Overall the addition of the RSF is facilitating the adsorption at the interface and the adsorption of the SDS molecules from lower concentrations and at high SDS concentration the surface tension is dominated by the surface activity of SDS.

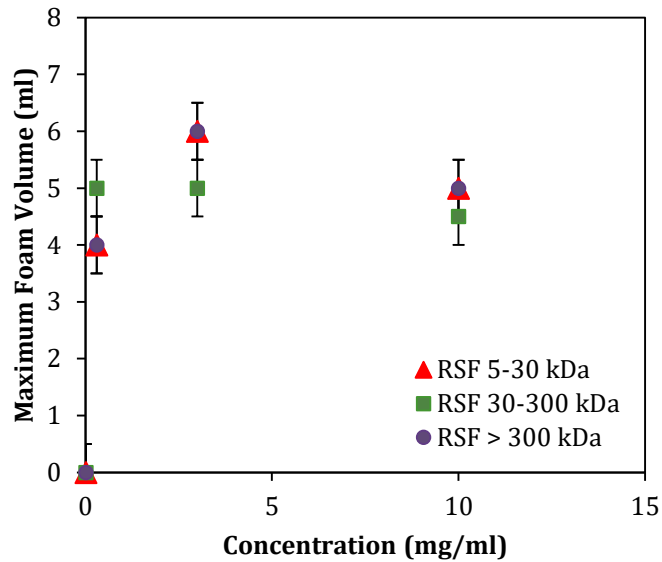
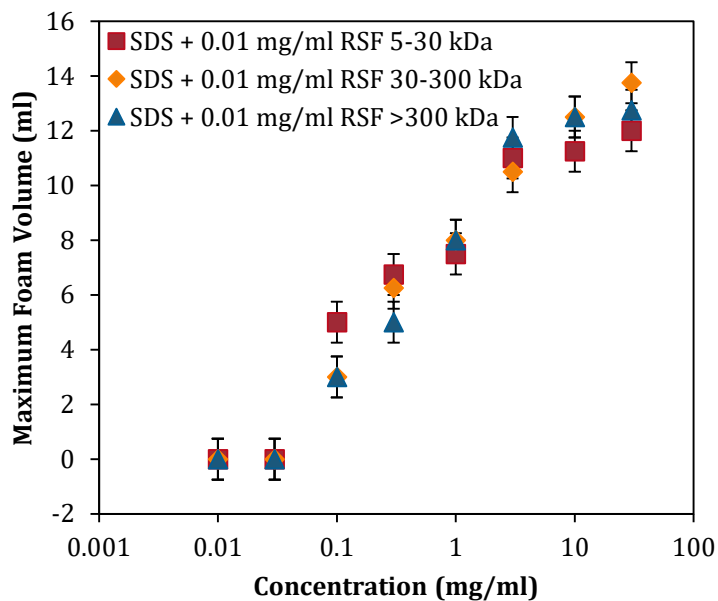


Figure 5.17 Foaming capacity of pure solutions of RSF 5-30 kDa, 30-300 kDa and over 300 kDa.

Foaming of RSF and SDS. Experiments were conducted to measure the foaming properties of the mixed solutions of RSF and SDS. Surface adsorption and the interactions between the molecules at the surface are essential in determining the foaming behaviour. As such examining the foaming can reveal information regarding the adsorption of molecules at the air-water interface.

Before studying the foaming ability of the mixed solutions the foam ability of pure RSF solutions was examined. As can be seen in Figure 5.17, the foaming ability of RSF solution is not very good, the maximum foam volume produced was around 6 ml. Protein solutions are typically known to have limited foaming abilities due to their size and slower diffusion to interfaces. At a concentration of 0.01 mg/ml the RSF solutions did not result in any foaming and at higher concentrations the foaming behaviour was roughly the same for all MW's of RSF.

(A)



(B)

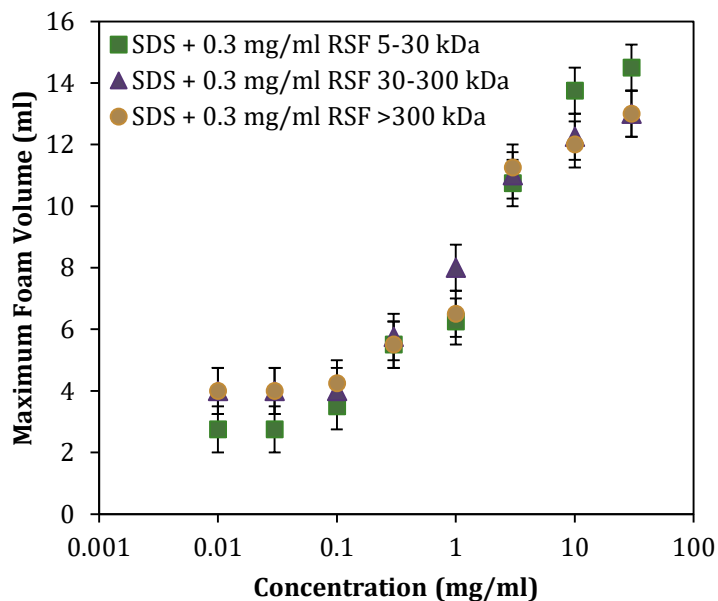


Figure 5.18 Foam ability of SDS with the addition of RSF. (A) addition of 0.01 mg/ml RSF, (B) addition of 0.3 mg/ml RSF.

When RSF was combined with SDS, as had been done in the surface tension experiments, the foam volume was much higher than pure RSF. Two concentrations of RSF were used, 0.01 mg/ml and 0.3 mg/ml. The results of the mixtures are summarised in Figure 5.18.

There appears to be no significant difference between the three molecular weights of RSF. The foam volume rises with SDS concentration up to around 14 ml for both concentrations of RSF. However, at the lower concentration of RSF it can be seen that addition of 0.3 mg/ml RSF resulted in higher foam volumes. For clarity this has been plotted on a separate graph for RSF 30-300 kDa, shown in Figure 5.19.

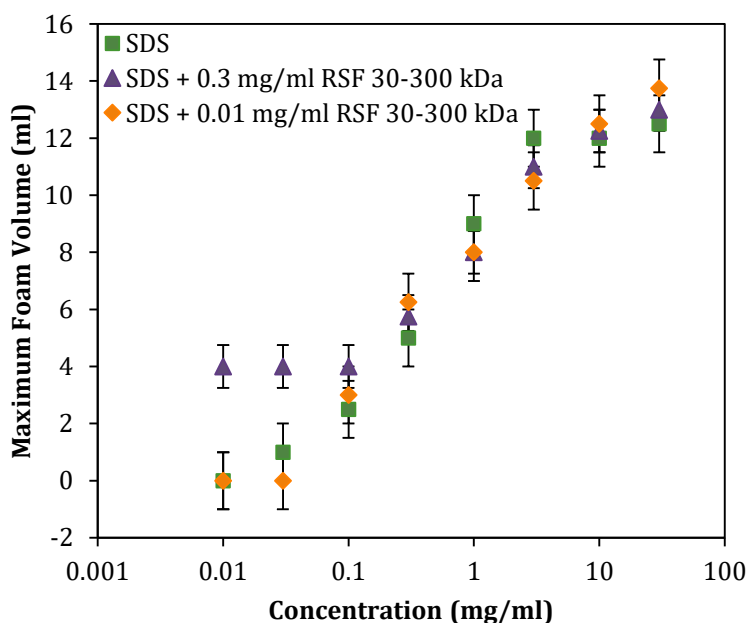


Figure 5.19 Addition of 0.01 and 0.3 mg/ml RSF 30-300 kDa to SDS solutions of varying concentration.

In Figure 5.19 the foam ability of pure SDS has also been overlaid in the graph and it becomes apparent that the foaming behaviour of the mixed solution is strongly influenced by that of SDS. Compared to RSF pure SDS surfactant has a much greater foaming ability. With a maximum foam volume of around 13 ml. For concentrations above 0.1 mg/ml of SDS, the addition of RSF does not seem to make any difference to the maximum foaming volume. However below 0.1 mg/ml SDS, addition of 0.3 mg/ml RSF caused a significant improvement in foaming volume relative to pure surfactant solution. On the other hand addition of 0.01 mg/ml RSF had no effect. However, the improvement seen by the

addition of 0.3 mg/ml RSF (below 0.1 mg/ml SDS) is no better than the foaming ability of pure RSF solutions of the same concentration. It is hence likely that the foaming below 0.1 mg/ml SDS is dominated by the foaming ability of RSF and beyond 0.1 mg/ml SDS, the far superior foaming ability of SDS become the dominating factor.

Stability of the foams was investigated by monitoring the foam volume over a period of 24h. The change in stability with concentration for SDS is shown in Figure 5.20, alongside the stability curves for the three MW's of RSF. The figure highlights concentration dependant stability for SDS solutions with a gradual decay over time which significantly accelerates after 2h. On the other hand, RSF shows very stable foams up to around 8h at which point there is a rapid decay in the foam.

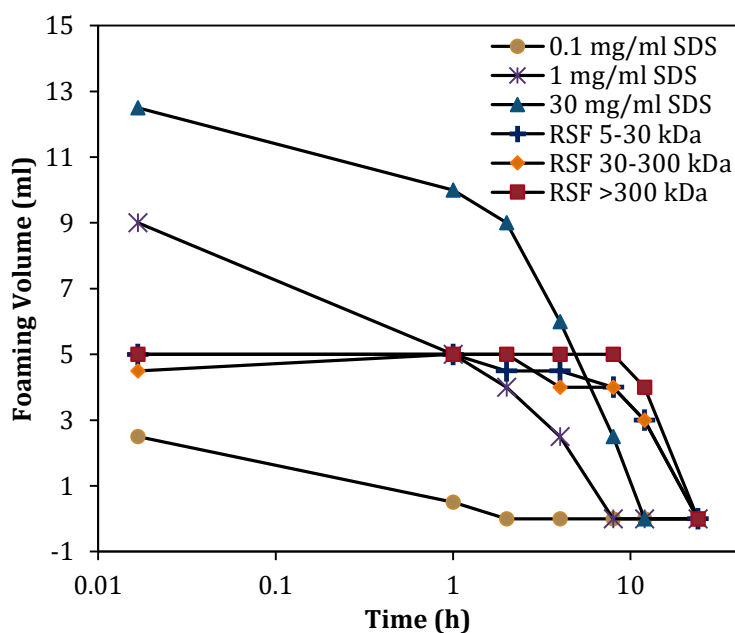
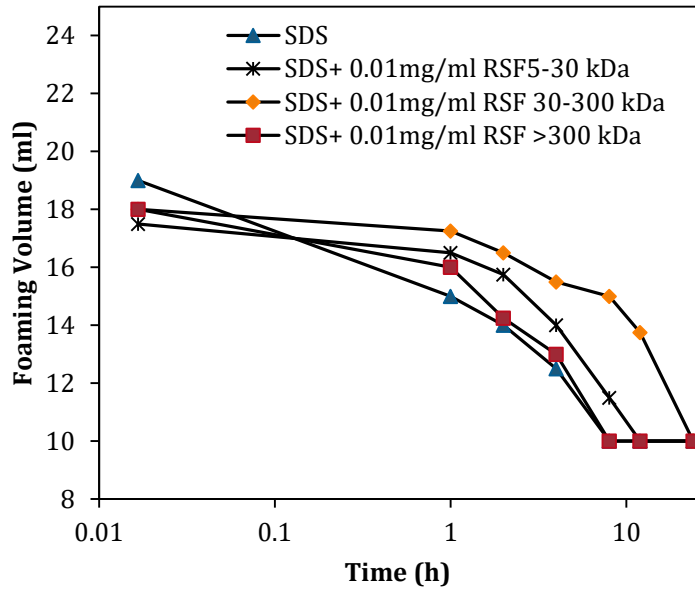


Figure 5.20 Foam stability of SDS and RSF solutions over a period of 24 h.

(A)



(B)

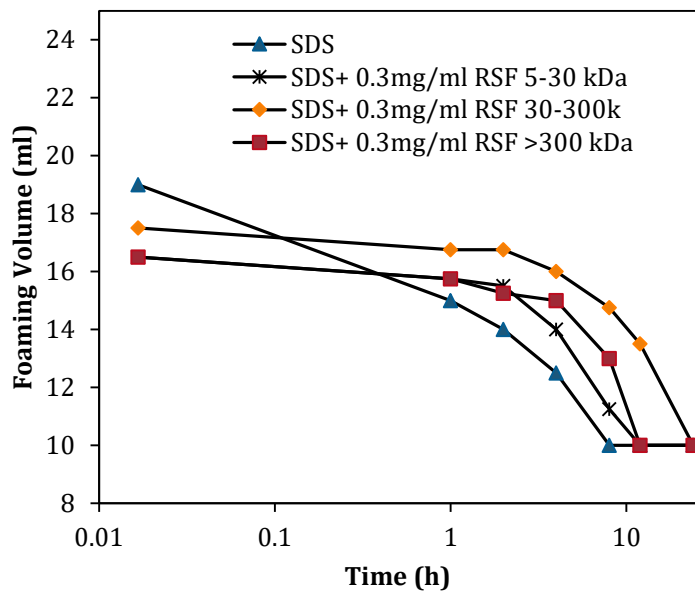


Figure 5.21 Stability of SDS solutions following the addition of (A) 0.01 mg/ml RSF, (B) 0.3 mg/ml RSF, over a period of 24 hours.

Addition of RSF to SDS solutions caused an improvement to the stability of the foam. The improved stability following addition of 0.01 and 0.3 mg/ml RSF is shown in Figure 5.21. It can be clearly seen that the foam remains stable for longer. The foam behaviour resembled that of the pure RSF solutions, especially when 0.3 mg/ml is added. It also

appears that the RSF fraction of 30-300 kDa resulted in more stable foams compared to the other two fractions at both 0.01 and 0.3 mg/ml concentrations.

Even at high concentrations the foam stability is improved with the addition of a small amount of RSF. Addition of RSF even at a concentration of 0.01 mg/ml caused a considerable increase in foam stability across the concentration range as can be seen in Figure 5.22. Addition of 0.3 mg/ml RSF resulted in higher foam stability but there appeared to be a deterioration of the stability with increasing SDS concentration likely due to SDS removing some RSF at higher concentrations as a result of competitive adsorption at the surface.

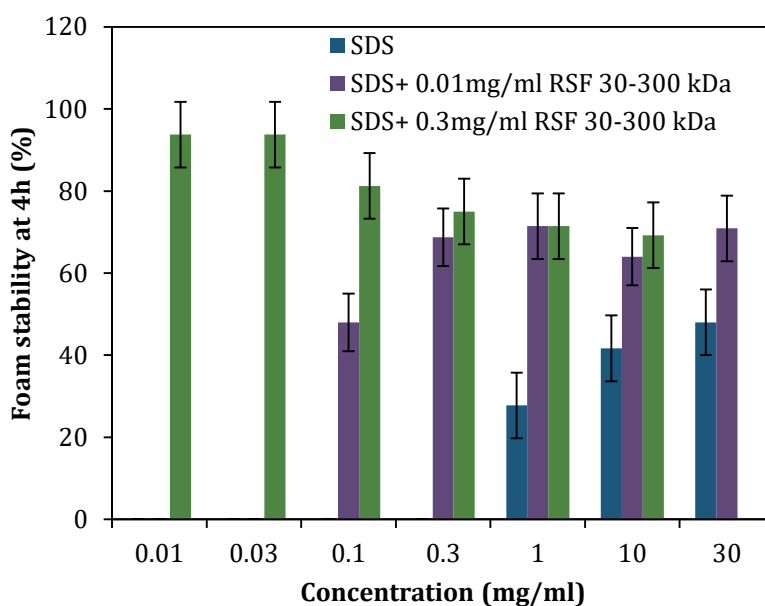


Figure 5.22 Foam stability of SDS and mixtures with RSF across the concentration range tested.

5.4.3 Co-adsorption with C₁₂TAB and foaming behaviour

Cationic surfactant use is often limited because of its higher toxicity and skin irritating properties, especially in relation to their use in skin and personal care products. Formulation with a milder surface active agent can result in an overall milder product. Surface tension measurements have been used to assess the surface active properties of mixed solutions of RSF and C₁₂TAB and any interactions between the two molecules.

Addition of RSF 5-30 kDa resulted in a large drop in surface tension across all concentrations below the surfactant CMC. Whilst above the CMC, RSF 5-30 kDa did not lower further the surface tension. The lowering of the surface tension below the CMC was RSF concentration dependant. The highest drop in surface tension was ~24 mN/m, relative to the pure surfactant solution, upon the addition of 0.3 mg/ml RSF. The CMC of the mixture also appears to be lowered by the addition of 0.1 and 0.3 mg/ml RSF 5-30 kDa but not with the addition of 0.01 mg/ml.

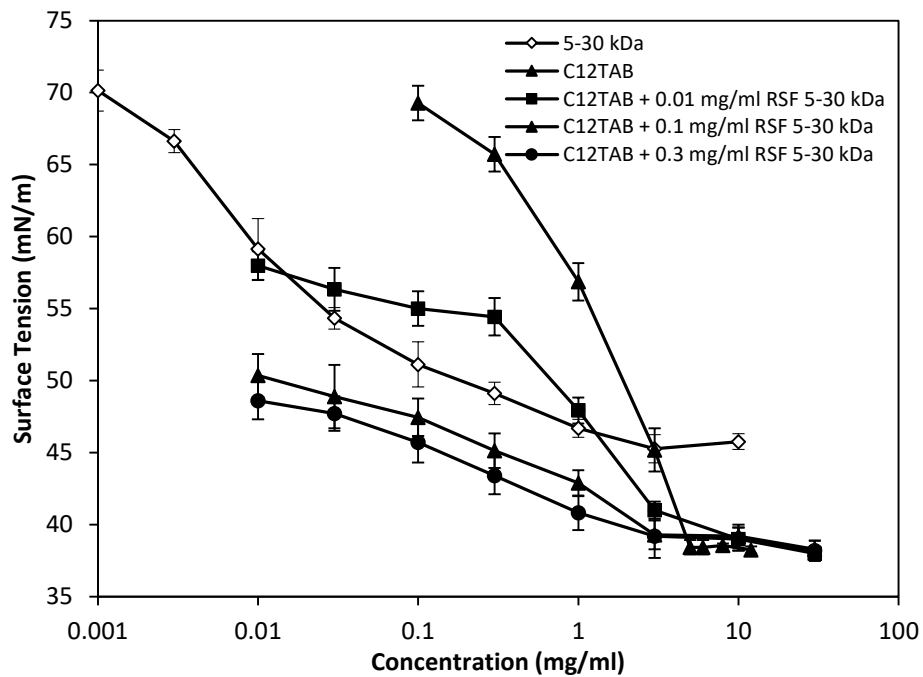


Figure 5.23 Surface tension curves for C₁₂TAB with the addition of RSF 5-30 kDa.

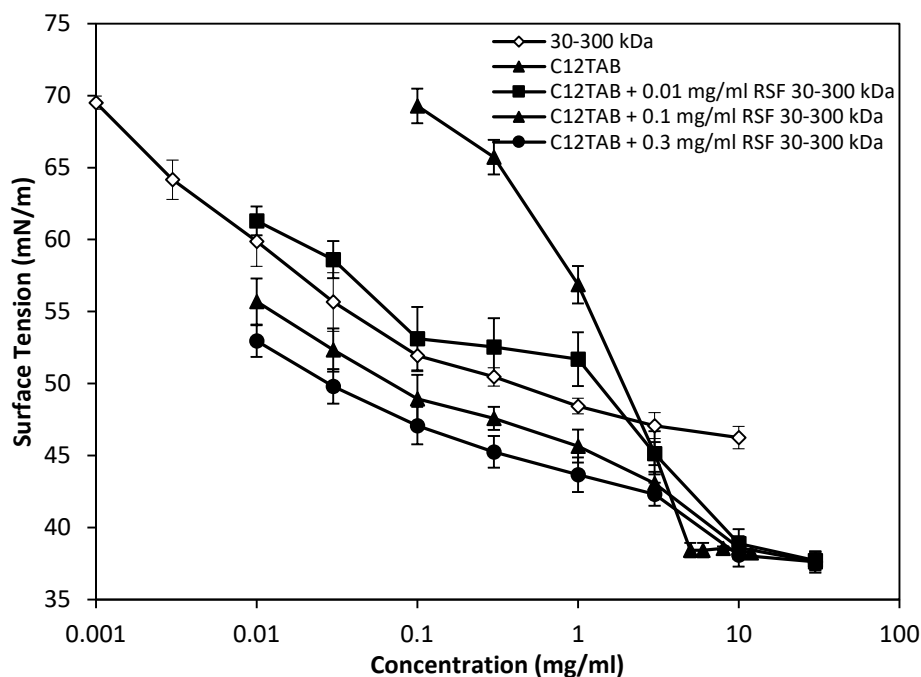


Figure 5.24 Surface tension curve for $C_{12}TAB$ with the addition of RSF 30-300 kDa.

Addition of RSF 30-300 kDa, to the surfactant also resulted in a lowering of the surface tension over most of the concentration range as shown in Figure 5.24. The lowering of the surface tension was RSF concentration dependant, below the CMC of the pure surfactant. The highest drop of surface tension resulted in a maximum fall of ~ 22 mN/m, relative to the pure surfactant solution, upon addition of 0.3 mg/ml RSF. There also was no apparent lowering of the CMC of the mixed solutions. Interestingly, the interaction of RSF 30-300 kDa with very low $C_{12}TAB$ concentrations of 0.01 mg/ml resulted in higher surface tension values than the pure RSF 30-300 kDa. This would suggest the presence of strong interactions between the two molecules which result in either lower adsorbed amount at the interface or less surface active complexes formed.

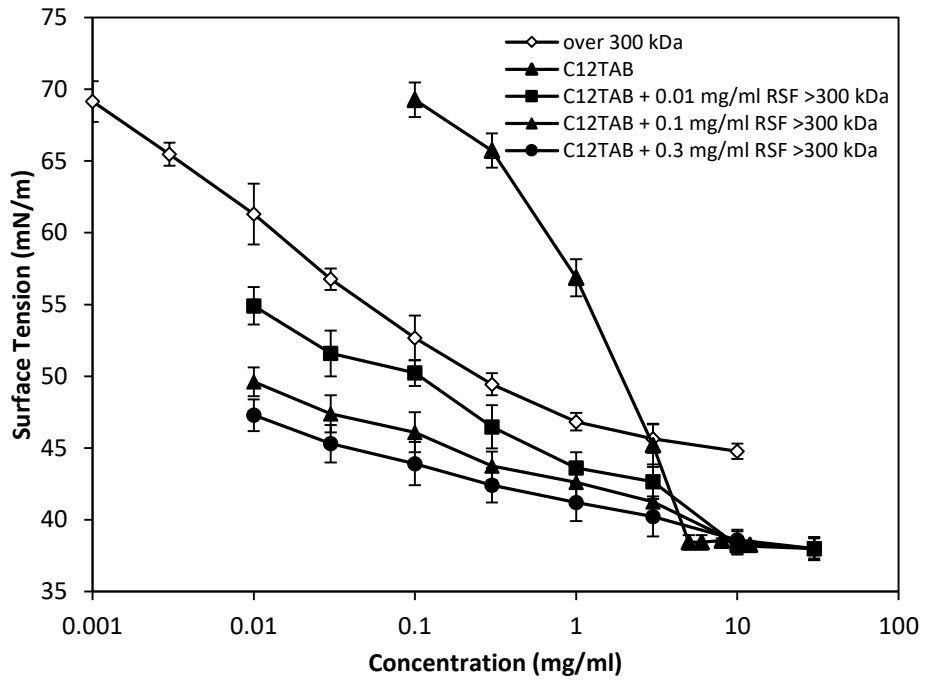


Figure 5.25 Surface tension curve for $C_{12}TAB$ with the addition of RSF over 300 kDa.

Addition of RSF over 300 kDa resulted in lowering of the surface tension below the CMC but no effect was seen above the CMC, as shown in Figure 5.25. The lowering of the surface tension was also RSF concentration dependant. Surface tension fell up to a maximum of 25 mN/m upon addition of 0.3 mg/ml RSF relative to the pure surfactant.

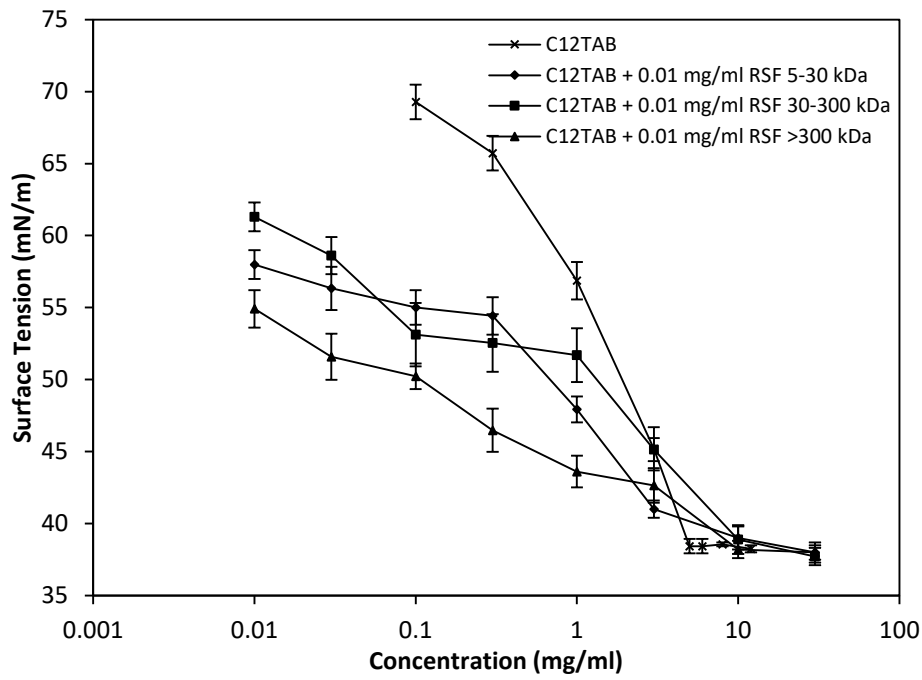


Figure 5.26 Comparison between the surface tension curves of the three RSF MW's following the addition of 0.01 mg/ml to C₁₂TAB solutions.

When comparing the RSF-surfactant curves between each other it can be seen that addition of over 300 kDa RSF fraction resulted in noticeably higher surface activity. Figure 5.26 highlights this for the addition 0.01 mg/ml RSF. However, Figure 5.26 also highlights the poorer surface activity by the other two RSF fractions.

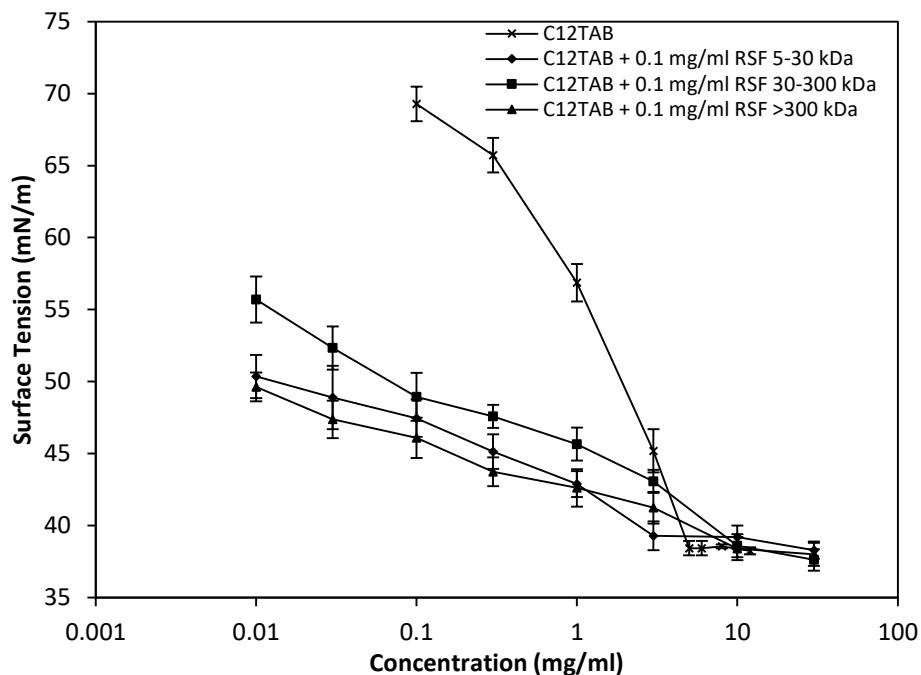


Figure 5.27 Comparison between the surface tension curves of RSF MW fractions at 0.1 mg/ml added to C₁₂TAB solutions.

Addition of 0.1 mg/ml RSF to C₁₂TAB resulted in even lower surface tension readings as can be seen in Figure 5.27. Over 300 kDa resulted in the lowest surface tension but 5-30 kDa is only marginally less surface active. Overall all three RSF MW surfactant mixtures appear to have similar slopes and throughout the concentration range studied are found within a maximum of ~5 mN/m from each other.

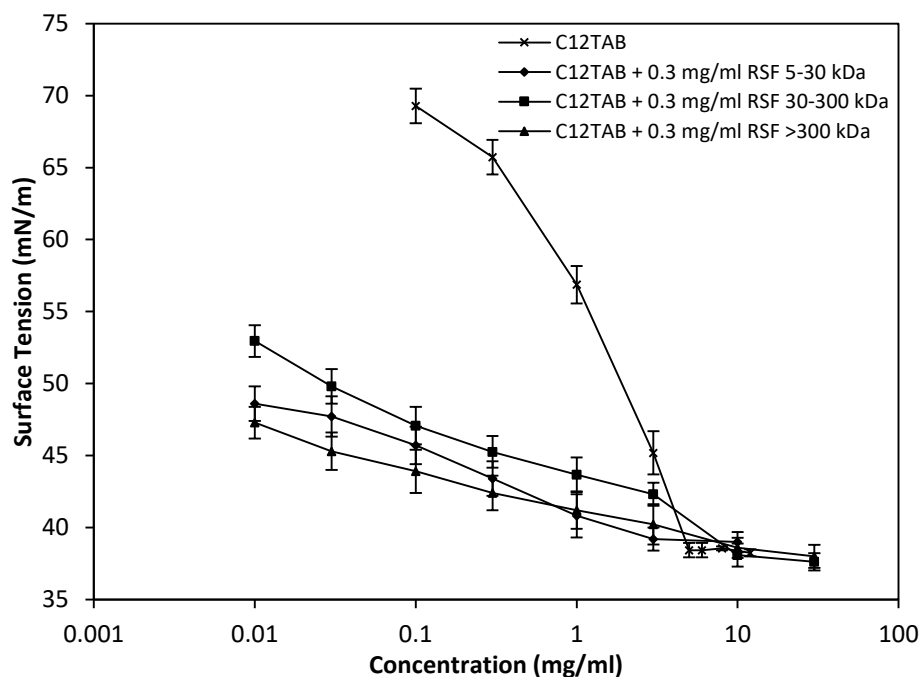


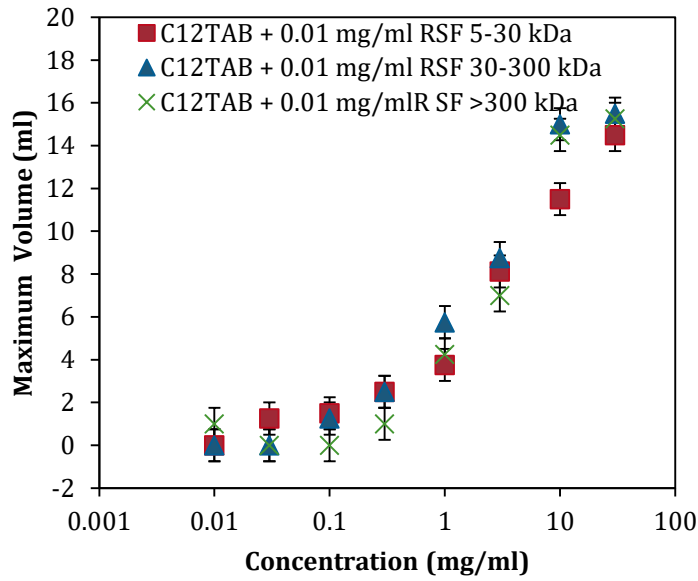
Figure 5.28 Comparison between the surface tension curves of RSF MW fractions at 0.3 mg/ml added to $C_{12}TAB$ solutions.

Addition of 0.3 mg/ml RSF caused a further lowering in the surface tension as seen in Figure 5.28. There is very little difference between the three RSF fractions, all are within less than 5 mN/m from each other at each concentration point. However, the graph does indicate that over 300 kDa resulted in the lowest surface tension and 30-300 kDa had a higher surface tension throughout.

The above results have the peculiarity of showing an opposite trend with regards to the RSF MW fraction which is most effective compared to the SDS results, i.e. over 300 kDa resulted in a greater surface tension reduction with $C_{12}TAB$ but with SDS it resulted in the least surface tension drop out of the RSF MWs. This is a clear indication that the two surfactants interact with the RSF peptides in different ways.

Foaming of C₁₂TAB with RSF.

(A)



(B)

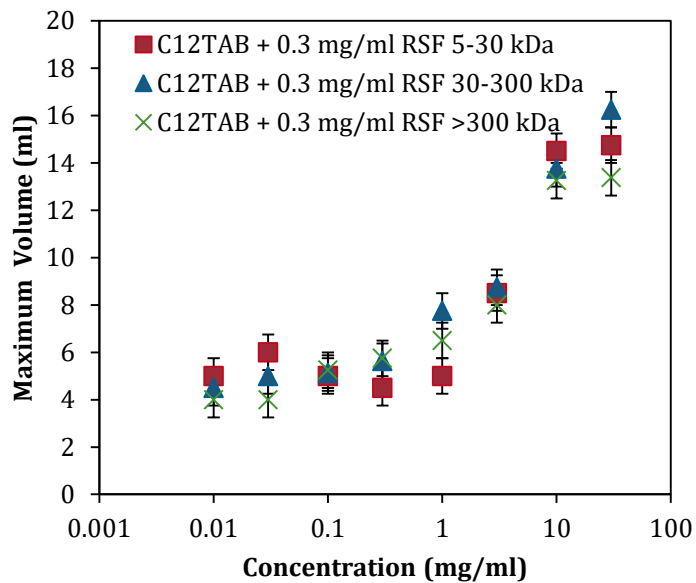


Figure 5.29 Foaming ability of C₁₂TAB solutions with the addition of (A) 0.01 mg/ml RSF, (B) 0.3 mg/ml RSF.

Following mixing with C₁₂TAB, there was no apparent difference between the three MW fractions of RSF. Figure 5.29 shows the increased foaming ability of the solutions with increasing C₁₂TAB concentration for both the addition of 0.01 and 0.3 mg/ml RSF.

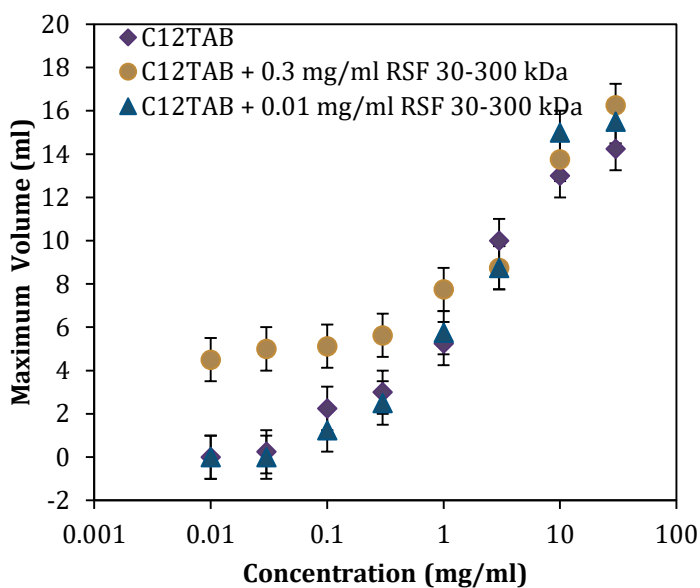


Figure 5.30 Addition of 0.01 and 0.3 mg/ml RSF 30-300 kDa to solutions of $C_{12}TAB$.

The addition of 0.3 mg/ml RSF resulted in a different foaming behaviour compared to the addition of 0.01 mg/ml RSF, but no significant differences between the RSF fractions at the respective added concentrations. As better highlighted in Figure 5.30, the overall foaming behaviour is dominated by $C_{12}TAB$'s foaming behaviour. Foaming ability of pure $C_{12}TAB$ solutions improved with concentration but the addition of RSF at 0.01 mg/ml made no difference to it. On the other hand, the addition of 0.3 mg/ml RSF showed a clear improvement in the foaming ability up to 1 mg/ml $C_{12}TAB$. However, at higher concentrations the addition of RSF does not result in any improvement over the pure surfactant foaming ability suggesting that the interface is dominated by the surfactant action.

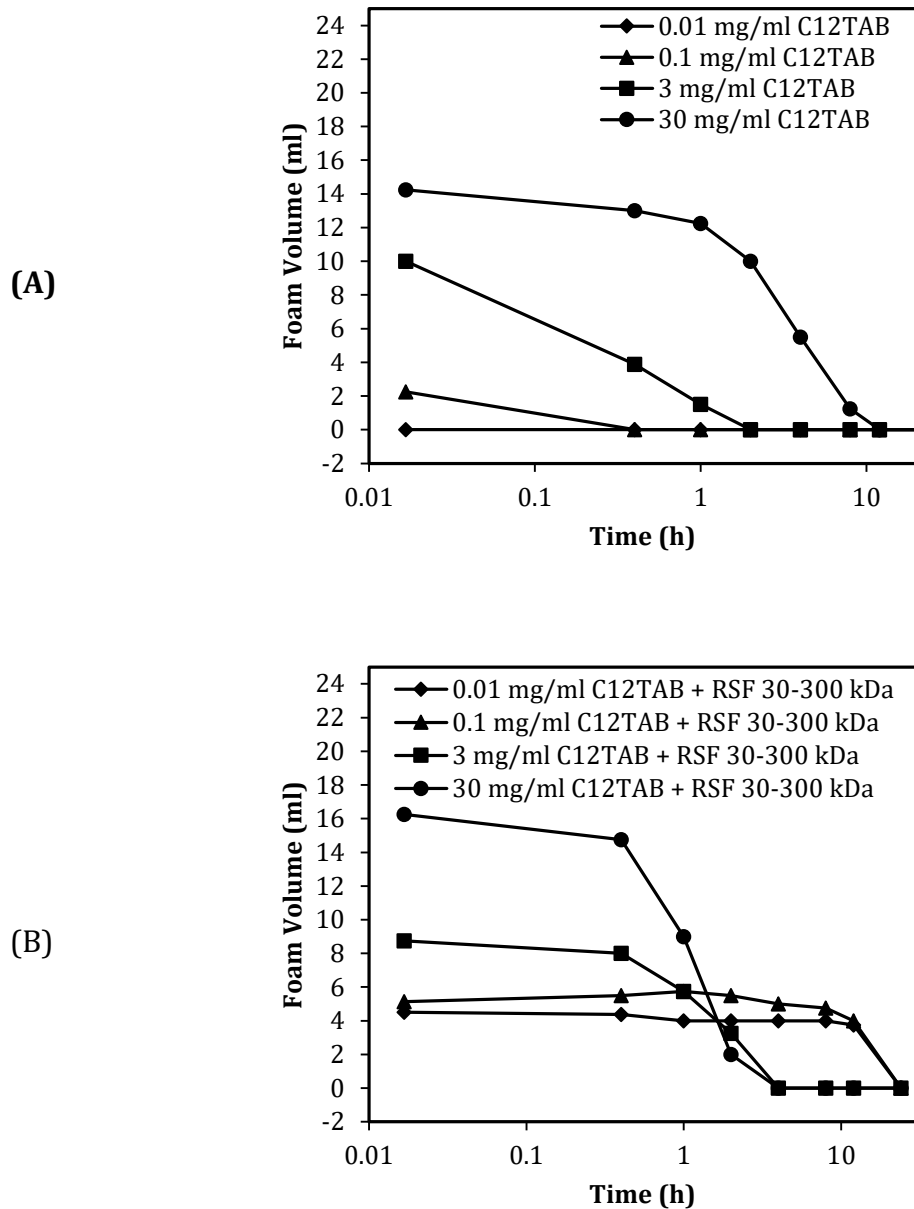


Figure 5.31 (A) Stability of C₁₂TAB, (B) stability following addition of 0.3 mg/ml RSF 30-300 kDa. Error bars omitted for clarity.

The foam stability was examined for pure C₁₂TAB solutions and it showed standard concentration dependant increase in stability with increasing concentration as can be seen in Figure 5.31(A). However the addition of 0.3 mg/ml RSF to the surfactants solutions resulted in a more complex behaviour as seen in Figure 5.31(B). At high surfactant concentrations the addition of RSF caused a drop in the foam stability whilst there is a

very clear improvement in the stability at low surfactant concentrations. This increased stability at low concentrations would appear to be a result of the RSF peptides dominating the surface interaction whilst at higher concentrations the surfactant dominates but is destabilised over-time by interaction with RSF peptides.

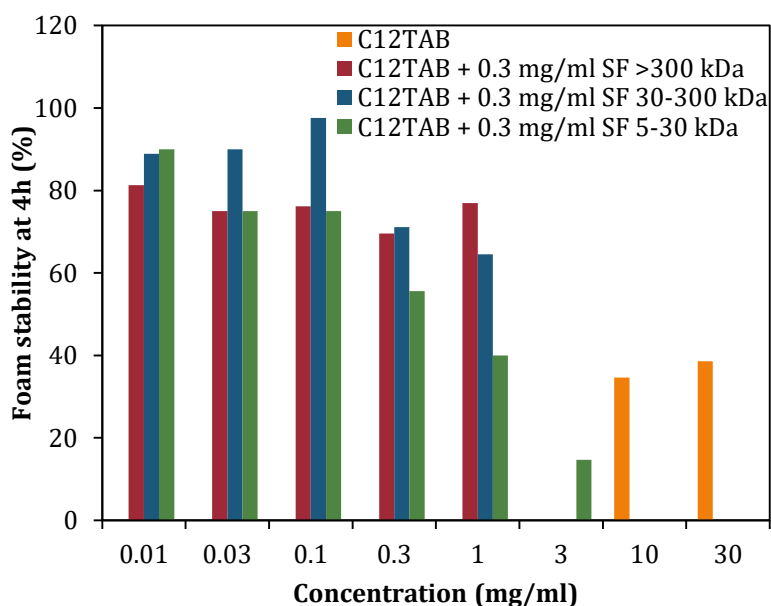


Figure 5.32 Foam stability as a percentage of initial foam of $C_{12}TAB$ and mixtures with RSF after 4 hours.

At the 4 hour mark, after foaming, the addition of RSF has helped maintain the foam stable whilst in the pure surfactants solution, the foam has mostly decomposed and is only present at concentrations above 10 mg/ml. Figure 5.32 also highlights the fall in stability as surfactants concentration increases in the mixed solutions. This is indication of the surface being replaced by surfactant at higher concentrations, leading to the stability imparted by the RSF molecules to gradually fall. At concentration above 1 mg/ml, mixed solutions had no foam left at the 4 hour mark. This is a clear indication of the presence of strong interactions between the RSF and $C_{12}TAB$ which result in lower surface elasticity and thereby more unstable foam.

5.5 Conclusion

Neutron reflection revealed that the adsorption of the peptides formed a uniform peptide layer at the air/water interface with nearly one third of the layer extending into the air phase. The thickness of the layer was found to increase with solution concentration from around 30 Å (at 0.003 mg/ml) to approximately 50 Å (at 10 mg/ml) while the respective surface excess gradually increased from around 0.4 mg/m² to 2.8 mg/m². However, the adsorbed amount started to plateau fairly soon whilst the thickness steadily increased. This gave an indication that the RSF which was found at the interface at the higher concentration must be arranged in a different structural conformation. Based on these results and on the literature, it was possible to propose a RSF model adsorption at the air-water interface. RSF is believed to initially adsorb perpendicular to the interface and as concentration increases the RSF peptide was forced to adopt a tighter configuration which causes it to be found with its backbone perpendicular to the surface. It is suggested that since the peptides are mostly in the water interface the peptides are arranged in such a way to shield the hydrophobic areas and expose their hydrophilic segments to the bulk solution. This may also be the reason for the weakening of surface elasticity since such aggregates would not be strongly cohesive. RSF layers were however found to be fairly stable with regards to both salt and pH. The adsorbed RSF was largely unaffected by ionic strength, with minor increase in the adsorbed amount of 0.2 mg/m² when NaCl concentration was raised to 1 M. Changes to pH caused a slight increase in the adsorbed amount when moving to both low and high pH with adsorbed amounts remaining very stable between pH 5-9.

Surface tension measurements revealed that RSF peptides were significantly more surface active than conventional surfactants at low concentrations. This is a very attractive result in terms of its potential use as a surfactant. Co-adsorption with surfactants revealed even lower surface tension values. Addition of RSF at very low concentrations of 0.01 to 0.3 mg/ml caused significant drop in the surface tension below the CMC of the pure surfactants and in most cases was seen to also reduce the CMC value. There appeared to be a RSF MW dependant reduction in the surface tension. However, the most effective MW fraction changed depending on the surfactant. With SDS, the 5-30 kDa fraction resulted in the lowest surface tensions, whilst with C₁₂TAB it was the larger > 300 kDa which resulted in the lower surface tensions. It is unclear why this was the case, but the results would indicate that the two surfactants interact with the RSF peptides in two different ways. Foaming experiments were not able to make the interactions any clearer as there appeared to be no major differences between the three RSF MW's ability to foam. Stability of the foams however revealed that RSF was very good at increasing foam stability at low surfactant concentrations. Foam stability appeared higher with SDS across the entire concentration range. Whilst stability with C₁₂TAB revealed that there were strong interactions taking place between the surfactant and the peptide, hence the increased stability at low surfactant concentrations rapidly deteriorated.

6 CONCLUSION

6.1 Conclusions

Interactions between surfactant-like peptides and conventional surfactants had not been looked at before. So experiments were carried out to assess their potential use together at the solid-liquid interface. Firstly, co-adsorption studies of V₆K with SDS confirmed the presence of strong interactions between the two oppositely charged molecules. There was a molar ratio dependence and consequent neutralization at molar unity resulting in zero adsorption. However below molar unity SDS adsorption could be enhanced at the interface due to like charge attraction by the positively charged lysine heads of the peptide. This was further confirmed when V₆K was pre-adsorbed and formed a stable bilayer or cylindrical micellar structure and could aid the adsorption of SDS onto its surface. This is a positive result as it showcases the potential for V₆K to modulate the adsorption of SDS (or any similarly negatively charged molecule). On the other hand, V₆K was found to be able to effectively shield the surface from the positively charged C₁₂TAB, when pre-adsorbed. Co-adsorption with C₁₂TAB however resulted in competitive adsorption and C₁₂TAB dominated the interface above its CMC. However, below its CMC V₆K was able to adsorb at the interface faster than C₁₂TAB and therefore

was found adsorbed at the interface. Overall the results show that surfactant-like peptides show promising adsorption and an interesting range of behaviours and interactions with conventional surfactants which give insight into potential ways to use these peptides.

Next, RSF peptide adsorption at the solid-liquid interface was characterised in detail. It showed that the RSF peptide could form a very stable and irreversibly adsorbed layer. But its adsorption was affected by pH and salt concentration. Increasing pH or ionic strength caused a reduction in the adsorbed amount. Pre-adsorbed layers of RSF were found to help SDS adsorption. However, increasing the SDS content above its CMC caused the near complete removal of RSF from the interface. On the other hand, cationic surfactant C₁₂TAB, removed a small amount of RSF from the interface and was found to coexist at the interface with a significant amount of RSF, even above the surfactants CMC. These results give an important insight into the interactions with conventional surfactants at the solid-liquid interface. Whilst the results showed that RSF was fairly easily removed from the interface by SDS, it would appear that it could be used in conjunction with a cationic surfactant at the solid-liquid interface.

Furthermore, the characterisation of RSF at the air-liquid interface revealed a very stable RSF layer which was not affected much by solution salt or pH changes. The results seem to confirm a structural change in the adsorbed RSF peptides at high bulk concentrations. The most significant result however comes from the co-adsorption with surfactants, which resulted in a substantial drop in surface tension with the addition of small amounts of RSF. As such the use of RSF together with surfactants, would greatly improve the surfactant and in applications which require surface tension lowering this would result in significantly lower amounts of surfactant needed. In addition, RSF was also able to help improve the stability of foams over all the concentration range tested, for SDS, and partially for C₁₂TAB.

Going back to the research motivations delineated in the introduction chapter, the use of peptides for their surfactant ability would seem justified. The overall results of the thesis show great potential in the use of designed surfactant-like peptides. Also, the use of RSF peptides did result in moderate surface activity, though not quite good as conventional surfactants. Nevertheless, RSF peptides demonstrated an exceptionally promising ability to lower surface tension when formulated with conventional surfactants and would thus contribute in making conventional surfactant solutions milder and more efficient. Hence the top-down approach of recovering peptides from larger proteins would appear to be promising, but will not likely yield anything functionally specific as carefully designed and synthesised surfactant-like peptides.

6.2 Future work

The results from the adsorption of V₆K at the solid-liquid interface helped elucidate for the first time the interactions that take place between cationic surfactants-like peptides and cationic and anionic surfactants. It would be interesting to investigate the use of V₆K in applications typically accomplished by conventional surfactants. These could range from coating of surfaces, delivery and solubilisation of drugs or use in personal care and hygiene products. Further work should also take the direction of investigating an anionic surfactant-like peptide in a similar fashion to try and expand on the use of this class of designed peptides.

The investigation on RSF's surfactant behaviour highlighted the potential that can come from extracting and recovering functional peptides from larger proteins. It can be a worthwhile process but improvements are needed in the procedure of identification, extraction and separation of the peptides to yield better fractions. However, if the cost of

such processes becomes too high, competing sources of functioning peptides will be preferred.

With specific regards to the RSF peptides, future work should attempt to elucidate the interactions that are taking place at the air-water interface in the presence of surfactants. For example, if the RSF peptides are able to form stable layers encompassing other molecules this could be used to help stabilise biomolecules which would otherwise denature at the air-water interface. Also the improved stability of foams upon surfactant addition would warrant some more exploration to identify how this stability is mediated and whether it can be exploited for the stabilisation of molecules or surfaces such as microbubbles.

7 REFERENCES

1. B. Kronberg, K. Holmberg and B. Lindman, *Surface Chemistry of Surfactants and Polymers*, 2014, DOI: 10.1002/9781118695968, 1-479.
2. S. Mishra and V. K. Tyagi, *Journal of Oleo Science*, 2007, **56**, 269-276.
3. J. Penfold, R. K. Thomas, P. X. Li, J. T. Petkov, I. Tucker, J. R. P. Webster and A. E. Terry, *Langmuir : the ACS journal of surfaces and colloids*, 2015, **31**, 3003-3011.
4. K. Esumi and M. Ueno, *Structure-performance relationships in surfactants*, Marcel Dekker, New York, 2nd ed rev. and expanded. edn., 2003.
5. F. M. Menger and C. A. Littau, *J Am Chem Soc*, 1993, **115**, 10083-10090.
6. I. Kralova and J. Sjoblom, *J Disper Sci Technol*, 2009, **30**, 1363-1383.
7. V. P. Torchilin, *Journal of controlled release : official journal of the Controlled Release Society*, 2001, **73**, 137-172.
8. T. A. Khan, H. C. Mahler and R. S. K. Kishore, *European Journal of Pharmaceutics and Biopharmaceutics*, 2015, **97**, 60-67.
9. A. Singh, J. D. Van Hamme and O. P. Ward, *Biotechnol Adv*, 2007, **25**, 99-121.
10. M. J. L. Castro, C. Ojeda and A. F. Cirelli, *Environmental Chemistry Letters*, 2014, **12**, 85-95.
11. S. B. Liu, L. Wei, L. Hao, N. Fang, M. W. Chang, R. Xu, Y. H. Yang and Y. Chen, *Acs Nano*, 2009, **3**, 3891-3902.
12. P. K. Kang and D. O. Shah, *Langmuir : the ACS journal of surfaces and colloids*, 1997, **13**, 1820-1826.
13. M. A. Malik, Z. Khan and S. A. Al-Thabaiti, *Sci Adv Mater*, 2011, **3**, 912-918.

14. M. le Maire, P. Champeil and J. V. Moller, *Bba-Biomembranes*, 2000, **1508**, 86-111.
15. S. F. Atkinson, D. R. Johnson, B. J. Venables, J. L. Slye, J. R. Kennedy, S. D. Dyer, B. B. Price, M. Ciarlo, K. Stanton, H. Sanderson and A. Nielsen, *Sci Total Environ*, 2009, **407**, 4028-4037.
16. P. T. Anastas and J. C. Warner, *Green chemistry : theory and practice*, Oxford University Press, Oxford, 1998.
17. H. a. S. Executive, The Registration Process, <http://www.hse.gov.uk/reach/regprocess.htm>).
18. K. Holmberg, *Handbook of applied surface and colloid chemistry*, Wiley, Chichester, 2002.
19. P. Foley, A. K. Pour, E. S. Beach and J. B. Zimmerman, *Chemical Society reviews*, 2012, **41**, 1499-1518.
20. M. K. Patel, A. Theiss and E. Worrell, *Resour Conserv Recy*, 1999, **25**, 61-78.
21. M. Nakagaki and S. Yokoyama, *Journal of Pharmaceutical Sciences*, **74**, 1047-1052.
22. L. H. Lin and K. M. Chen, *Colloid Surface A*, 2006, **275**, 99-106.
23. R. E. W. Hancock and M. G. Scott, *Proceedings of the National Academy of Sciences*, 2000, **97**, 8856-8861.
24. T. J. Hall-Manning, G. H. Holland, G. Rennie, P. Revell, J. Hines, M. D. Barratt and D. A. Basketter, *Food and Chemical Toxicology*, 1998, **36**, 233-238.
25. J. D. Desai and I. M. Banat, *Microbiol Mol Biol R*, 1997, **61**, 47-&.
26. A. Varvaresou and K. Iakovou, *Lett Appl Microbiol*, 2015, **61**, 214-223.
27. M. B. Linder, G. R. Szilvay, T. Nakari-Setala and M. E. Penttila, *Fems Microbiol Rev*, 2005, **29**, 877-896.
28. J. N. Israelachvili, *Intermolecular and surface forces*, Academic, 2nd ed. edn., 1991.
29. B. Lindman and H. Wennerstrom, *Topics in current chemistry*, 1980, **87**, 1-87.
30. S. Paria and K. C. Khilar, *Advances in colloid and interface science*, 2004, **110**, 75-95.
31. D. Attwood, *Kolloid-Zeitschrift und Zeitschrift für Polymere*, 1969, **232**, 788-792.
32. P. H. Elworthy and C. B. Macfarlane, *Journal of Pharmacy and Pharmacology*, 1962, **14**, 100T-102T.
33. M. N. Jones, *J Colloid Interf Sci*, 1967, **23**, 36-42.
34. F. M. Menger and S. A. A. Rizvi, *Langmuir : the ACS journal of surfaces and colloids*, 2011, **27**, 13975-13977.

35. F. M. Menger, S. A. A. Rizvi and L. Shi, *Langmuir : the ACS journal of surfaces and colloids*, 2011, **27**, 7963-7965.
36. F. M. Menger, L. Shi and S. A. A. Rizvi, *Langmuir : the ACS journal of surfaces and colloids*, 2010, **26**, 1588-1589.
37. P. X. Li, Z. X. Li, H.-H. Shen, R. K. Thomas, J. Penfold and J. R. Lu, *Langmuir : the ACS journal of surfaces and colloids*, 2013, **29**, 9324-9334.
38. P. X. Li, R. K. Thomas and J. Penfold, *Langmuir : the ACS journal of surfaces and colloids*, 2014, **30**, 6739-6747.
39. H. Xu, P. X. Li, K. Ma, R. K. Thomas, J. Penfold and J. R. Lu, *Langmuir : the ACS journal of surfaces and colloids*, 2013, **29**, 9335-9351.
40. R. Zhang and P. Somasundaran, *Advances in colloid and interface science*, 2006, **123-126**, 213-229.
41. R. Atkin, V. S. J. Craig, E. J. Wanless and S. Biggs, *Advances in colloid and interface science*, 2003, **103**, 219-304.
42. M. Rabe, D. Verdes and S. Seeger, *Advances in colloid and interface science*, 2011, **162**, 87-106.
43. T. Nylander, Y. Samoshina and B. Lindman, *Advances in colloid and interface science*, 2006, **123-126**, 105-123.
44. F. Tiberg, J. Brinck and L. Grant, *Curr Opin Colloid In*, 1999, **4**, 411-419.
45. R. Zhang and P. Somasundaran, *Advances in colloid and interface science*, 2006, **123-126**, 213-229.
46. E. M. Lee, R. K. Thomas, P. G. Cummins, E. J. Staples, J. Penfold and A. R. Rennie, *Chem Phys Lett*, 1989, **162**, 196-202.
47. J. Penfold, I. Tucker, J. Petkov and R. K. Thomas, *Langmuir : the ACS journal of surfaces and colloids*, 2007, **23**, 8357-8364.
48. K. Nakanishi, T. Sakiyama and K. Imamura, *J Biosci Bioeng*, 2001, **91**, 233-244.
49. G. Fragneto-Cusani, *J Phys-Condens Mat*, 2001, **13**, 4973-4989.
50. X. Zhao, F. Pan, L. Garcia-Gancedo, A. J. Flewitt, G. M. Ashley, J. Luo and J. R. Lu, *Journal of the Royal Society, Interface / the Royal Society*, 2012, **9**, 2457-2467.
51. F. Pan, Z. Lu, I. Tucker, S. Hosking, J. Petkov and J. R. Lu, *J Colloid Interf Sci*, 2016, **484**, 125-134.
52. A. Fan, P. Somasundaran and N. J. Turro, *Langmuir : the ACS journal of surfaces and colloids*, 1997, **13**, 506-510.
53. Y. Samoshina, T. Nylander, V. Shubin, R. Bauer and K. Eskilsson, *Langmuir : the ACS journal of surfaces and colloids*, 2005, **21**, 5872-5881.
54. S. Manne and H. E. Gaub, *Science*, 1995, **270**, 1480-1482.

55. J. Penfold and R. K. Thomas, *Curr Opin Colloid In*, 2014, **19**, 198-206.
56. R. K. Thomas, *Annual Review of Physical Chemistry*, 2004, **55**, 391-426.
57. J. Penfold, R. M. Richardson, A. Zorbakhsh, J. R. P. Webster, D. G. Bucknall, A. R. Rennie, R. A. L. Jones, T. Cosgrove, R. K. Thomas, J. S. Higgins, P. D. I. Fletcher, E. Dickinson, S. J. Roser, I. A. McLure, A. R. Hillman, R. W. Richards, E. J. Staples, A. N. Burgess, E. A. Simister and J. W. White, *J Chem Soc Faraday T*, 1997, **93**, 3899-3917.
58. J. R. Wright, *Nat Rev Immunol*, 2005, **5**, 58-68.
59. E. Z. Ron and E. Rosenberg, *Environmental Microbiology*, 2001, **3**, 229-236.
60. C. Bechara and S. Sagan, *FEBS Letters*, 2013, **587**, 1693-1702.
61. A. Giuliani, G. Pirri, A. Bozzi, A. Di Giulio, M. Aschi and A. C. Rinaldi, *Cellular and molecular life sciences : CMLS*, 2008, **65**, 2450-2460.
62. M. D. Dwyer, L. Z. He, M. James, A. Nelson and A. P. J. Middelberg, *Journal of the Royal Society, Interface / the Royal Society*, 2013, **10**.
63. R. V. Ulijn and A. M. Smith, *Chemical Society reviews*, 2008, **37**, 664-675.
64. X. Zhao, F. Pan, H. Xu, M. Yaseen, H. Shan, C. A. Hauser, S. Zhang and J. R. Lu, *Chemical Society reviews*, 2010, **39**, 3480-3498.
65. S. G. Zhang, *Nat Biotechnol*, 2003, **21**, 1171-1178.
66. A. F. Dexter and A. P. J. Middelberg, *Ind Eng Chem Res*, 2008, **47**, 6391-6398.
67. M. S. Ekiz, G. Cinar, M. A. Khalily and M. O. Guler, *Nanotechnology*, 2016, **27**.
68. D. K. Warren, W. W. Quadir, C. S. Hollenbeak, A. M. Elward, M. J. Cox and V. J. Fraser, *Crit Care Med*, 2006, **34**, 2084-2089.
69. C. K. Bower, J. Mcguire and M. A. Daeschel, *Appl Environ Microb*, 1995, **61**, 992-997.
70. S. G. Zhang, L. Yan, M. Altman, M. Lassel, H. Nugent, F. Frankel, D. A. Lauffenburger, G. M. Whitesides and A. Rich, *Biomaterials*, 1999, **20**, 1213-1220.
71. S. Vauthey, S. Santoso, H. Gong, N. Watson and S. Zhang, *Proceedings of the National Academy of Sciences of the United States of America*, 2002, **99**, 5355-5360.
72. G. v. Maltzahn, S. Vauthey, S. Santoso and S. Zhang, *Langmuir : the ACS journal of surfaces and colloids*, 2003, **19**, 4332-4337.
73. S. Santoso, W. Hwang, H. Hartman and S. Zhang, *Nano Letters*, 2002, **2**, 687-691.
74. S. Vauthey, S. Santoso, H. Y. Gong, N. Watson and S. G. Zhang, *Proceedings of the National Academy of Sciences of the United States of America*, 2002, **99**, 5355-5360.

75. J. Wang, S. Han, G. Meng, H. Xu, D. Xia, X. Zhao, R. Schweins and J. R. Lu, *Soft Matter*, 2009, **5**, 3870-3878.
76. H. Xu, J. Wang, S. Han, J. Wang, D. Yu, H. Zhang, D. Xia, X. Zhao, T. A. Waigh and J. R. Lu, *Langmuir : the ACS journal of surfaces and colloids*, 2009, **25**, 4115-4123.
77. C. Chen, F. Pan, S. Zhang, J. Hu, M. Cao, J. Wang, H. Xu, X. Zhao and J. R. Lu, *Biomacromolecules*, 2010, **11**, 402-411.
78. S. Han, S. Cao, Y. Wang, J. Wang, D. Xia, H. Xu, X. Zhao and J. R. Lu, *Chemistry – A European Journal*, 2011, **17**, 13095-13102.
79. F. Pan, X. Zhao, S. Perumal, T. A. Waigh, J. R. Lu and J. R. Webster, *Langmuir : the ACS journal of surfaces and colloids*, 2010, **26**, 5690-5696.
80. X. B. Zhao, F. Pan, S. Perumal, H. Xu, J. R. Lu and J. R. P. Webster, *Soft Matter*, 2009, **5**, 1630-1638.
81. J. R. Lu, S. Perumal, I. Hopkinson, J. R. P. Webster, J. Penfold, W. Hwang and S. Zhang, *J Am Chem Soc*, 2004, **126**, 8940-8947.
82. A. L. Demain and P. Vaishnav, *Biotechnol Adv*, 2009, **27**, 297-306.
83. I. M. Banat, R. S. Makkar and S. S. Cameotra, *Appl Microbiol Biot*, 2000, **53**, 495-508.
84. M. M. Muller, J. H. Kugler, M. Henkel, M. Gerlitzki, B. Hormann, M. Pohnlein, C. Syldatk and R. Hausmann, *J Biotechnol*, 2012, **162**, 366-380.
85. Y. Corvis, A. Walcarius, R. Rink, N. T. Mrabet and E. Rogalska, *Anal Chem*, 2005, **77**, 1622-1630.
86. A. G. P. Samaranyaka and E. C. Y. Li-Chan, *Journal of Functional Foods*, 2011, **3**, 229-254.
87. A. Moure, H. Domínguez and J. C. Parajó, *Process Biochemistry*, 2006, **41**, 447-456.
88. P. A. Harnedy and R. J. FitzGerald, *Journal of Functional Foods*, 2012, **4**, 6-24.
89. C. Rondel, B. Portet, I. Alric, Z. Mouloungui, J. F. Blanco and F. Silvestre, *J Surfactants Deterg*, 2011, **14**, 535-544.
90. M. Dimitrijevic-Dwyer, L. Z. He, M. James, A. Nelson, L. G. Wang and A. P. J. Middelberg, *Soft Matter*, 2012, **8**, 5131-5139.
91. D. N. Rockwood, R. C. Preda, T. Yucel, X. Wang, M. L. Lovett and D. L. Kaplan, *Nature protocols*, 2011, **6**, 1612-1631.
92. R. L. Horan, K. Antle, A. L. Collette, Y. Z. Huang, J. Huang, J. E. Moreau, V. Volloch, D. L. Kaplan and G. H. Altman, *Biomaterials*, 2005, **26**, 3385-3393.
93. S. W. Ha, H. S. Gracz, A. E. Tonelli and S. M. Hudson, *Biomacromolecules*, 2005, **6**, 2563-2569.

94. C. Z. Zhou, F. Confalonieri, M. Jacquet, R. Perasso, Z. G. Li and J. Janin, *Proteins*, 2001, **44**, 119-122.
95. P. Jiang, H. F. Liu, C. H. Wang, L. Z. Wu, J. G. Huang and C. Guo, *Mater Lett*, 2006, **60**, 919-925.
96. L. S. Wray, X. Hu, J. Gallego, I. Georgakoudi, F. G. Omenetto, D. Schmidt and D. L. Kaplan, *J Biomed Mater Res B*, 2011, **99B**, 89-101.
97. G. T. Cheng, X. Wang, S. J. Tao, J. Xia and S. Xu, *J Appl Polym Sci*, 2015, **132**.
98. K. Tsubouchi, H. Nakao, Y. Igarashi, Y. Takasu and H. Yamada, *Journal of Insect Biotechnology and Sericology*, 2003, **72**, 65-69.
99. H. Yamada, H. Nakao, Y. Takasu and K. Tsubouchi, *Mat Sci Eng C-Bio S*, 2001, **14**, 41-46.
100. A. E. Thurber, F. G. Omenetto and D. L. Kaplan, *Biomaterials*, 2015, **71**, 145-157.
101. Z. Wang, Y. S. Zhang, J. X. Zhang, L. Huang, J. Liu, Y. K. Li, G. Z. Zhang, S. C. Kundu and L. Wang, *Sci Rep-Uk*, 2014, **4**.
102. P. Aramwit, S. Kanokpanont, W. De-Eknamkul and T. Srichana, *J Biosci Bioeng*, 2009, **107**, 556-561.
103. B. Panilaitis, G. H. Altman, J. S. Chen, H. J. Jin, V. Karageorgiou and D. L. Kaplan, *Biomaterials*, 2003, **24**, 3079-3085.
104. R. Valluzzi, S. P. Gido, W. Muller and D. L. Kaplan, *Int J Biol Macromol*, 1999, **24**, 237-242.
105. R. Valluzzi, S. P. Gido, W. P. Zhang, W. S. Muller and D. L. Kaplan, *Macromolecules*, 1996, **29**, 8606-8614.
106. R. Valluzzi and S. P. Gido, *Biopolymers*, 1997, **42**, 705-717.
107. Y. H. Yang, C. Dicko, C. D. Bain, Z. G. Gong, R. M. J. Jacobs, Z. Z. Shao, A. E. Terry and F. Vollrath, *Soft Matter*, 2012, **8**, 9705-9712.
108. D. S. Sivia, *Elementary scattering theory : for X-ray and neutron users*, Oxford University Press, Oxford, 2011.
109. T. L. Crowley, *Physica A: Statistical Mechanics and its Applications*, 1993, **195**, 354-374.
110. J. R. Lu, E. M. Lee and R. K. Thomas, *Acta Crystallographica Section A*, 1996, **52**, 11-41.
111. O. S. Heavens, *Optical properties of thin solid films*, Butterworths, London, 1955.
112. J. Penfold and R. K. Thomas, *J Phys-Condens Mat*, 1990, **2**, 1369-1412.
113. L. Nevot and P. Croce, *Revue De Physique Appliquee*, 1980, **15**, 761-779.

114. R. A. Cowley and T. W. Ryan, *Journal of Physics D-Applied Physics*, 1987, **20**, 61-68.
115. M. Born and E. Wolf, *Principles of optics : electromagnetic theory of propagation, interference and diffraction of light*, Pergamon, Oxford, 4th ed. edn., 1970.
116. A. Nelson, *J Appl Crystallogr*, 2006, **39**, 273-276.
117. H. G. Tompkins, *A user's guide to ellipsometry*, Academic Press, Boston ; London, 1993.
118. H. G. Tompkins and E. A. Irene, *Handbook of ellipsometry*, William Andrew Pub. ; Heidelberg, Germany : Springer, Norwich, N.Y., 2005.
119. J. A. De Feijter, J. Benjamins and F. A. Veer, *Biopolymers*, 1978, **17**, 1759-1772.
120. X. B. Zhao, F. Pan, P. Coffey and J. R. Lu, *Langmuir : the ACS journal of surfaces and colloids*, 2008, **24**, 13556-13564.
121. B. S. Murray and R. Ettelaie, *Curr Opin Colloid In*, 2004, **9**, 314-320.
122. P. Wilde, A. Mackie, F. Husband, P. Gunning and V. Morris, *Advances in colloid and interface science*, 2004, **108**, 63-71.
123. R. J. Pugh, *Advances in colloid and interface science*, 1996, **64**, 67-142.
124. R. Pons, P. Taylor and T. F. Tadros, *Colloid and Polymer Science*, 1997, **275**, 769-776.
125. A. Saint-Jalmes, M. L. Peugeot, H. Ferraz and D. Langevin, *Colloids and Surfaces A: Physicochemical and Engineering Aspects*, 2005, **263**, 219-225.
126. A. R. Mackie, A. P. Gunning, P. J. Wilde and V. J. Morris, *J Colloid Interf Sci*, 1999, **210**, 157-166.
127. E. Dickinson, R. Ettelaie, B. S. Murray and Z. P. Du, *J Colloid Interf Sci*, 2002, **252**, 202-213.
128. A. R. Cox, F. Cagnol, A. B. Russell and M. J. Izzard, *Langmuir : the ACS journal of surfaces and colloids*, 2007, **23**, 7995-8002.
129. D. R. Ekserova and P. M. Krugliakov, *Foam and foam films : theory, experiment, application*, Elsevier, Amsterdam ; New York, 1998.
130. J. J. Bikerman, *Foams : theory and industrial applications*, Reinhold, New York, 1953.
131. J. Ross and G. D. Miles, *Oil & Soap*, 1941, **18**, 99-102.
132. S. G. Zhang, D. M. Marini, W. Hwang and S. Santoso, *Curr Opin Chem Biol*, 2002, **6**, 865-871.
133. X. Zhao and S. Zhang, *Macromolecular bioscience*, 2007, **7**, 13-22.
134. C. Chen, J. Hu, P. Zeng, F. Pan, M. Yaseen, H. Xu and J. R. Lu, *Biomaterials*, 2014, **35**, 1552-1561.

135. A. Dehsorkhi, V. Castelletto, I. W. Hamley, J. Seitsonen and J. Ruokolainen, *Langmuir : the ACS journal of surfaces and colloids*, 2013, **29**, 14246-14253.
136. J. Hu, C. Chen, S. Zhang, X. Zhao, H. Xu and J. R. Lu, *Biomacromolecules*, 2011, **12**, 3839-3843.
137. J. Penfold, R. K. Thomas and H. H. Shen, *Soft Matter*, 2012, **8**, 578-591.
138. M. R. Infante, L. Pérez, A. Pinazo, P. Clapés, M. C. Morán, M. Angelet, M. T. García and M. P. Vinardell, *Cr Chim*, 2004, **7**, 583-592.
139. S. Y. Han, W. W. Xu, M. W. Cao, J. Q. Wang, D. H. Xia, H. Xu, X. B. Zhao and J. R. Lu, *Soft Matter*, 2012, **8**, 645-652.
140. T. J. Deming, *Soft Matter*, 2005, **1**, 28-35.
141. S. J. Keeler and H. S. M. Lu, *Journal*, 2009.
142. H. Heerklotz and J. Seelig, *Biophysical journal*, 2001, **81**, 1547-1554.
143. D. Jayawardane, F. Pan, J. R. Lu and X. B. Zhao, *Soft Matter*, 2015, **11**, 7986-7994.
144. J. Penfold, I. Tucker, E. Staples and R. K. Thomas, *Langmuir : the ACS journal of surfaces and colloids*, 2004, **20**, 7177-7182.
145. X. Zhang, D. Taylor, R. Thomas, J. Penfold and I. Tucker, *Langmuir : the ACS journal of surfaces and colloids*, 2011, **27**, 3569-3577.
146. J. Penfold, I. Tucker and R. K. Thomas, *Langmuir : the ACS journal of surfaces and colloids*, 2005, **21**, 11757-11764.
147. C. Tanford, *J Phys Chem-US*, 1972, **76**, 3020-&.
148. A. Mohr, T. Nylander, L. Piculell, B. Lindman, V. Boyko, F. W. Bartels, Y. Liu and V. Kurkal-Siebert, *ACS applied materials & interfaces*, 2012, **4**, 1500-1511.
149. X. L. Zhang, J. Penfold, R. K. Thomas, I. M. Tucker, J. T. Petkov, J. Bent and A. Cox, *Langmuir : the ACS journal of surfaces and colloids*, 2011, **27**, 10464-10474.
150. C. N. Mulligan, *Environ Pollut*, 2005, **133**, 183-198.
151. L. Rodrigues, I. M. Banat, J. Teixeira and R. Oliveira, *J Antimicrob Chemoth*, 2006, **57**, 609-618.
152. E. Bouyer, G. Mekhloufi, V. Rosilio, J. L. Grossiord and F. Agnely, *Int J Pharmaceut*, 2012, **436**, 359-378.
153. J. M. Campos, T. L. M. Stamford, L. A. Sarubbo, J. M. de Luna, R. D. Rufino and I. M. Banat, *Biotechnol Progr*, 2013, **29**, 1097-1108.
154. I. A. Nnanna and J. Xia, Protein-based surfactants : synthesis, physicochemical properties, and applications, Marcel Dekker, New York, 2001.
155. H. Tao, B. Marelli, M. M. Yang, B. An, M. S. Onses, J. A. Rogers, D. L. Kaplan and F. G. Omenetto, *Advanced Materials*, 2015, **27**, 4273-4279.

156. D. H. Kim, J. Viventi, J. J. Amsden, J. L. Xiao, L. Vigeland, Y. S. Kim, J. A. Blanco, B. Panilaitis, E. S. Frechette, D. Contreras, D. L. Kaplan, F. G. Omenetto, Y. G. Huang, K. C. Hwang, M. R. Zakin, B. Litt and J. A. Rogers, *Nat Mater*, 2010, **9**, 511-517.
157. A. S. Lammel, X. Hu, S. H. Park, D. L. Kaplan and T. R. Scheibel, *Biomaterials*, 2010, **31**, 4583-4591.
158. G. S. Perrone, G. G. Leisk, T. J. Lo, J. E. Moreau, D. S. Haas, B. J. Papenburg, E. B. Golden, B. P. Partlow, S. E. Fox, A. M. S. Ibrahim, S. J. Lin and D. L. Kaplan, *Nat Commun*, 2014, **5**.
159. E. M. Pritchard, X. Hu, V. Finley, C. K. Kuo and D. L. Kaplan, *Macromolecular bioscience*, 2013, **13**, 311-320.
160. R. S. H. Lam and M. T. Nickerson, *Food Chem*, 2013, **141**, 975-984.
161. J. D. Xia, J. H. Qian and I. A. Nnanna, *J Agr Food Chem*, 1996, **44**, 975-979.
162. W. Norde, T. A. Horbett and J. L. Brash, *Acs Sym Ser*, 2012, **1120**, 1-34.
163. M. Malmsten, *Biopolymers at interfaces*, Marcel Dekker, New York, 2nd ed. edn., 2003.
164. E. Dickinson, *Food Hydrocolloid*, 2011, **25**, 1966-1983.
165. R. Adjonu, G. Doran, P. Torley and S. Agboola, *J Food Eng*, 2014, **122**, 15-27.
166. W. A. M. Mutilangi, D. Panyam and A. Kilara, *J Food Sci*, 1996, **61**, 270-&.
167. S. B. Zhang and Q. Y. Lu, *Food Hydrocolloid*, 2015, **47**, 51-60.
168. H. Korhonen and A. Pihlanto, *Int Dairy J*, 2006, **16**, 945-960.
169. J. R. Lu, T. J. Su and R. K. Thomas, *J Phys Chem B*, 1998, **102**, 10307-10315.
170. J. R. Lu, T. J. Su, R. K. Thomas and J. Penfold, *Langmuir : the ACS journal of surfaces and colloids*, 1998, **14**, 6261-6268.
171. R. J. Green, T. J. Su, J. R. Lu and J. Penfold, *J Phys Chem B*, 2001, **105**, 1594-1602.
172. R. J. Green, T. J. Su, J. R. Lu and J. R. P. Webster, *J Phys Chem B*, 2001, **105**, 9331-9338.
173. X. L. Zhang, J. Penfold, R. K. Thomas, I. M. Tucker, J. T. Petkov, J. Bent and A. Cox, *Langmuir : the ACS journal of surfaces and colloids*, 2011, **27**, 10464-10474.
174. A. Ajisawa, *The Journal of Sericultural Science of Japan*, 1998, **67**, 91-94.
175. D. Jayawardane, F. Pang, J. R. Lu and X. B. Zhao, *Langmuir : the ACS journal of surfaces and colloids*, 2016, **32**, 8202-8211.
176. C. W. P. Foo, E. Bini, J. Hensman, D. P. Knight, R. V. Lewis and D. L. Kaplan, *Appl Phys a-Mater*, 2006, **82**, 223-233.

177. F. J. Zhang, M. W. A. Skoda, R. M. J. Jacobs, R. A. Martin, C. M. Martin and F. Schreiber, *J Phys Chem B*, 2007, **111**, 251-259.
178. M. Lundin, U. M. Elofsson, E. Blomberg and M. W. Rutland, *Colloid Surface B*, 2010, **77**, 1-11.
179. T. J. Su, J. R. Lu, R. K. Thomas, Z. F. Cui and J. Penfold, *J Colloid Interf Sci*, 1998, **203**, 419-429.
180. G. Fragneto, R. K. Thomas, A. R. Rennie and J. Penfold, *Langmuir : the ACS journal of surfaces and colloids*, 1996, **12**, 6036-6043.
181. A. Renault, J. F. Rioux-Dube, T. Lefevre, S. Pezennec, S. Beaufils, V. Vie, M. Tremblay and M. Pezolet, *Langmuir : the ACS journal of surfaces and colloids*, 2009, **25**, 8170-8180.
182. L. Wang, H. G. Xie, X. Y. Qiao, A. Goffin, T. Hodgkinson, X. F. Yuan, K. Sun and G. G. Fuller, *Langmuir : the ACS journal of surfaces and colloids*, 2012, **28**, 459-467.
183. X. F. Wei, Z. D. Chang and H. Z. Liu, *J Surfactants Deterg*, 2003, **6**, 107-112.
184. R. J. Green, T. J. Su, H. Joy and J. R. Lu, *Langmuir : the ACS journal of surfaces and colloids*, 2000, **16**, 5797-5805.